T.R.
GEBZE TECHNICAL UNIVERSITY
GRADUATE SCHOOL OF NATURAL AND APPLIED SCIENCES

DEVELOPING AN EFFICIENT SYNTHESIS METHOD FOR GRAPHENE

BETÜL GÜRÜNLÜ
A THESIS SUBMITTED FOR THE DEGREE OF
DOCTOR OF PHILOSOPHY
DEPARTMENT OF CHEMICAL ENGINEERING

GEBZE
2019

T.R.

GEBZE TECHNICAL UNIVERSITY

GRADUATE SCHOOL OF NATURAL AND APPLIED SCIENCES

DEVELOPING AN EFFICIENT SYNTHESIS METHOD FOR GRAPHENE

BETÜL GÜRÜNLÜ

A THESIS SUBMITTED FOR THE DEGREE OF DOCTOR OF PHILOSOPHY

DEPARTMENT OF CHEMICAL ENGINEERING

THESIS SUPERVISOR

PROF. DR. MAHMUT RAHİM BAYRAMOĞLU

GEBZE

2019

T.C.
GEBZE TEKNİK ÜNİVERSİTESİ
FEN BİLİMLERİ ENSTİTÜSÜ

GRAFEN SENTEZİ İÇİN ETKİN BİR YÖNTEM GELİŞTİRİLMESİ

BETÜL GÜRÜNLÜ
DOKTORA TEZİ
KİMYA MÜHENDİSLİĞİ ANABİLİM DALI

DANIŞMANI
PROF. DR. MAHMUT RAHİM BAYRAMOĞLU

GEBZE
2019

GEBZE TEKNİK ÜNİVERSİTESİ	**DOKTORA JÜRİ ONAY FORMU**

GTÜ Fen Bilimleri Enstitüsü Yönetim Kurulu'nun 26/06/2019 tarih ve 2019/09 sayılı kararıyla oluşturulan jüri tarafından 12/09/2019 tarihinde tez savunma sınavı yapılan Betül Gürünlü'nün tez çalışması Kimya Mühendisliği Anabilim Dalında DOKTORA tezi olarak kabul edilmiştir.

JÜRİ

ÜYE
(TEZ DANIŞMANI) : PROF. DR. MAHMUT RAHİM BAYRAMOĞLU (GTÜ)

ÜYE : PROF. DR. HÜSEYİN DELİGÖZ (İÜ)

ÜYE : PROF. DR. MAHMET ALİ FARUK ÖKSÜZÖMER (İÜ)

ÜYE : DR ÖĞR. ÜYESİ ÇİĞDEM TAŞDELEN YÜCEDAĞ (GTÜ)

ÜYE : DR. ÖĞR. ÜYESİ ÖMÜR ARAS (BTÜ)

ONAY

Gebze Teknik Üniversitesi Fen Bilimleri Enstitüsü Yönetim Kurulu'nun
...../...../..... tarih ve ...../..... sayılı kararı.

SUMMARY

In recent years, a great deal of concentration has addressed the electronic and morphological characteristics of carbonaceous substances. Nowadays, particularly, graphene is the most popular subjects in condensed-matter physics and materials science. It is utilized in different area such as desalination of seawater, smartphones, computers, satellites, planes, cars, building materials, obtaining protective coatings and rust free cars, nuclear clean up, transistors, sensors, electron microscopy, Li ion batteries, super capacitors, and bionics. Mechanical cleaving (exfoliation), chemical exfoliation, chemical synthesis, and thermal chemical vapor deposition (CVD) synthesis are the most commonly used methods today. Some other techniques are also reported such as unzipping nanotube and microwave synthesis. In graphene synthesis, starting material is usually graphite. But different starting materials are also used in literature such as; rice husks, fenugreek seeds, melamine, hibiscus flower petals, camphor, polyaniline, urea, humanin, alfalfa plants, petroleum asphalt. In this thesis study, different methods for graphene synthesis were studied, and their performances were compared with the help of different characterization techniques. Among all these methods, a new and improved method was developed for graphene synthesis.

Keywords: Graphene synthesis, molten salt media, polysaccharides, graphene characterization.

ÖZET

Son yıllarda, karbonlu maddelerin elektronik ve morfolojik özellikleri dikkate değerdir. Günümüzde özellikle grafen, yoğun madde fiziği ve malzeme biliminde en popüler konulardır. Deniz suyunun tuzunun giderilmesi, akıllı telefonlar, bilgisayarlar, uydular, uçaklar, arabalar, inşaat malzemeleri, koruyucu kaplamalar ve paslanmaz araçlar, nükleer temizleme, transistörler, sensörler, elektron mikroskobu, Li-ion piller, süper kapasitörler gibi farklı alanlarda kullanılmaktadır. Mekanik soyulma, kimyasal soyulma, kimyasal sentez ve termal kimyasal buhar biriktirme (CVD) sentezi günümüzde en yaygın kullanılan yöntemlerdir. Sıkıştırılmış nanotüp ve mikrodalga sentezi gibi başka teknikler de bildirilmiştir. Grafen sentezinde başlangıç materyali genellikle grafittir. Ancak literatürde; pirinç kabuğu, çemen tohumu, melamin, hibiskus çiçek yaprakları, kafuru, polianilin, üre, humanin, alfalfa bitkileri, petrol asfaltı gibi pek çok doğal malzeme aşağıdan yukarı sentez çalışmasında karbon başlangıç maddesi olarak kullanılmıştır. Bu tez çalışmasında, grafen sentezi için farklı yöntemler geliştirilmiştir ve bunların performansları farklı karakterizasyon teknikleri yardımıyla kıyaslanmıştır. Bu yöntemler arasında grafen sentezi için yeni bir yöntem geliştirilmiştir.

Anahtar kelimeler: Grafen sentezi, eriyik tuz ortamı, polisakkaritler, grafen karakterizasyonu.

ACKNOWLEDGEMENTS

I would like to express my deep and sincere gratitude to my supervisor, Prof. Mahmut Bayramoglu, who not only shared his profound scientific knowledge with me but also taught me great lessons of life. His support, suggestions and encouragement gave me the drive and will to complete this work. I would also like to thank my family for their support and assistance during my study.

TABLE of CONTENTS

	Page
SUMMARY	v
ÖZET	vi
ACKNOWLEDGEMENTS	vii
TABLE of CONTENTS	viii
LIST of ABBREVIATIONS and ACRONYMS	x
LIST of FIGURES	xii
LIST of TABLES	xv
1. INTRODUCTION	1
2. LITERATURE REVIEW	3
2.1. Top-down Processes	5
2.1.1. Micromechanical Exfoliation (ME) of Graphene from Graphite	5
2.1.2. Anodic Bonding	7
2.1.3. Laser Ablation	9
2.1.4. Liquid Phase Exfoliation (LPE)	9
2.1.4.1. LPE of Graphene Directly from Graphite	9
2.1.4.2. LPE of Graphite Oxide	10
2.1.4.3. Ultrasound Energy	11
2.1.5. Detonation	12
2.1.6. Chemical Synthesis	12
2.1.6.1. Microwave Energy	12
2.2. Bottom-up Processes	13
2.2.1. Solvothermal/Pyrolsis Methods	13
2.2.2. Epitaxial Growth of Graphene on SiC	14
2.2.3. Chemical Vapor Deposition (CVD)	14
2.3. Characterization Techniques	15
2.3.1. Atomic Force Microscopy (AFM) Spectroscopy	15
2.3.2. Raman Spectroscopy	16
2.3.3. Rayleigh Scattering	17
2.3.4. X-Ray Diffraction (XRD)	17

2.3.5. X-Ray Photoelectron (XPS) Spectroscopy 17
2.3.6. Low Energy Electron Diffraction (LEED) 18
3. EXPERIMENTAL STUDY 19
3.1. Molten-Salt Solution Method 19
3.1.1. Bottom-up Approach 20
3.1.2. Top-down Approach 23
3.2. Microwave Energy Method 28
3.3. Ultrasound Energy Method 30
4. RESULTS & DISCUSSION 33
4.1. Molten-Salt Solution Method Results 33
4.1.1. Bottom-up Approach 33
4.1.2. Top-down Approach 45
4.2. Microwave (MW) Assisted Method Results 58
4.3. Ultrasound (US) Assisted Method Results 64
5.CONCLUSION 69

REFERENCES 72
BIOGRAPHY 79
APPENDIX 80

LIST of ABBREVIATIONS and ACRONYMS

Abbreviations and Acronyms		**Explanations**
GGr	:	Graphene from graphite
GO	:	Graphene oxide
RGO	:	Reduced graphene oxide
GN	:	Graphene nanoplatelet
GF	:	Graphene from fructose
GS	:	Graphene from starch
GM	:	Graphene from mannose
GA	:	Graphene from arabinose
GX	:	Graphene from xylose
GG	:	Graphene from glucose
DMSO	:	Dimethyl sulfoxide
PA	:	Perchloric acid
DMF	:	N,N Dimethyl formamide
A	:	Surface area
l	:	Sample thickness
σ	:	Electrical conductivity
ME	:	Mechanically exfoliated
MS	:	Molten salt
MW	:	Microwave
US	:	Ultrasonic treatment
LPE	:	Liquid phase exfoliation
XPS	:	X-ray Photo Electron Spectroscopy
SEM	:	Scanning Electron Microscopy
TEM	:	Transmission Electron Microscopy
HRTEM	:	High Resolution Transmission Electron Microscopy
UV-vis	:	Ultraviolet visible spectroscopy
HOPG	:	Highly oriented pyrolytic graphite
STM	:	Scanning tunneling microscopy
LEED	:	Low-energy electron diffraction

SLG	:	Single layer graphene
N	:	Number of graphene layers
THF	:	Tetrahydrafuran
DBE	:	Dibasic ester
EMIMAc	:	1- ethyl-3-methylimidazolium acetate
CNT	:	Carbon nanotube
GIC	:	Graphite intercalated compound
IL	:	Ionic liquid
TEA	:	Tetra ethyl ammonium
SiC	:	Silicon Carbide
EG	:	Ethylene glycol
ED	:	Ethylene diamine
n_Hexa	:	n-Hexadecane
OCTA	:	1-octanol
λ	:	X-ray wavelength (0.15406 nm)
K	:	Constant that depends on the crystallite shape (0.89)
L	:	Thickness of crystallite
θ	:	Scattering angle for XRD
$\beta(2\theta)$	:	Half-width of the diffraction line
βexp	:	Experimental half-width
$\beta instr$	:	The experimental broading which was measured with silicon sample
N_{GP}	:	Number of graphene layer
D_{002}	:	Overall thickness of graphene
d_{002}	:	Thickness of a graphene layer
wG	:	Band position in Raman wave numbers
CG	:	Commercial graphene
CGr	:	Commercial graphite
CB	:	Carbon Black
FWHM	:	Full width at half maximum
Ra	:	Rougness average
Rq	:	Root mean square roughness
RMS	:	Roughness mean square

LIST of FIGURES

Figure No:		Page
2.1:	a) sp^2 hybrids carbon atoms in graphene b) sp^2 hybrids of graphene carbon atoms connected to adjacent ones.	4
2.2:	A flow chart of graphene synthesis methods.	4
2.3:	a) Optical micrograph of ME piece including of parts with different thickness. b) Calculation of the number of graphene layers by Raman spectra.	6
2.4:	An easy way for producing single- and few-layered graphene by the micromechanical exfoliation of graphite. a) 1) Attach a very thin piece of HOPG onto a scotch tape. 2–4) Fold and unfold as shown to get ultrathin (almost invisible) flakes of graphite on the tape. b) Select an area having very thin flakes, move them onto a available substrate like SiO_2/Si. Remove the tape from the substrate. c) Typical image of a few-layer flake by optical microscope d) AFM image of graphene flakes.	7
2.5:	The illustration of the basic methods for graphene synthesis. (a) Micromechanical exfoliation. (b) Anodic bonding. (c) Photocleavage. (d) Liquid phase cleavage. (e) Growth on SiC. (f) Precipitation/Segregation from carbon onto metal substrate. (g) Chemical vapor deposition. (h) Molecular Beam epitaxy. (i) Chemical synthesis from benzene.	8
2.6:	Primary and secondary sonochemistry for synthesis of nanomaterials. In order to build functional nanomaterials, first metal atoms are generated via sonolysis of weak metal-carbon bonds from volatile organometallic composites in diminishing bubble then spread in the mass liquid. Secondary sonochemical samples can be synthesized from chemically active materials such as organic radicals producing in the bubble, but then disperse in the liquid and afterwards react with solution precursor in order to synthesize a kind of nanomaterials.	11

2.7:	Atomically resolved STM image of a graphene sample grown on SiC(0001) at 1400 °C for 8 min.	14
2.8:	Raman output of graphene layers with different thicknesses.	16
2.9:	X-ray diffraction spectrum of graphene nanosheets.	17
2.10:	Typical LEED patterns of graphene and h-BN films on single-crystal surfaces.	18
3.1:	Experimental set-up.	20
3.2:	XRD spectra of industrial graphene nanoplatelets entitled as a) GN5, b) GN15, and c) GN25.	22
3.3:	Block diagram of experimental set – up.	24
3.4:	Keithley 2400 Sourcemeter.	26
3.5:	Copper cylindrical container and a copper cap.	26
3.6:	Electrical conductivity measurement set-up.	27
3.7:	Malvern Zetasizer Nano ZS Laser Particle Size Distribution Meter.	27
3.8:	Microwave oven.	29
3.9:	Ultrasound device.	31
3.10:	Perkin Elmer Lambda 35 UV/vis Spectrometer.	32
4.1:	Graphene Product Yields at 600 °C and 800 °C.	35
4.2:	XRD patterns for graphene products at 600 °C.	36
4.3:	XRD patterns for graphene products at 800 °C.	37
4.4:	Raman spectra of GA800, GC600 and GA600 graphene products.	39
4.5:	Raman spectra of graphene from graphite at 600 °C.	40
4.6:	SEM images of GF800, GM800, GS600, GX600, GF600, GM600.	42
4.7:	Survey-scanned XPS spectra and fine-scanned spectra of a) GA600, b) GA800 and c) GF600.	43
4.8:	a) XRD patterns of CGr, GGr500, GGr600, GGr700 & GGr800 b) UV absorbance peaks of commercial graphite and c) graphene d) UV analyses of obtained graphene products from graphite at different temperatures.	46
4.9:	Particle size distribution (DLS) analyses of graphene products.	47
4.10:	Raman spectra of RGO, CG, GGr500, GGr700, and GGr800.	49
4.11:	Survey-scanned XPS spectra and fine-scanned spectra of a) GGr600 and b) GGr800.	51

4.12: SEM images of graphene products. 54
4.13: TEM images of graphene products. 55
4.14: AFM images and line profiles of graphene samples. 56
4.15: XRD spectrum of expanded graphite products, which was obtained in EG by using MW energy. 59
4.16: XRD spectrum of expanded graphite products, which was obtained in ammonia by using MW energy. 60
4.17: XRD spectrum of expanded graphite products, which was obtained in DMF by using MW energy. 60
4.18: XRD spectrum of Natural graphite. 60
4.19: XRD spectrums of MW supported synthesized graphene products. 62
4.20: Relation between electrical conductivity and dipole moment. 63
4.21: Relation between layer numbers and electrical conductivity. 63
4.22: UV spectrums of MW based synthesized graphene products. 64
4.23: UV-Vis spectrums of US-assisted graphene products and CG. 65
4.24: AFM results of US-assisted graphenes a) G-DMSO, b) G-DMF, and c) G-PA. 66
4.25: DLS analysis results of synthesized samples a) G-PA, b) G-DMSO, c) G-DMF. 67

LIST of TABLES

Table No:		Page
3.1:	Comparison of the graphene synthesis methods.	19
4.1:	List of experiments and product yields.	34
4.2:	Layer numbers of MS-derived graphene products.	38
4.3:	I_{2D}/I_G and I_D/I_G values of GA800, GC600 and GA600.	40
4.4:	Electrical conductivities of MS-derived graphene products.	41
4.5:	Electrical conductivities of commercial graphene, commercial graphite, carbon black, and reduced graphene oxide.	41
4.6:	Contribution from differently bonded carbons extracted through peak de-convolution for C1s region for GA600, GA800 and GF800.	45
4.7:	C1s and O1 regions' atomic ratio values for GA600, GA800 and GF800.	45
4.8:	Particle size values of synthesized graphene samples and commercial products.	48
4.9:	Layer numbers of synthesized graphene samples and commercial products.	50
4.10:	I_D/I_G ratio of synthesized graphene and commercial products.	50
4.11:	Contribution from differently bonded carbons extracted through peak de-convolution for C1s region for GGr600, and GGr800.	53
4.12:	C1s and O1 regions' atomic ratio values and peak for GGr600, and GGr800.	53
4.13:	Results of experiments that were done by using ammonia.	58
4.14:	Microwave tests that were conducted by using DMF, EG and ED.	59
4.15:	Layer numbers of final products calculating from XRD results.	61
4.16:	Electrical conductivities, dipole moments, layer numbers and dielectric constants of MW supported graphene products.	62
4.17:	Particle size results of US-assited synthesized samples.	68

1. INTRODUCTION

Graphene is a one layer of carbon atoms organized in a honeycomb lattice [Tassin, Koschny and Soukoulis, 2013]. It is the block of graphite that is used in pencil tips, but graphene is an extraordinary matter with a multitude of astounding specialities that named it as wonder material [Lohar, 2017].

Graphene is the thinnest substance at one atom thick, and also fabulously strong around 200 times stronger than steel [Lohar, 2017]. Apart from that, graphene is a superb conductor of heat and electricity and has exciting light absorption capabilities. It is truthfully a material with wide potential for integrating in nearly any industry.

Graphene is a highly varied material, and can be merged with other materials (involving gases and metals) to synthesize various materials with different exceptional qualities. Researchers proceed to examine its unexplored properties and possible applications such as touchscreens (for LCD or OLED displays), computer chips, transistors, batteries, supercapacitors, energy production, DNA sequencing, water filters, antennas, solar cells, and spintronics.

Graphene gathers much interest particularly after Geim and Novoselov win the 2010 Nobel Prize in physics by obtaining it in 2004. To produce high-quality graphene in high amount is not easy and affordable. Most companies are using chemical vapor deposition (CVD) based processes. Also, mechanical and chemical exfoliation and chemical synthesis are the most preferred ways today. Another methods are unzipping of a nanotube and microwave irradiation [Bhuyan et al., 2016].

In graphene synthesis, starting material is usually graphite. But different starting materials are also used in literature such as; rice husks [Lu et al., 2015], fenugreek seeds [Park et al., 2017], melamine [Zhang et al., 2014], hibiscus flower petals [Ray et al., 2015], camphor [Ravani et al., 2013], polyaniline [Wang et al., 2012], urea [Wakeland et al., 2010], humanin [Gurunathan et al., 2013], alfaalfa plants [Qu et al., 2013], petroleum asphalt [Li et al., 2013].

In this thesis study, a new and improved method is developed for graphene synthesis, which is called as molten salt derived method. Also different starting materials are used when applying this new method. Then, synthesized graphene

flakes were identified by different characterization techniques. Graphene samples, which were synthesized by using bottom-up method, have the low electrical conductivity values. On the other hand, graphene samples that are produced by top-down method have better electrical conductivity performances than them. For this reason, graphene was synthesized by using top-down methodology in molten salt media at the other temperatures such as 500 °C to 800 °C by increasing 100 °C temperature step. The electrical conductivities of synthesized products will be measured by using 4-point probe technique. Also; SEM, XRD, AFM, XPS, Raman characterization were conducted and Raman and XRD analyses were used in order to calculate the layer numbers of graphene and these results were also compared with each other.

2. LITERATURE REVIEW

Graphene is a 2D material, which was firstly discovered by Geim and Novoselov in 2004. They won Nobel Prize in Physics by synthesizing of 2D of carbon crystal having sp^2 bond by Scotch-tape method in 2010 [Eswaraiah et al., 2011], [Akbar et al., 2015]. Graphene is a thin nanoplatelet, which can be produced by cleaving of graphite. Graphite can be downed into the single graphene sheet level [Lee, 2010]. Graphene is a one atomic layer having 0.34 nm thicknesses. It is a hexagonal shaped plane consisting of sp^2-carbon atoms [Liu et al., 2011], [Baatar, 2008], [Chen et al., 2008], [Bolotin et al., 2008], [Sung, 2009]. Graphene can be seemed as either uncoiled single-walled carbon nanotubes or a wide atomic sheet of graphite [Novoselov et al., 2005]. Graphene has superior mechanical strength, thermal conductivity, optical transparency, high mobility, room temperature quantum Hall effect and great electronic properties like Dirac-particles having a linear dispersion, transport energy gap and simply absorption coefficient of lights, thus it will become the favorable prospect after the silicon time [Geim and Novoselov, 2007], [Nair et al., 2008].

This new 2D material has a prominent importance in present day. It is a quickly developing subject that flourishing novel concepts at incredible speed [Gong, 2011]. Graphene is extensively used substance in electronic industry such as field-effect transistor, transparent electrode, etc. The recent developments in surface area, optical, magnetic, and mechanical properties of functionalized graphene and the unique electronics have arised new attitude of green technology and creative discovery for present complications such as photonic and electronic usages for ultrahigh-frequency graphene-based apparatus, anode for li-ion battery, material science, ceramics, light natural gas tanks, medical science, sensors to identify sickness, supercapacitor, solar cell, desalination of seawater, smartphones, computers, satellites, planes, cars, building materials, obtaining protective coatings and rust free cars, nuclear clean up, transistors, sensors, electron microscopy, and bionics.

Graphene molecular structure includes of sp^2 hybrid carbon atoms that were presented in Figure 2.1a. Sp^2 hybrids supply σ bonds with adjacent carbon atoms.

Each of σ bonds has the length of 1.42 A°. Excellent mechanical characteristics of graphene are obtained under favour of σ bonds.

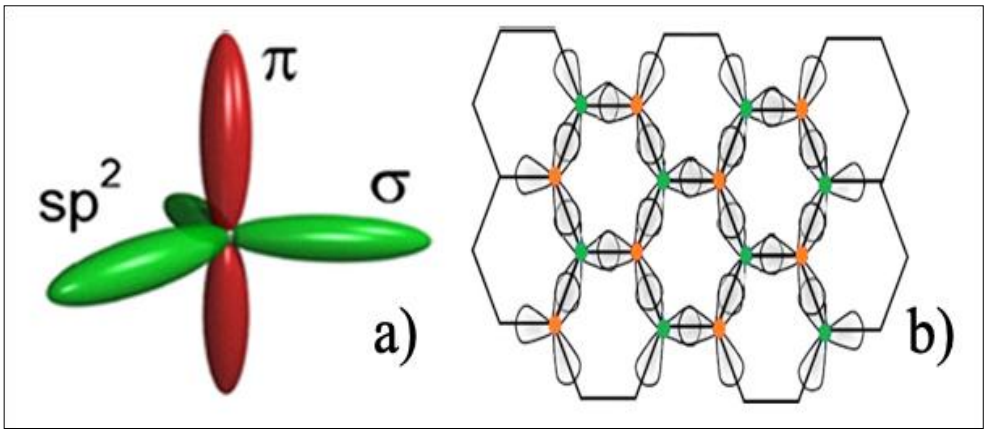

Figure 2.1: a) sp^2 hybrids carbon atoms in graphene b) sp^2 hybrids of graphene carbon atoms connected to adjacent ones.

Also, the p orbitals near carbon atoms tie to construct a halffilled π bond. This π bond supplied energy bands and electronic features of graphene [Vaziri, 2011], [Kim, 2008]. Linking of sp^2 hybrids of graphene carbon atoms with adjacent ones is presented in Figure 2.1. Graphene synthesis ways are primarily separated under two main groups entitling as bottom-up and top-down methods as seen as in Figure. 2.2 [Bhuyan et al., 2016].

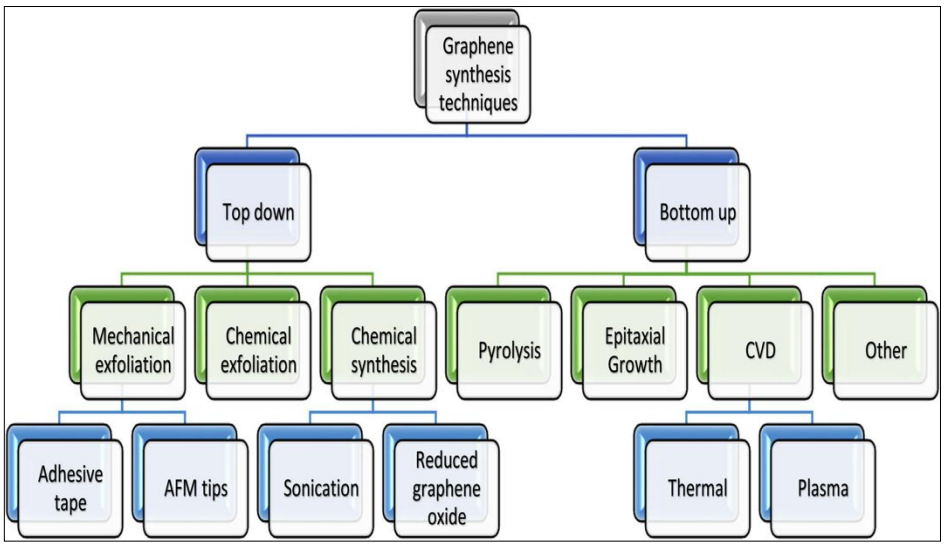

Figure 2.2: A flow chart of graphene synthesis methods.

2.1. Top-down Processes

In first approach graphene is synthesized by using graphite or graphite-oxide with the help of different methods. Basically exfoliation of carbon materials is a relatively economical and easy way to produce graphene [Lopez et al., 2016]. In top-down approach, carbon materials such as graphite, carbon nanotubes are starting substances, and they are peeled by using chemical, electrochemical or physical ways [Sridhar et al., 2010]. Main top down approaches micromechanical exfoliation, cleavage of graphite intercalated compounds (GICs), unzipping of carbon nanotubes (CNTs), arc discharge, cleavage of graphene oxide, and liquid phase exfoliation.

2.1.1. Micromechanical Exfoliation (ME) of Graphene from Graphite

Geim and Novoselov gained the Nobel Prize in 2010 by using micromechanical exfoliation including Scotch tape method. They obtained one layer graphene by cleaving of graphite. This method is significantly easy method for synthesizing of few or multi layered graphene. On the other hand, it is not suitable for large scale production.

Crystal synthesizers have applied micromechanical exfoliation for years. Lu et al. can achieve to produce few layered graphene from graphite in a controllable way and they reported that flat plates have less friction than the graphite plates [Lu et al., 2015]. Novoselov et al. presented the optical micrograph of single layer graphene using adhesive tape in Figure 2.3a [Novoselov et al., 2004]. Micromechanical exfoliation ensures graphene products with size limited, high quality layers. Number of layers can easily be determined by the means of elastic and inelastic light scattering. An eloquent and non-devastating observing of doping, deficiencies, stress, disorder, chemical alterations and borders are provided by Raman spectroscopy as seen in Figure 2.3b [Bonaccorso et al., 2012].

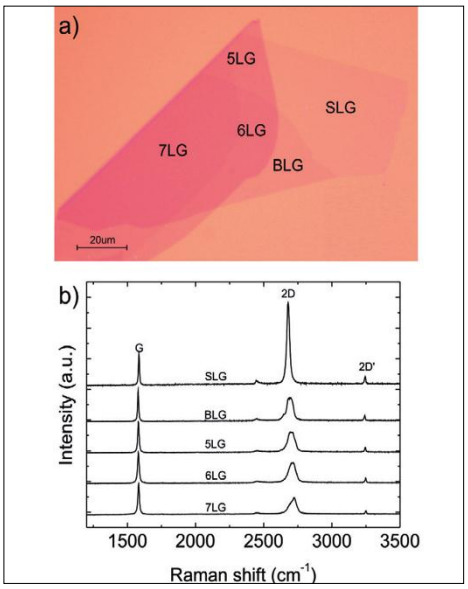

Figure 2.3: a) Optical micrograph of ME piece including of parts with different thickness. b) Calculation of the number of graphene layers by Raman spectra.

Highly oriented pyrolytic graphite (HOPG) was used for synthesis of graphene by using micromechanical cleavage by Novoselov et al. and they measure straightly 2D electronic features of graphene [Novoselov et al., 2004]. Pure monatomic 2D crystals are steady in an isolated condition. Researchers can be determined thermal, electronic and optical properties of several tens of microns sized graphene and few layered graphene pieces by carrying them to SiO_2/Si and other substrates.

Novoselov et al. proposed a detailed way that includes millimeter thick platelets of HOPG as starting carbon material and the steps such as patterning, etching, photoresist, an adhesive-tape peel-off, and an ultrasonic rinse [Novoselov et al., 2004]. Then they defined an eloquent formula for obtaining graphite by means of the process including an exfoliated HOPG surface was mechanically abraded against solid surface. This constantly remaining behind rubble of crystallites on the surface and single- and few-layered graphene can usually be found among them. Thus, the easiness of this method, a diverseness of variants have turned into advantageous, and Figure 2.4 a, b draws a formality that merely works an adhesive tape, that is chosen by plenty. This method has turned into labelling as the scotch tape method.

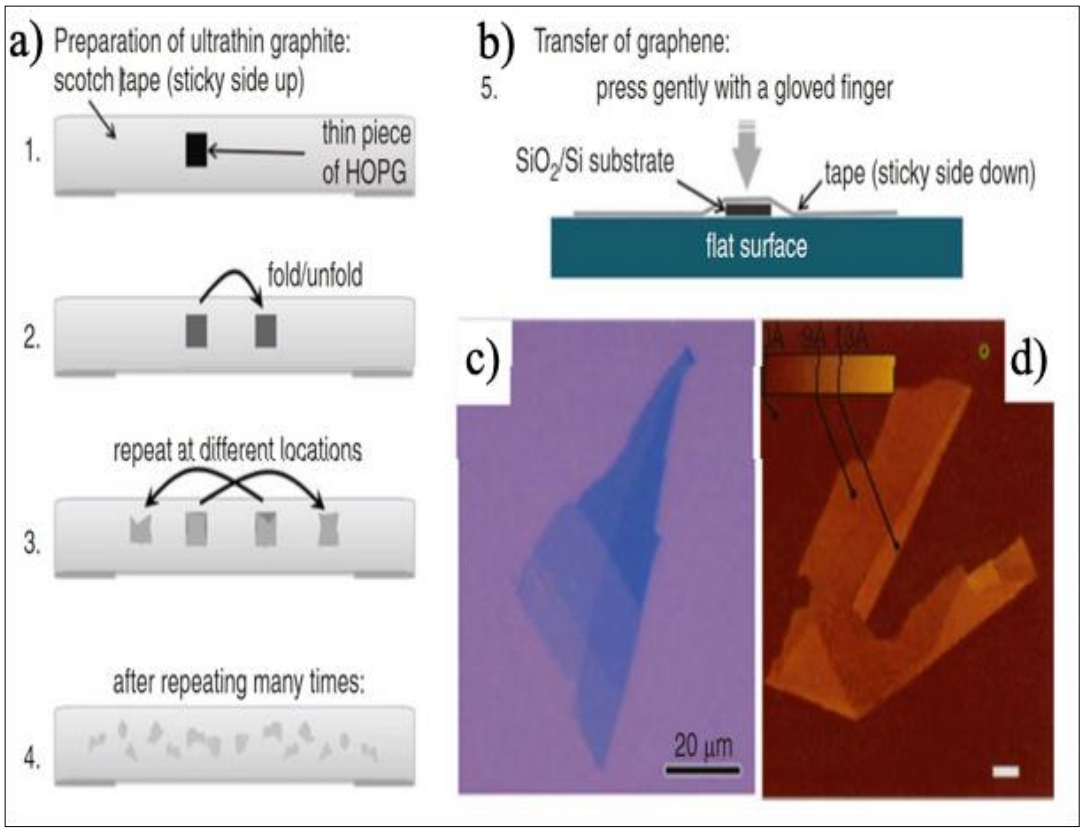

Figure 2.4: An easy way for producing single- and few-layered graphene by the micromechanical exfoliation of graphite. a) 1) Attach a very thin piece of HOPG onto a scotch tape. 2–4) Fold and unfold as shown to get ultrathin (almost invisible) flakes of graphite on the tape. b) Select an area having very thin flakes, move them onto a available substrate like SiO_2/Si. Remove the tape from the substrate. c) Typical image of a few-layer flake by optical microscope d) AFM image of graphene flakes.

Si wafer having ~300-nm-thick oxide layer can be preferred as an applied substrate. Graphene is nearly transparent, but graphene can be seen by using Si wafer oxide thickness and even using an optical microscope as seen in Figure 2.4c. Flat and folded areas of graphene layer thickness can be seen by using an atomic force microscopy (AFM) as presented its image in Figure 2.4d [Kar and Talapatra, 2012].

2.1.2. Anodic Bonding

Anodic bonding is usually chosen in the microelectronics area to bond Si wafers to glass in order to eleminate the impurities and humidity. While using this way to produce single layer graphene (SLG), graphite is used and pressed on a glass. Then, a high voltage in the order of few kVs is applied between the graphite and

metal back contact as shown in Figure 2.5b and glass is heated around 200 °C for 10 – 20 mins.

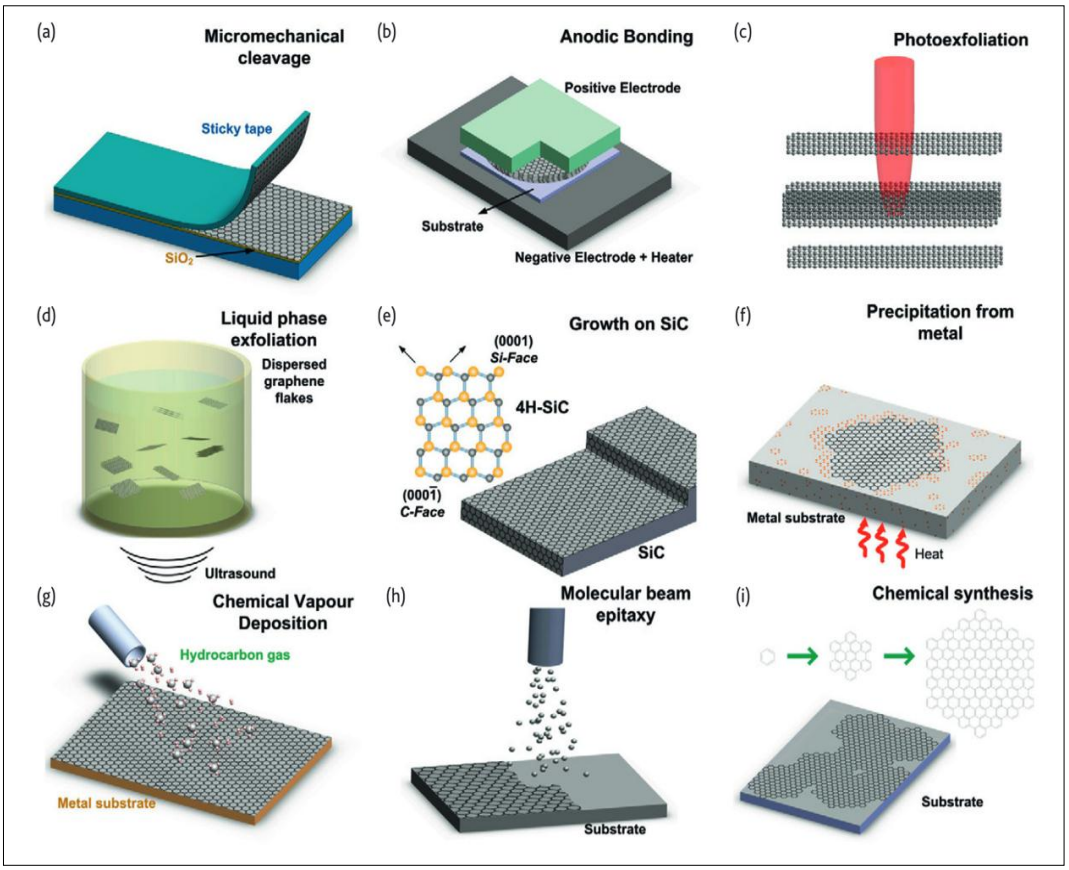

Figure 2.5: The illustration of the basic methods for graphene synthesis. (a) Micromechanical exfoliation. (b) Anodic bonding. (c) Photocleavage. (d) Liquid phase cleavage. (e) Growth on SiC. (f) Precipitation/Segregation from carbon onto metal substrate. (g) Chemical vapor deposition. (h) Molecular Beam epitaxy. (i) Chemical synthesis from benzene.

When a positive voltage is used in the top contact, a negative charge deposites in the glass face sighting the positive electrode, resulting the accumulation of Na_2O contaminations in the glass into Na^+ and O_2^- ions. Na^+ goes to the back contact and O_2^- stays at the graphite-glass interface building a high electric field. Several layers of graphite involving SLGs bond to the glass by electrostatic interaction and can be peeled off; also the number of layers and their size can differ with changing temperature and/or applied voltage. In the magnitude of millimeter in width graphene flakes can be produced by anodic bonding [Bonaccorso et al., 2012].

2.1.3. Laser Ablation

Laser ablation vanishes a material from a solid face by using laser beam. The irradiation causing the separation of whole or fragmentary layer is named as photocleavage. Graphite flakes are ablated/exfoliated by the means of laser pulses. The accurate patterning of graphene is provided by tuning the laser energy density. Dhar et al. informed that while the number of layers (N) is lowering from 7 to 1, required laser energy demand for cleavage increases. Dhar et al. explained that this process is best applied in vacuum or inert environment [Dhar et al., 2011].

2.1.4. Liquid-Phase Exfoliation (LPE)

Liquid phase cleavage is an eloquent and productive way for synthesizing of single and few layered graphene. Solvent – carbon source suspension was first sonicated for preparation of exfoliation. Prepared graphene dispersion was stabilized by used solvent. Solvent type has also importance in productivity of the graphene dispersion [Jiang et al., 2017].

Solvent settles both stability of synthesized graphene mixture and its productiveness. Tetrahydrafuran (THF) and N,N-dimethyl-formamide (DMF) are advantageous solvents to get high quality of graphene merely they are poisonous and show low efficiency. Dibasic ester (DBE) is an a nontoxic and environmental-friendly solvent and it was used for cleavage of graphite by Jiang et al. Its surface tension is 35.6 mJ/m^{-2} and solubility parameter is 9.7 [Jiang et al., 2017].

2.1.4.1. LPE of Graphene from Graphite

The concept of liquid phase cleavage is fundamentally a conjunction of the two approaches – mechanical cleavage from graphite and liquid phase media that is commonly implemented to graphene oxide (GO). Expansible graphite can be synthesized by chemical embolism of sulfuric acid and nitric acid. Liquid-phase exfoliation (LPE) has been considered as one of the most feasible approach for industrial production of graphene due to its scalability and low cost. The LPE, a new top-down method, can obtain a stable dispersion of monolayer or few-layer defect-

free graphene, which only involves the exfoliation of natural graphite via high-shear mixing or sonication [Randviir et al., 2014]. The LPE of graphite is especially critical for the manufacturing of conducting inks and the other top-down synthesis methods for electronics. Because the graphene products synthesized by LPE contain no defects and oxide groups, they are more suitable for use in the electronics industry than that are produced by other techniques.

The LPE is based on the exfoliation of graphite via the graphite intercalated compounds (GICs) way. The LPE method basically includes three subsequent processes: (1) dispersion of graphite in a solvent, (2) exfoliation, and (3) purification [Ciesielski, and Samori, 2014]. The LPE involves three different mechanisms according to the synthesis method used. The first one, known as normal force, is based on the exertion of a normal force to overcome the Van der Waals attraction while two graphite sheets are peeling. The second one, known as shear force, consists of the exertion of a lateral or shear force to promote the movement of two graphite sheets. The last one is based on the graphite fragmentation during graphite exfoliation, producing the breakage of graphite particles or sheets into smaller pieces. This last mechanism has a disadvantage that fragmentation reduces graphene lateral size thus, small-area graphene is obtained.

2.1.4.2. LPE of Graphite Oxide

LPE is an adaptable approach which can be used for graphite intercalated compound (GIC) and graphite oxide exfoliation apart from graphite [Bonaccorso, 2012]. During the observing the graphite flakes's activity, Brodie surprisingly achieved the oxidation of graphite by using fuming nitric acid and potassium chlorate ($KClO_3$) in 1859. In 1898, Staduenmaier modified Brodie's method by adding $KClO_3$ and concentrated sulphuric acid to the reaction media. Kohlschtter and Haenni examined graphite oxide flakes in 1918, and in 1948, Ruess and Vogt announced the first TEM images displaying the single GO sheets. In 1958, Hummers mixed potassium permanganate, sulphuric acid, and sodium nitrate and add to mixture to the reaction media and achieved to modified the method [Bonaccorso, 2012].

2.1.4.3. Ultrasound Energy

LPE has the advantage of the easy exfoliation of the smaller graphite pieces due to the lower Van der Waals interactions taking place between them. In LPE method, the graphite was exfoliated in an appropriate solvent to give graphene through the breakage of van der Waals bonds in presence of ultrasound energy. Ultrasound waves include the cycles for rarefaction and compression. High intensity ultrasound energy leads to high-energy chemical reactions in the solvent which contains graphite. Carbon products can be synthesized from volatile/non-volatile starting materials via sonochemistry by following mechanisms, which are illustrated in Figure 2.6 [Xu et al., 2013].

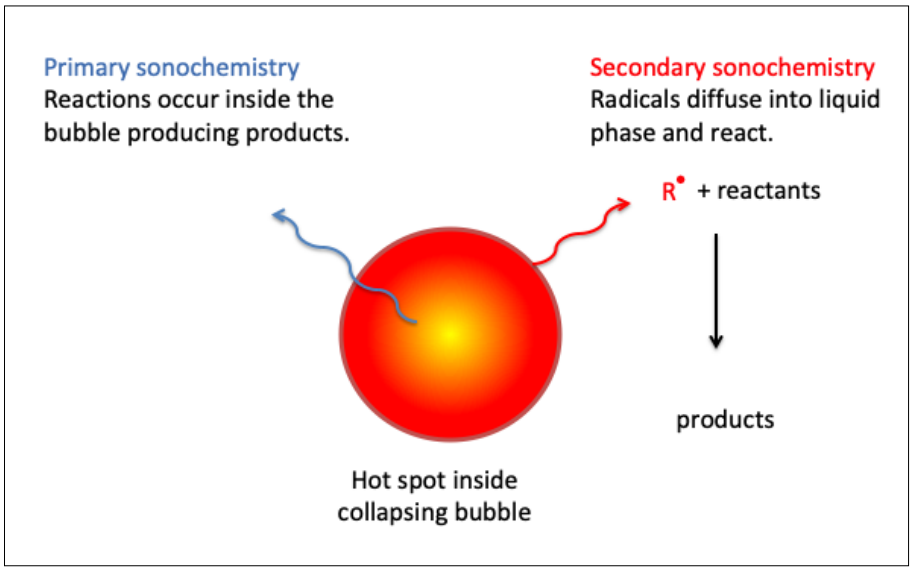

Figure 2.6: Primary and secondary sonochemistry for synthesis of nanomaterials. In order to build functional nanomaterials, first metal atoms are generated via sonolysis of weak metal-carbon bonds from volatile organometallic composites in diminishing bubble then spread in the mass liquid. Secondary sonochemical samples can be synthesized from chemically active materials such as organic radicals producing in the bubble, but then disperse in the liquid and afterwards react with solution precursor in order to synthesize a kind of nanomaterials.

The exfoliation step of the LPE can be conducted by the sonication of graphite using different solvents. There are two types of sonication: tip and bath sonication. In this study, tip sonication treatment was applied to the graphite-sovent dispersions. Chun et al. stated that epoxy/graphene shown better improvement in the mechanical

properties due to direct ultrasonication of tip sonication, that generates higher sound pressures and intensity compared to bath sonication which is indirect ultrasonication [Chun et al., 2018], [Schnyder et al., 2001]. Graphite is directly sonicated in a solvent, which should have similar surface energy to graphite, enabling a stable graphite solution [Whitener and Sheehan, 2014]. Several studies have been performed in order to find the most appropriate solvent as well as the optimum operation conditions for the sonication process [Yi and Shen, 2015], [Blake et al., 2008], [Ciesielski, and Samorì, 2014], [Hernandez et al., 2008].

2.1.5. Detonation

Lately, Schniepp and coworkers suggested a process to synthesize functionalized single graphene sheets in bulk quantities via thermal expansion of GO [Schniepp et al., 2006]. The mechanism of cleavage is mainly the expansion of CO_2 developing to the interstices between the graphene sheets for the duration of the quick heating. High temperature and powerful shock wave can be generated by a rapid decomposition of explosives. Synthesizing of graphite nanopowders by using detonation has been investigated. Wang et al. produced graphene nanosheets (GNS) by detonation including whole oxidation of natural graphite (NG), quick decomposition of detonatives, and cleavage of GO [Wang et al., 2011]. The synthesized GNS were analyzed and the cleavage mechanism of GO was suggested.

2.1.6. Chemical Synthesis

2.1.6.1. Microwave Energy

Raccichini et al. applied heat as fast as possible in order to obtain the rapid expansion of the graphene layers of graphite [Raccichini et al., 2015]. Reaction media was heated to 250 °C and had exposed to this temperature for 90 s without stirring before cooling below 30 °C. In order to distribute the microwaved graphite, -(EMIMAc) was used as an ionic liquid (IL). The mixture of graphite and IL was microwaved and sonicated.

Solvents determining stability and productivity of graphene dispersion should choose for synthesis. For example, according to Jiang et al. tetrahydrofuran (THF) and N,N-dimethyl-formamide (DMF) are suitable solvents for obtaining high quality of graphene, on the other hand they are highly toxic and show low efficiency [Jiang et al., 2017]. For this reason, dibasic ester (DBE) which is an enviromental and nontoxic solvent was chosed for cleavage of graphite. DBE's surface tension is 35.6 mJ/m^{-2} and its solubility parameter is equal to 9.7. Therefore, its surface energy is compatible with that of graphite, this ensures to decrease the mixing enthalpy. Same researchers study with ammonia in order to exfoliate the graphite layers by intercalation. Dispersion was sonicated under 40 kHz frequency and 300 W power for 1.5 hours and then obtained homogeneous dispersion was evaporated in order to remove DBE from synthesized graphene by using rotary evaporator at 50 ˚C and 180 r/min.

2.2. Bottom-up Processes

Bottom-up approach implements carbon atoms as building blocks; epitaxial growth of graphite on SiC surfaces, chemical vapor deposition are the most sophisticated ones. Mechanism of bottom-up process proceeds in two steps; C-radicals production by decomposition of a carbon precursor until the amount of solved C is saturated and the sublimation of C atoms [Akbar et al., 2015] Various organic molecules are used in this approach, such as naphthalene, phenanthrene, alfalfa plant, glucose, cellulose, etc. For example; Liu et al. used molten salt in order to synthesize the graphene from glucose using as sole reagent in bottom-up method [Liu et al., 2014].

2.2.1. Solvothermal/Pyrolysis Methods

Graphene sheets could be easily separated by pyrolization of sodium ethoxide via sonication. The dimension of synthesized graphene sheets with is up to 10 μm. The benefits of this method were being economical, easy fabrication, obtaining highly pure and functionalized graphene in low temperature.

2.2.2. Epitaxial Growth onto Silicon Carbide (SiC)

Berger et al. suggested another approach for graphene synthesis in 2004 [Berger et al., 2004]. In this procedure, graphene crystals were synthesized on the Si-terminated (0001) surface of single-crystal 6H-SiC via thermal desorption of Si. The SiC faces were first produced via oxidation or H_2 etching. The oxide was then eleminated via electron bombardment-assisted heating in ultrahigh vacuum (~10-10 Torr) to 1000 °C. The deoxidized substances were heated to 1250 °C to 1450 °C for 1–20 min. A scanning tunneling microscope (STM) image of graphene synthesized by heating SiC at 1400 °C for 8 min can be seen in Figure 2.7. This method has been finely tuned thus can controllably synthesize monolayer graphene on SiC substrates [Rollings et al., 2006].

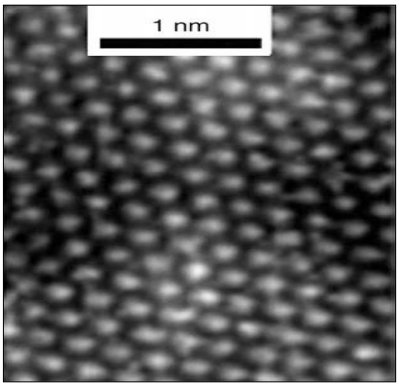

Figure 2.7: Atomically resolved STM image of a graphene sample grown on SiC(0001) at 1400 °C for 8 min.

This process for the direct synthesis of large-domain graphene on an insulating underlayer produced an important step toward accomplishing graphene-based nanoelectronics on a semiconductor-processable substrate [Kar and Talapatra, 2012].

2.2.3. Chemical Vapor Deposition (CVD)

A metal substrate is located in a flow mode furnace heating to a temperature between 750 °C and 1000 °C in the existence of a mixture of Ar and H_2 at a fixed chamber pressure P in an ordinary CVD method. Begin with stabilizing the target temperature, the flow is held for 30 - 60 min to decontaminate and make ready the

surface of the metal. The carbon source, ethylene and methane is fed to the cool end of the furnace for a length of time. After the cooling, single and multilayered graphene were found on the surface. Temperature, feed-gas concentration, chamber pressure and time are the factors controlling layer thickness and domain sizes of graphene are different for each metal. Yu et al. practised CH_4:H_2:Ar = 0.15:1:2 with a whole gas flow rate of 315 sccm [Yu et al., 2008]. For instance, the sort of graphene synthesized on Ni foils relied on the cooling rate, with multilayer graphene synthesized only when cooling rate was set to 10 °C/s. Thin layers of pre-patterned Ni could be employed to fabricated large-scale patterned growth of graphene filmes could be moved onto various substrates [Kim et al., 2009].

2.3. Characterization Techniques

As single layer graphene cannot be characterized by optical microscopes on a significant number of substrates, building a precise and economical method for characterizing the synthesized graphene is an important problem. Transmission electron microscopy (TEM), Rayleigh scattering, Atomic force microscopy (AFM), X-ray diffraction (XRD) and Raman spectroscopy are the most common identification techniques that are being used today. The structural and electrical properties of graphene were also examined with FT-IR, SEM, XPS, and 4-point probe conductivity method [Lee et al., 2010].

2.3.1. Atomic Force Microscopy (AFM) Spectroscopy

Atomic Force Microscopy (AFM) is one of the most commonly used characterization methods for graphene. It is benefited while determining of the thickness of synthesized graphene. Different size parameters can be measured by AFM. Roughness average (Ra), the most commonly preferred parameter to investigate the roughness property of graphene product, is less sensitive to big peaks and valleys, and it is calculated by measuring the surfaces height alterations. Root mean square roughness (Rq) value is the square root of the total of the squares of the particular heights and depths from the average level [Choi and Lee, 2011]. The roughness mean square (RMS) value, which gives the average height deflections of

the average level, was estimated by measuring the heights of surfaces of microscopic peaks and valleys. The number of graphene layers, N, is calculated via Eq. (2.1) by assuming the single layer graphene (SLG) thickness as 0.335 nm:

$$N = (t_{measured} - 0.4)/0.335 \tag{2.1}$$

where $t_{measured}$ is the thickness determined by AFM to exclude the increase in thickness contributed by the substrate – graphene and graphene – tip interactions. The value of 0.4 is the arbitrary magnitude (equivalent to three graphene layers assuming a 0.335 nm spacing). N can be calculated via AFM by measuring the height of the deposited graphene flakes [Cameron et al., 2016]. The height of SLG is strongly affected by the structure. For example, when SiO_2 and mica are chosen as substrates, the heights of SLG are ~1 nm and 0.4 nm, respectively [Ferrari et al., 2015].

2.3.2. Raman Spectroscopy

Raman spectroscopy is based on inelastic interactions of phonons on the sample and it is the best technique for the qualitative analysis of the graphene. Raman is able to identify the number of layers and measures the doping and quality of the flakes. Typical Raman output of graphene layers with different thicknesses was given in Figure 2.8.

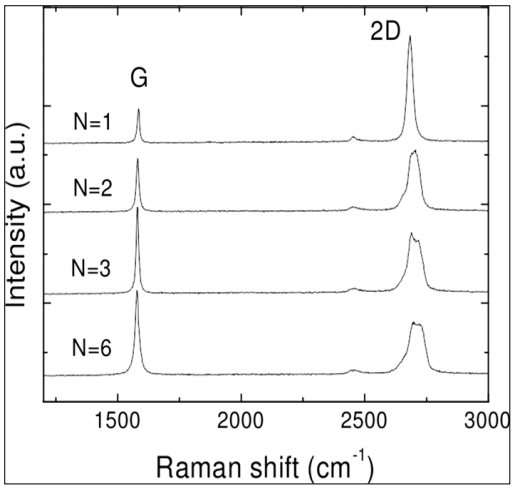

Figure 2.8: Raman output of graphene layers with different thicknesses.

2.3.3. Rayleigh Scattering

Although Rayleigh scattering is a nondetrimental, rapid and delicate method, it is not frequently used for characterization of graphene. It is a feasible method to recognize single and multi layer graphene. Its working mechanism depends on the interaction of light with substance through elastic scattering. An image contrast has a high importance and is described as distinction between the substrate and sample intensity.

2.3.4. X-Ray Diffraction (XRD)

X-ray diffraction (XRD) is a powerful technique for characterizing graphene. Typical XRD spectra of graphene includes three peaks; a sharp 002 peak at 26.3°, 101 peak at 44.6°, and 100 peak at 43.2° that can be seen in Figure 2.9. The thickness of graphene layer can determine by the intensity of the 002 peak.

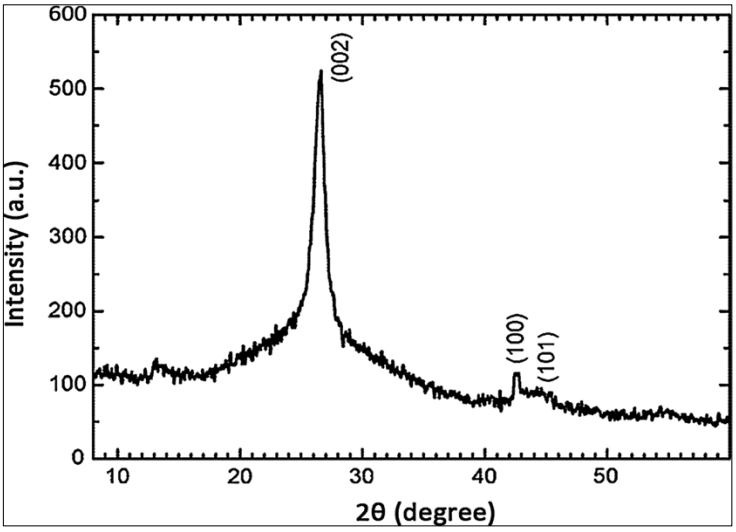

Figure 2.9: X-ray diffraction spectrum of graphene nanosheets.

2.3.5. X-ray Photoelectron Spectroscopy (XPS)

X-ray photoelectron spectroscopy (XPS) is a suitable method in order to characterize a substance's surface chemistry with extraordinary selectivity.

Elemental composition, electronical state of elements, empirical formula can be measured and also chemical states on a surface can be recognized.

The measurement procedure of XPS includes the following steps: First, X-ray irradiates the solid surface, then emitted electrons and kinetic energy on the top 10 nm are examined. Ejected electrons over a range of kinetic energies are counted and builds a photoelectron spectrum. Recorded spectrum involves peaks of atoms emitting electrons of a particular characteristic energy. Apart from hydrogen, other surface elements can be quantified and recognized by the means of the energies and intensities.

This method is a highly crucial for the surface or thin film composition studies having high importance in performance for research and industrial applications. XPS is a highly strong way to characterize graphene and its variations.

2.3.6. Low Energy Electron Diffraction (LEED)

The symmetry of graphene is usually determined by when the graphene is on the conductive substrates, but LEED cannot handle graphene transferred to SiO_2/Si substrates due to the charging effect. On the other hand, although transmission electron microscopy can produce electron diffraction on post-transferred graphene, this way is too regional [Lu et al., 2017].

Monolayer graphene on single-crystal surfaces were imaged by LEED as seen as in Figure 2.10. The presence of diffraction ring segments indicating rotational disorder of graphene can be seen in Figure 2.10.

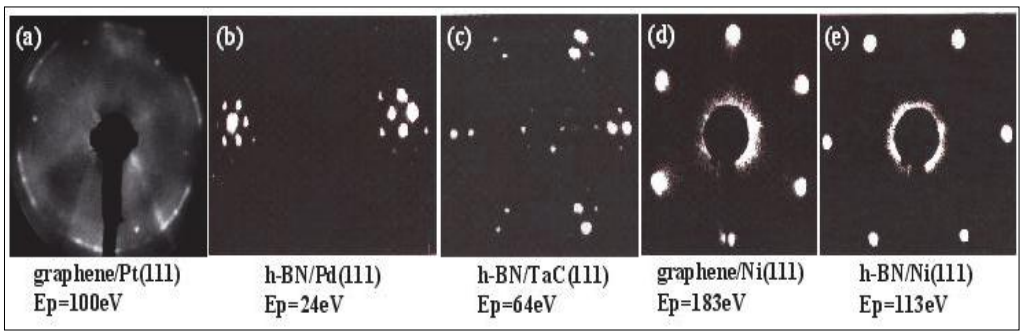

Figure 2.10: Typical LEED patterns of graphene and h-BN films on single-crystal surfaces.

3. EXPERIMENTAL STUDY

In this study, the most efficient synthesis methods and characterization techniques of graphene were used. As the scope of thesis, physical synthesis methods was studied and then graphene flakes will be identified by various characterization methods. For this aim, different types of starting carbonaceous sources such as glucose, fructose, cellulose, etc. was used. Various eutectic salt mixtures such as LiCl/KCl were used as molten state for reaction environment. Table 3.1 compares the graphene synthesis methods according to their qualities, sizes, amounts, complexities and controllabilities.

Table 3.1: Comparison of the graphene synthesis methods.

Method	Quality	Size	Amount	Complexity	Controllability
Adhesive Tape	√	x	X	√	x
Liquid phase	x	x	√	√	x
Graphite oxide	-	x	√	X	x
Epitaxial growth	x	√	X	√	√
CVD	x	√	√	√	√

As a scope of this study, molten salt solution method, microwave assisted method and ultrasound energy assisted method were used. For molten salt solution method, top down and bottom up approaches were followed. For bottom up approach, different types of polysaccharides such as arabinose, fructose, glucose, mannose, xylose, cellulose, and starch were used as a starting carbon material. As a scope of top down approach, graphite was used as a starting carbon source. For microwave assisted method and ultrasound energy assisted method, different solvents were used.

3.1. Molten Salt Solution Method

Molten salt method was examined into two main sub-categories; bottom-up and top down approaches.

3.1.1. Bottom-up Approach

For bottom-up approach in this study, a procedure was built by the help of the study which Liu et al. developed [Liu et al., 2014]. Reactor was designed and made. Reactor made of stain steel 310, temperature controller, thermocouple, heating jacket, gas flowmeter are main equipments of the study. Experimental set-up was built and completed in this work package as shown in Figure 3.1. Reactor made of stain steel 310, temperature controller, thermocouple, heating jacket, gas flowmeter, two valves are the main equipment of the study.

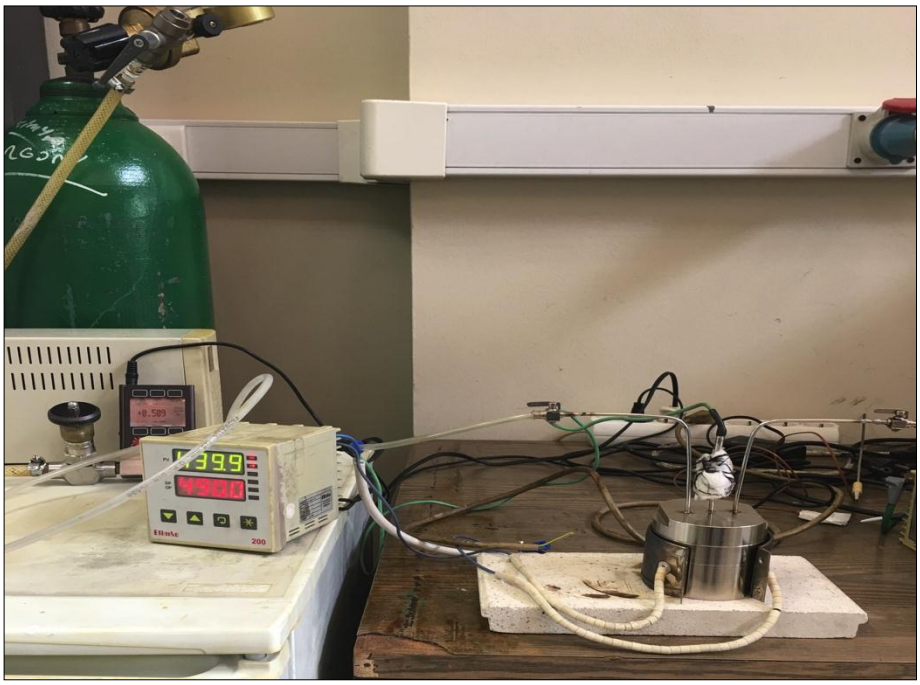

Figure 3.1: Experimental set-up.

Saccharides used as a carbon materials in our way are cheap and simply supplied. On the other hand, unlike other ways, this way is very cheap because of the use of lesser chemicals. Graphene was produced by heating different types of monosaccharides such as glucose, xylose, arabinose, fructose, and polysaccharides such as microcrystalline cellulose and starch under flowing argon or nitrogen atmosphere in a stainless steel reactor with a ceramic heater. Used chemicals were purchased from various producers. D(-)-Fructose was sustained from Merck KGaA. Graphite powder was obtained from XG Sciences, Inc. D(+)-Xylose was purchased

from Merck KGaA. DL-Arabinose was bought from Alfa Aesar. D-(+)-Mannose, 99% was obtained from Alfa Aesar. Kalium Chlorid was obtained from Riedel-de-Haën. Lithium Chloride was bought from Merck. D(+)-Glucose monohydrate was purchased from Riedel de Haën.

A saccharide was blended with eutectic composition of LiCl/KCl (45/55 by weight) with a ratio (1:10) and the powders were pestled into an agate mortar. The powder mixture was put into a ceramic crucible and then placed into the reactor. First, the system was vacuumed then purged with the Ar/Ni gas for 5 min. After starting step, the system was heated to reaction temperature 600/800 °C with 20 °C min^{-1} ramp rate and kept for 5 h. The system was eventually cooled to room temperature; meanwhile, Ar/Ni gas flow was contuined to fed to the system until the temperature decreased below 50 °C. Also, graphite was used as a starting carbon material in the same recipe for building an alternative way to Hummers' method using high amount of chemicals. The acquired block of products was crushed into particles and washed with water to remove the salts. The resulted carbon product was dried in a drying oven at 60 °C for overnight. The final carbon yield with respect to saccharide after drying of the samples was between 75 and 83% (calculated by assuming the products were 100% carbon).

X-ray diffraction (XRD) was made with a Rigaku D-Max 2200 Series equipped with Cu-Kα radiation (λ = 1.54 A°) at a scanning rate of 3° per minute. The tube voltage was 40 kV and the current was 40 mA. The intensity was determined over a 2θ angular range of 2–90°. XRD analyses of commercial graphene nanoplatelets were conducted. These commercial graphene nanoplatelets (GN) have 6-8 nm thickness and 5, 15 and 25 microns wide and are labeled as GN5, GN15 and GN25 respectively. XRD patterns of all industrial types of graphene shows a broad peak at about 2θ = 26.5° as shown in Figure 3.2.

The surface morphologies of the synthesized graphenes were observed by Philips XL 30 SFEG Scanning Electron Microscope (SEM). Raman spectra were recorded at a Renishaw inVia Raman Microscope using a 5× optical lens, a 532 nm laser diode with 50 mW as the excitation source. XPS measurements were made by Thermo Scientific K-Alpha X-ray Photoelectron Spectrometer which has energy range between 100-4000eV, source-defined analysis area from 30-400 μm, 180° double focusing hemispherical analyzer and 128-channel detector.

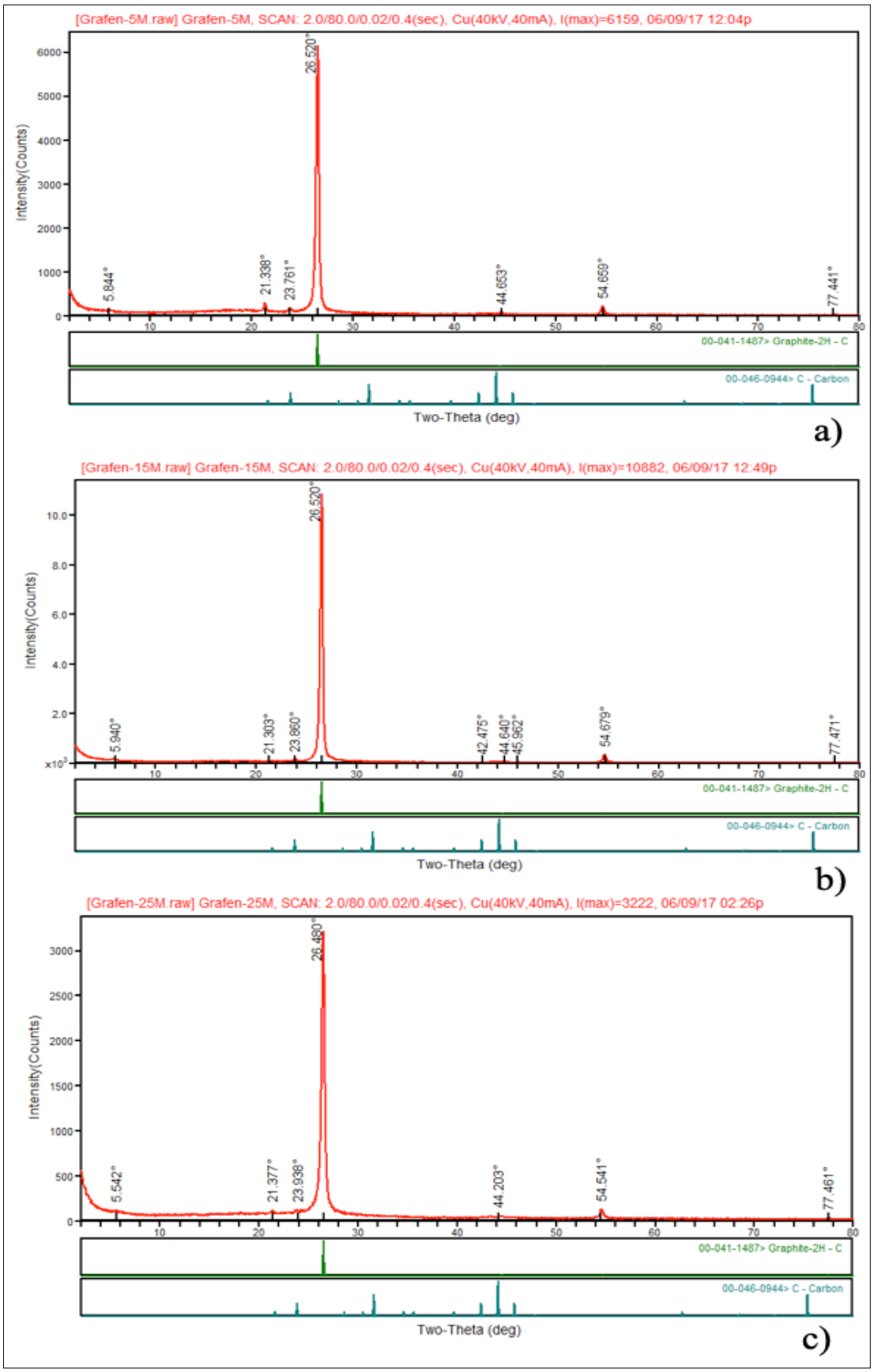

Figure 3.2: XRD spectra of industrial graphene nanoplatelets entitled as a) GN5, b) GN15, and c) GN25.

Also, electrical conductivity of the industrial graphene nanoplatelet has been measured by four-point probe analysis. Electrical conductivities of graphene products, and also commercial graphene (CG) were measured by Keithley 2400 Sourcemeter. First, graphene powders were placed in a copper cylindrical container, which has a copper cap. Then, graphene powders were compressed by a hydraulic press under 50 bar for 0.5 hours. The electrical resistivities of graphene powders were determined by 4-point probe method. A pressure was applied onto the graphene powder in copper mould during the electrical conductivity measurement by a joiner's clamp. The conductivity σ was then estimated according to $\sigma = l/AR$. After pre-experiments, 23 experiments were conducted by using saccharides in molten salt media with following the same procedure, which was described at above.

3.1.2. Top-down Approach

An environmentally friendly method developed for synthesizing graphene from graphite in molten salt mixture of LiCl/KCl, as an alternative to most traditional methods such as Hummers' method depending heavily on chemical consumption. The exfoliation of graphite in the eutectic salt mixture of LiCl/KCl, which has several advantages like simplicity, high productivity, low cost and short processing times compared to present techniques. Graphite can be converted into nanoporous carbons in an ionic molten-salt (MS) medium, and through fine-tuning of the synthesis conditions the process yields more pure graphene. For this purpose, a series of experiments at different temperatures were conducted to investigate the effect of temperature on product quality.

Natural flake graphite, grade 3061, was purchased from Asbury Graphite Mills, Inc., New Jersey. Commercial graphene was obtained from XG Sciences, Michigan, US. Other chemicals used in the experiments were of analytical grade; lithium chloride (Merck), potassium chloride (Riedel de Haen), sulphuric acid (95-97%, Merck), potassium permanganate (Merck), sodium hydroxide (Sigma Aldrich), L-ascorbic acid (Carlo Erba), hydrochloric acid (37%, J.T.Baker).

Graphene was synthesized by heating graphite under flowing argon or nitrogen atmosphere in a stainless steel reactor surrounded by a ceramic heater. The experimental set-up is presented in Figure 3.3. The system temperature was

controlled by Elimko E-200 Series digital temperature controller. The graphite was blended with the eutectic composition of LiCl/KCl (45/55 by weight) with a ratio (1:10) and the powders were mixed by squeezing in an agate mortar. The blend was then placed in a ceramic crucible locating into the reactor. First, vacuum is applied and argon/nitrogen gas was given to the system for 5 min. After the starting procedure, the system was heated to the desired temperature with 20 °C min^{-1} heating rate and kept at this temperature for 5 h. Finally, the system was cooled to room temperature by turning off the power; meanwhile, the gas flow was fed until the temperature decreased below 50 °C. The gained block of products was broken into smaller particles and then washed with an adequate amount of water in order to remove the salts. The carbon product was dried in a drying oven at 60 °C for overnight.

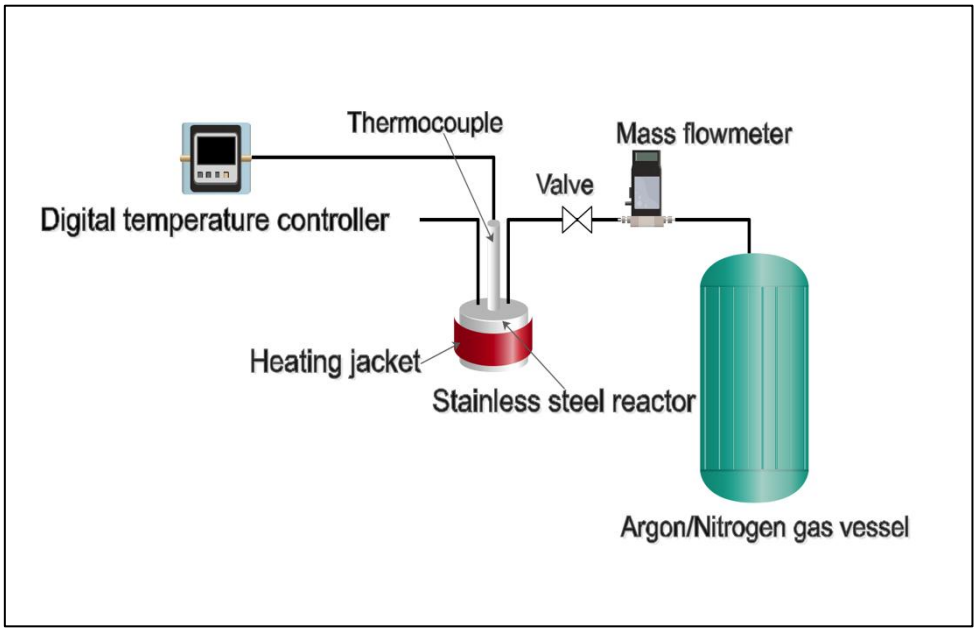

Figure 3.3: Block diagram of experimental set – up.

For comparison, reduced graphene oxide (RGO) was produced by modified Hummers method; 1 g of graphite was added to 50 mL concentrated sulphuric acid while stirring in an ice-water bath. Then, 3 g potassium permanganate was tardily added by keeping the temperature below 55 °C. Next step is stirring of the suspension at 25 °C for 25 min and sonication in an ultrasonic bath (Elmasonic S, 30H) for 5 min. After applying the stirring-sonication step for 12 times, the reaction

was satisfied by the addition of 200 mL-distilled water. An extra 2h ultrasonic treatment was applied. After adjusting the pH to 6 by the addition of 1M sodium hydroxide solution, additional sonication of the obtained suspension was carried out for 1h. 10 gL-ascorbic acid was dissolved in 100 mL distilled water, and then was tardily mixed with the exfoliated graphite oxide suspension at room temperature. The reduction was performed at 95 °C for 1h. The resultant black precipitates were easily filtered by cellulose filter paper and were washed with a 1M hydrochloric acid solution and distilled water to neutralize the pH of the suspension product. Finally, the filtrate was dried in a drying oven to get RGO powder.

X-ray diffraction (XRD) spectra were determined with a Rigaku D-Max 2200 Series equipped with Cu-Kα radiation (λ = 1.54 A°) at a scanning rate of 3° per minute. The tube voltage was 40 kV and the current was 40 mA. XPS analyses were performed by Thermo Scientific K-Alpha X-ray Photoelectron Spectrometer which has energy range between 100-4000eV, source-defined analysis area from 30-400 μm, 180° double focusing hemispherical analyzer and 128-channel detector.

Raman spectra were recorded at a Renishaw inVia Raman Microscope using a 5× optical lens, a 532 nm laser diode with 50 mW as the excitation source. UV–vis spectral analyses were done by using a Perkin Elmer Precisely Lambda 35 UV/vis Spectrometer. An ultrasonicated suspension of the product in water was prepared for the UV analyses. The ultrasonication was performed using an ultrasonic (US) generator (BANDELIN ® HD 2200 SONOPULS, 200 W, 35 kHz) equipped with a horn type probe was used to deliver pulsed ultrasound with controllable power.

The microstructures of the synthesized graphene were determined using a scanning electron microscope (FEI PHILIPS XL30 SFEG SEM) and a transmission electron microscope (Hitachi HT7800 TEM operating at 120 kV). The atomic force microscope (AFM) images for the graphene samples were taken with a Veeco NanoScope IV at contact mode.

Particle sizes of the products were determined by using Malvern Zetasizer Nano ZS Laser Particle Size Distribution Meter. Samples were prepared by dispersing in ethylene glycol and agitating at 1600 rpm by IKA® MS 1 shaker.

Electrical conductivity of the products were measured by Keithley 2400 Sourcemeter, which is given at Figure 3.4. First, powder products were put in a cylindrical copper container having a copper cap. Then, they were compressed by a hydraulic press under 50 bar for half an hour. The electrical resistivity of products

was determined by 4-point probe method. Powdered products locating in copper mould were pressed by a joiner’s clamp during the electrical resistivity measurement.

Figure 3.4: Keithley 2400 Sourcemeter.

Powdered products were put in a copper cylindrical container having a copper cap that is seen in Figure 3.5. Then, 50 bar pressure is applied onto samples by a hydraulic press for half an hour. The electrical resistivity of graphene powders was measured by 4-point probe method.

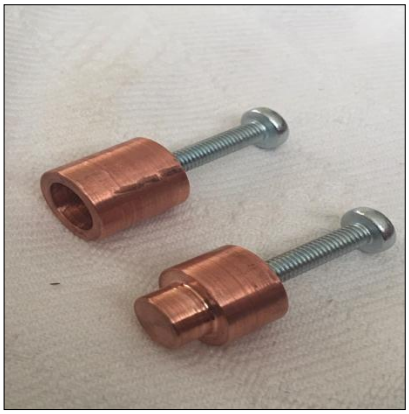

Figure 3.5: Copper cylindrical container and a copper cap.

Graphene powder in copper mould is compressed by using joiner's clamp during the electrical resistivity measurement which is seen at Figure 3.6. The electrical conductivity, σ was calculated by the following equation; $\sigma = l/AR$ where l, is the length of graphene powder in copper mould and A, is the surface area of the graphene powdered placed in copper mould.

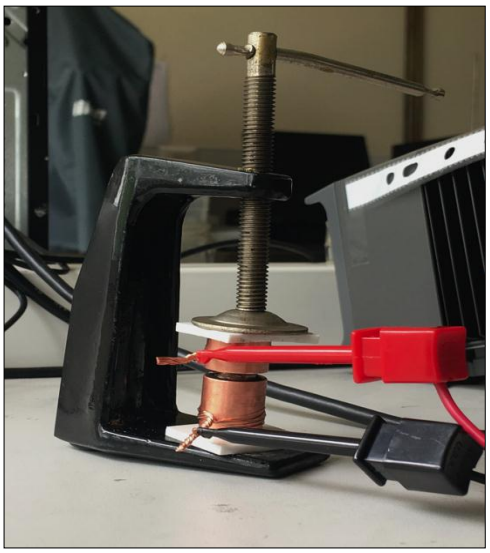

Figure 3.6: Electrical conductivity measurement set-up.

As a pretreatment for particle size distribution analyses, synthesized products were distributed in ethylene glycol by using an ultrasonic generator (model BANDELIN HD 2200 SONOPULS, 200 W, 35 kHz). Particle size distribution analyses of the products were also carried out by Malvern Zetasizer Nano ZS Laser Particle Size Distribution Meter which is given in Figure 3.7.

Figure 3.7: Malvern Zetasizer Nano ZS Laser Particle Size Distribution Meter.

3.2. Microwave Energy Method

Devices, which are converting electrical energy to electromagnetic radiation, are called as microwaves ovens. They involve a waveguide, a magnetron, a transformer, a stirrer and a control panel. Microwave energy based devices vibrate the molecules of substances by generating electromagnetic waves; occurred vibration causes friction and finally this friction reveals the heat.

Various types of process conditions were followed on previous studies. There are various kinds of chemicals taking part in literature such as hydrogen peroxide, ammonium, ammonium peroxidisulphate, sodium hydroxide, glutaric acid, tetrafluoroborate, dibasic ester, tetra ethyl ammonium (TEA), and tionin acetate salt. There are different types of pretreatments before microwave (MW) irridation such as sonication, thermal shock at high temperature, annealing, washing by water/methanol or other chemicals, filtration, and drying. A large scale of operating temperature in microwave oven are studied such as 250 °C, 200 °C, 170 °C [Janowska et al., 2010], [Al-Hazmi et al., 2015], [Matsumoto et al., 2015].

In our studies, we used graphite (natural flake graphite, grade 3061; purchased from Asbury Graphite Mills, Inc., New Jersey) as starting carbon source. Different solvents were used such as 25% ammonia solution (Merck KGaA), N,N-Dimethyl formamide (Merck KGaA), ethylene glycol (ZAG Chemicals) and ethylene diamine (Merck KGaA).

The procedure of MW treatment was summarized as following: First, natural graphite is added to ammonia, then obtained suspension was sonicated by ultrasound energy device (BANDELIN ® HD 2200 SONOPULS), under conditions 200 W, 35 kHz, mode 5 and 50% power for 30 min. Secondly, reaction was performed in Milestone Start-S model microwave oven (which is seen in Figure 3.8) for half an hour at 120 °C temperature and 1 bar pressure by applying 50, 100 or 200 Watt energy. Pressure controller was active and thermocouple was adjusted carefully.

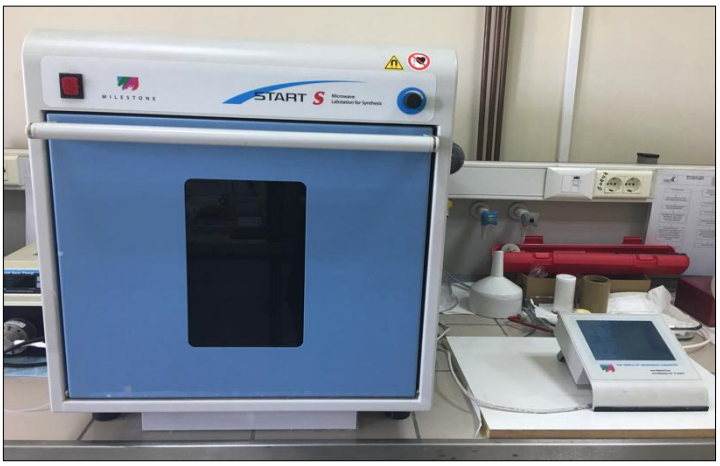

Figure 3.8: Microwave oven.

Apart from ammonia tests, additional experiments were carried out by using different chemicals such as N,N-Dimethyl formamide (DMF), ethylene glycol (EG) and ethylene diamine (ED). First, 0.1 gr natural graphite was dispersed in 50 ml DMF and obtained dispersion was sonicated for 10 min. Then, microwave irradiation was applied for 30 min under 180 °C. Electrical conductivity was determined by Keithley 2400.

Another experiment was done by using 50 ml EG and 0.1 gr graphite. First, 10 min sonication was applied to the dispersion and 60 min microwave irradiation was applied at 180 °C. Another experiment was carried out by using ED. 0.1 gr natural graphite and 50 ml ethylene diamine were mixed and sonicated by ultrasonic enery by BANDELIN ® HD 2200 SONOPULS, under 200 W, 35 kHz, mode 5 and 50% power conditions for 10 min. After that, microwave energy was applied under 180 °C and 200 W energy conditions for 30 min.

Additional microwave tests were carried out by using different types of solvents such as n-Hexadecane (n_Hexa), dimethylsulfoxide (DMSO), sodium hydroxide (NaOH), 1-octanol (OCTA), and perchloric acid (PA). The pristine graphite powder, grade 3061 was purchased from Asbury Graphite Mills, Inc., New Jersey. Other chemicals used in the experiments were of analytical grade; n-Hexadecane (Merck), dimethylsulfoxide (Merck), sodium hydroxide (J.T. Baker), 1-octanol (Merck), perchloric acid (Merck), N,N-Dimethyl formamide (Merck), Ethylene glycol (ZAG Chemicals), and ethylene diamine (Merck). 0.1 gr natural graphite and 50 ml solvent were mixed and sonicated by ultrasonic enery by BANDELIN ® HD 2200 SONOPULS, under 200 W, 35 kHz, mode 5 and 50%

power conditions for 10 min. After that, microwave energy was applied under 180 °C temperature and 200 W energy conditions for 30 min. Then, the resulting mixture was centrifuged at 1200 rpm for 30 min. First black sediment is removed, then the supernatant was vacuum-filtered by using a 0.22 μm Nylon membrane.

X-ray diffractograms were obtained with a Rigaku D-Max 2200 Series equipped with Cu-Kα radiation (λ = 1.54 A°) at a scanning rate of 3° per minute. The tube voltage was 40 kV and the current was 40 mA. The intensity was determined over a 2θ angular range of 2–90°. Electrical conductivities of synthesized products were measured by Keithley 2400 Sourcemeter. Each sample was measured by applying following procedure; first, it was placed in a copper cylindrical container which has a copper cap and it was compressed by a hydraulic press under 50 bar for half an hour. The electrical resistivities of obtained products were determined by 4-point probe method. Synthesized powder sample were compressed in copper mould with the help of a joiner's clamp during the electrical conductivity measurement. The conductivity σ was then estimated according to σ = l/AR. The obtained powder was characterized via ultraviolet–visible (UV-vis) spectroscopy. The spectrum has an operation range (UV Perkin Elmer, Lambda 35) of 200 to 700 nm.

3.3. Ultrasound Energy Method

The aim of this study is to focus on the exfoliation conditions as well as the main characteristics of the obtained graphene, such as size, yield, or graphene type (multilayer, few-layer, bilayer, or single-layer). Exfoliation conditions are directly related to the characteristics of the synthesized powder. Therefore, it is important to focus on the exfoliation parameters, including sonication and centrifugation conditions, and the solvents which assist the sonication.

Chemicals used in the study are as follows: Graphite fine powder (Extra pure, Asbury Inc., New Jersey), graphene nanoplatelets (XG Sciences, Michigan, US) Dimethyl sulfoxide - DMSO (Merck), N,N-Dimethylformamide - DMF (Merck), Perchloric acid 70-72% - PA (Merck) . DMF is a polar (hydrophilic) aprotic solvent with a high boiling point. DMF solvent molecule is polar and aprotic due to the existence of C=O and C-N groups and absence of O-H and N-H bonds, respectively. DMSO is a polar aprotic solvent that can dissolve a wide range of organic

compounds. It has also high dissolving power. The hydrogen atoms of DMSO are also quite resistant to removal in free-radical reactions, and consequently DMSO is useful as a solvent for carbon synthesis [MacGregor, 1967]. It has been shown that, the perchlorate ion is one of the best intercalating species at low acid concentrations [Beck et al., 1981]. The anion intercalation can subsequently damage the sp^2 lattice due to side reactions such as GO and carbon dioxide (CO_2) formation [Alsmeyer, and McCreery, 1992], [Kötz et al., 1993]. However, by employing concentrated PA and with a careful selection of the intercalation potential, the contribution of those reactions, and consequently the creation of defects in the carbon network, can be minimized [Zhang, and Wang, 1995], [Schnyder et al., 2001].

Graphene nanosheets were prepared by the sonication of graphite colloids in DMF, DMSO, and PA solvents without templates or surfactants. These solvents are able to vigorously exfoliate the material at the highest concentration and also they can keep the exfoliated 2D materials in a stabilized mode for the longest time. Nanolayers of graphite were exfoliated sonochemically and acted as starting material for the growth of graphene nanosheets. This graphite to graphene transformation mechanism has been driven thermodynamically by means of higher free energy of graphite than that of graphene nanosheets.

0.3 g graphite was dispersed in 50 ml solvent such as DMSO, DMF and PA. Obtained dispersions were sonicated by the means of BANDELIN ® HD 2200 SONOPULS (which is given in Figure 3.9) equipped with a VS 190 T sonotrode, 200 W, 50 % amplitude for 3 hours.

Figure 3.9: Ultrasound device.

Then, these dispersions were subjected to 60 minutes centrifugation (Elektromag, M 4812 P) at 3000 rpm to remove the unexfoliated part of graphite; after the heavier particles were settled down, supernatant parts were decanted and collected in separate vials.

UV–vis spectral measurements were acquired using a Perkin Elmer Precisely Lambda 35 UV/vis Spectrometer as seen in Figure 3.10. UV–Visible spectra (Perkin Elmer, Lambda 35) were measured from 200 to 800 nm. Samples for AFM were prepared by droppping the graphene dispersions onto glass pieces (0.7 x 0.7 mm^2) and measurements were made in contact (tapping) mode, with 10.00 μm scan size, and 20.35 Hz scan rate by using Digital Instruments Nanoscope. Samples for XRD were prepared by depositing onto glass pieces (0.7 x 0.7 mm^2) and X-ray diffraction (XRD) patterns were obtained with a Rigaku D-Max 2200 Series equipped with Cu-Kα radiation (λ = 1.54 A°) at a scanning rate of 3°per minute. The tube voltage was 40 kV and the current was 40 mA.

Figure 3.10: Perkin Elmer Lambda 35 UV/vis Spectrometer.

Also, an extensive study of the particle size distribution was carried out by an analytical technique such as dynamic light scattering (DLS) method by using Malvern Zetasizer Nano ZS Laser Particle Size Distribution Meter.

4. RESULTS & DISCUSSION

Molten salt solution method, microwave energy-assisted method and ultrasound energy-assisted method were studied and the final products were obtained. Synthesized carbon products were analyzed by applying different characterization techniques such as XRD, AFM, SEM, TEM, and XPS.

4.1. Molten Salt Solution Method Results

Two different approaches were used as a scope of molten salt solution method. First approach is called as bottom-up approach, which is based on the building of graphene from saccharides. Second approach is named as top-down approach that is based on exfoliation of graphite to graphene.

4.1.1. Bottom-up Approach

Yield results were presented at Table 4.1. Eight of them were performed at 600 °C, fifteen of them were carried out at 800 °C. 800 °C temperature range experiments were done twice in order to ensure the repeatability of the yield results.

Arabinose, xylose, mannose, starch, and fructose showed better yield values at 600 °C. Temperature did not have a significant effect on yield values for glucose and graphite. The results showed that the highest and lowest graphene yields were obtained from graphite and xylose, respectively. The reason that graphite gave highest yield is graphite has the same molecular honeycomb structure with graphene. Because the main challenge is to bond the carbon rings obtained from saccharides in order to form a smooth graphene honeycomb structure.

Among all saccharide based starting materials studied, starch was the best raw material to get the highest yield of the graphene at 600 °C. Among all saccharide based starting materials studied, glucose gave the highest graphene yields at 800 °C.

Table 4.1: List of experiments and product yields.

Exp. No	Exp. Date	Starting Carbon source	Reaction temp. (°C)	Abbreviation	Yield (w%)
1	13.07.2017	DL-Arabinose	600	GA600	77.50
2	18.07.2017	D(+)-Xylose	600	GX600	55.81
3	02.08.2017	D(+)-Glucose Monohydrate	600	GG600	72.11
4	17.08.2017	D(+)-Mannose	600	GM600	69.56
5	22.08.2017	Cellulose	600	GC600	71.62
6	24.08.2017	Starch	600	GS600	86.25
7	12.09.2017	D(-)-Fructose	600	GF600	69.06
8	13.09.2017	Graphite	600	GGr600	96.00
9	18.09.2017	DL-Arabinose	800	GA800	65.31
10	03.10.2017	D(+)-Xylose	800	GX800	18.80
11	05.10.2017	D(+)-Xylose	800	GX800	19.80
12	10.10.2017	D(+)-Glucose Monohydrate	800	GG800	63.30
13	12.10.2017	D(+)-Glucose Monohydrate	800	GG800	71.35
14	16.10.2017	Cellulose	800	GC800	34.68
15	18.10.2017	Cellulose	800	GC800	50.45
16	23.10.2017	D(+)-Mannose	800	GM800	65.81
17	24.10.2017	D(+)-Mannose	800	GM800	58.30
18	25.10.2017	D(-)-Fructose	800	GF800	51.30
19	26.10.2017	D(-)-Fructose	800	GF800	52.30
20	27.10.2017	Starch	800	GS800	59.23
21	30.10.2017	Starch	800	GS800	67.34
22	31.10.2017	Graphite	800	GGr800	96.00
23	01.11.2017	Graphite	800	GGr800	94.00

Among these results, sixteen of the results are given in Figure 4.1. Eight of them are yield values belong to 600 °C and the other eight of them are yields obtained at 800 °C. Yields at 600 °C and yields at 800 °C were compared.

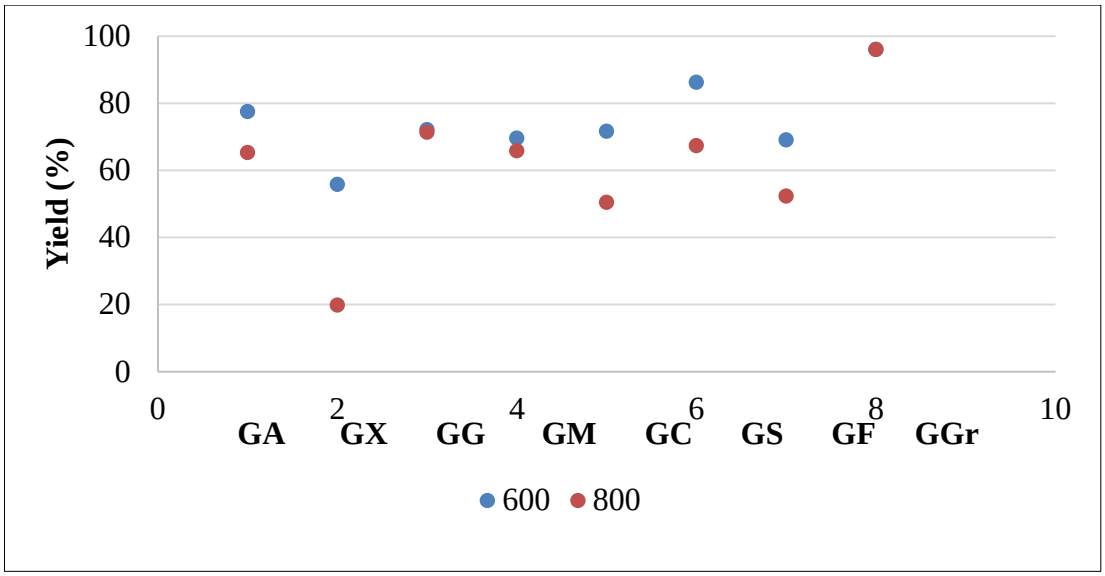

Figure 4.1: Graphene Product Yields at 600 °C and 800 °C.

According to Figure 4.1, yields at 600 °C are greater than 800 °C. Especially, the yield of GX (graphene from xylose) obtained at 600 °C is three times greater than 800 °C. Yield of GA (graphene from arabinose), GF (graphene from fructose), GS (graphene from starch), and GC (graphene from cellulose) at 600 °C are 1.2 – 1.5 fold greater than the ones belong to 800 °C.

XRD analyzes were performed to understand if the synthesized products were graphene. Layer number of synthesized products was determined by XRD analyses results. Since the layers of MS derived graphene samples are non-uniformly distributed, and therefore the samples have non-uniform thickness, Scherrer equation is insufficient [Andonovic et. al, 2015]. Ruammaitree et al. preferred to use Laue functions model including graphene thickness distribution and certain parameters as an alternative to Scherrer equation for evoluating the results of XRD analyses [Ruammaitree et al., 2013].

XRD patterns of graphene products which were obtained from different saccharide types such as xylose, arabinose, fructose, glucose, cellulose, mannose, starch and also graphite at 600 °C are shown in Figure 4.2.

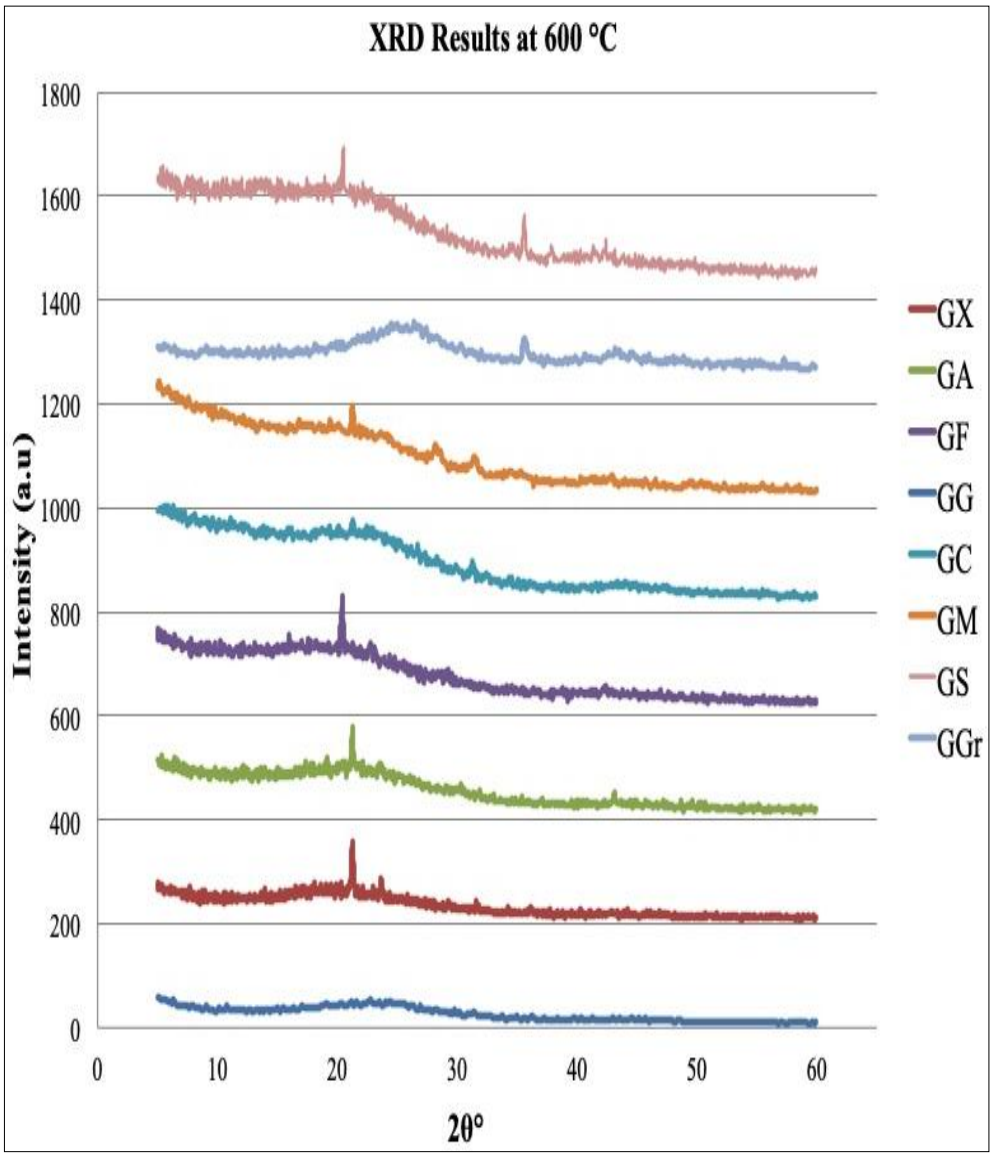

Figure 4.2: XRD patterns for graphene products at 600 °C.

According to Figure 4.2, GS, GM (graphene from mannose), GC, GF, GA, GX give peak at 2 θ = 23° around. GM, GX and GC also show peak at 2 θ = 32°. GS and GGr show peak at 36.4°. It can be understand that most of the graphene products give a weak and broad diffraction peak at 2 θ = 23°, corresponding to the diffraction of the (002) plane. In addition, GA and GS show the peak at 2 θ ~ 43°, corresponding to the (100) crystal plane of graphene.

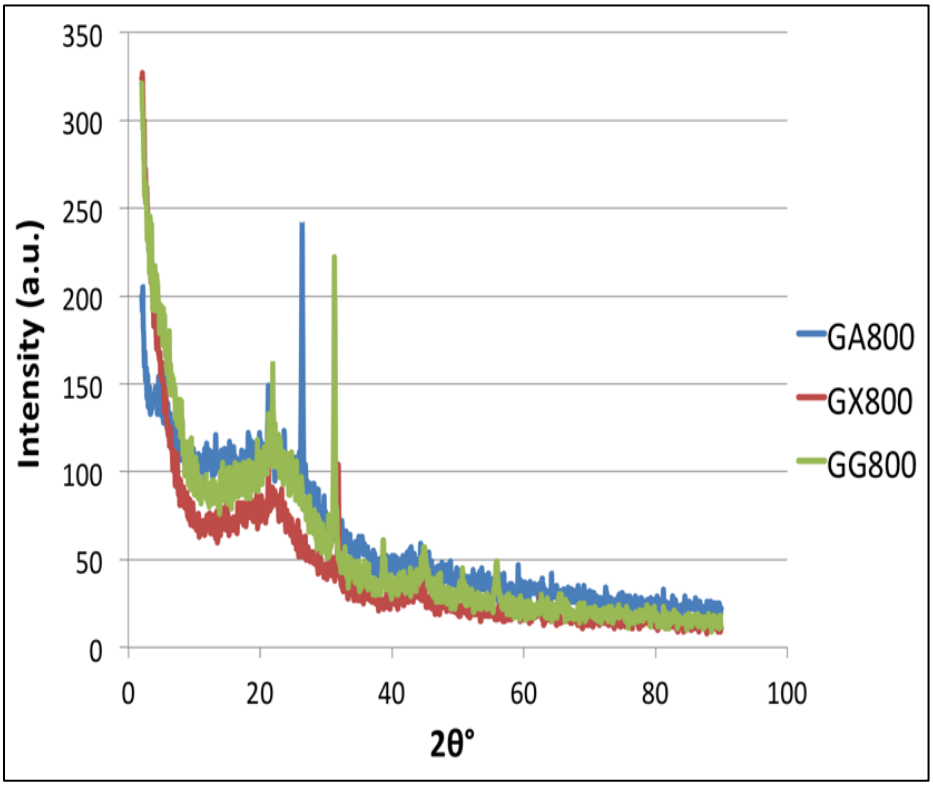

Figure 4.3: XRD patterns for graphene products at 800 °C.

As shown in Figure 4.3, XRD patterns of MS derived graphene products at 800°C exhibit a slightly increased peak at 2 θ =23° in all of the XRD patterns which are typical to graphene as expressed in previous papers [Liu et al., 2014], [Garaj et al., 2010]. Liu et al. reported that XRD pattern of graphene like structures, which are derived from glucose in molten salt media at 800 °C, show a hump at 2 θ = 23º [Liu et al., 2014], [Akbar et al., 2015]. Some of the graphenes synthesized at 800 °C show amorphous structure in their XRD patterns.

Graphene thickness can be calculated by using Scherrer's equation, which is expressed by

$$\beta(2\theta)=K\lambda/L\cos\theta \qquad (4.1)$$

where L is the thickness of crystallite, graphene thickness, K is a constant dependent on the crystallite shape (0.89), λ is the X-ray wavelength (0.15406 nm), and θ is scattering angle.

The half-width of the diffraction line β(2θ) (in rad) was taken as the experimental half-width (βexp) and was corrected for experimental broading (βinstr) according to Eq. (4.2)

$$\beta(2\theta) = (\beta exp^{\wedge 2} - \beta instr^{\wedge 2})^{\wedge (1/2)} \quad (4.2)$$

βinstr was measured experimentally with a silicon sample. From Scherrer's equation, the number of graphene layer (N_{GP}) can be calculated using the following equation (4.3) with the help of the magnitudes D_{002} (layer thickness of graphene) and d_{002} (the thickness of one graphene layer).

$$N_{GP} = D_{002}/d_{002} \quad (4.3)$$

As seen in Table 4.2, layer numbers varies between 2 - 42. The products, which have less than 1 layer, can be classified as carbonitic structures. The products, which have layers between 2 – 10, can be specified as graphene. The products that have layers more than 20, can be named as graphite.

Table 4.2: Layer numbers of MS-derived graphene products.

Code	Layer Numbers
CGr	31.22
CG	24.25
GG600	0.438
GA600	7.0354
GX600	37.809
GF600	6.832
GM600	42.52
GC600	0.736
GS600	0.371
GA800	0.558
GX800	37
GF800	3.085
GS800	8.067
GC800	5.559
GG800	1.21
GM800	7.43

The Raman spectra and the sorption curves for the MS-derived products at the two separate temperatures (600°C and 800 °C) are also given in Figure 4.4. It can be understood that graphene layers with different thicknesses show differences in G bands. As thick and disorganized amorph carbon structure turned to a single layer graphene, the I_D/I_G ratio decreases and the intensity of the 2D hump increases in the Raman spectra [Ferrari et al., 2000], [Ferrari, 2007], [Choucair et al., 2009]. I_D/I_G value of GC600 is 0.73 and, I_D/I_G of GA800 is 0.85 and I_D/I_G of GA600 is 0.77. Thus, it can be concluded that GC600 is thinner than GA600.

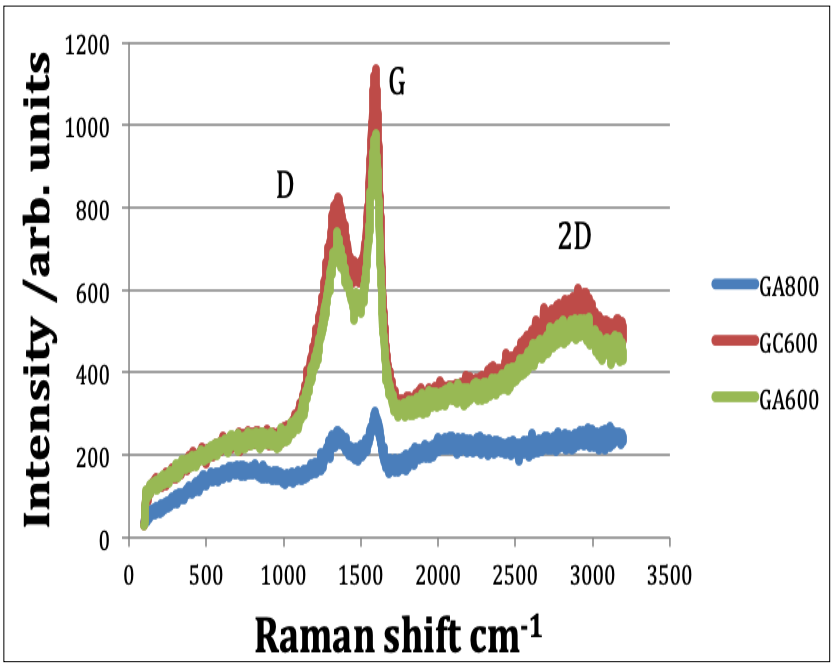

Figure 4.4: Raman spectra of GA800, GC600 and GA600 graphene products.

As it is known from existing literature, The 2D peak shapes of graphite and graphene are different. Although, the 2D peak shape changes with the number of graphene layers but if the samples have more than 10 layers of graphene, the peak becomes similar to that of graphite. Also, the 2D peak shifts to higher wavenumbers. For example, 2D peak for graphite appears at ~ 2750 cm^{-1} but for thin layer (<5 layers) of graphene the peak appears at ~ 2700 cm^{-1}.

As it is summarized in Table 4.3, I_D/I_G ratio of GA600, GC600, GA800 is respectively 0.76, 0.65 and, 0.85 which show that the graphene products have few-layers. Also, as the temperature increases, I_D/I_G ratio also increases.

Table 4.3: I_{2D}/I_G and I_D/I_G values of GA800, GC600 and GA600.

	GA800	GC600	GA600
I_{2D}/I_G	0.87	0.49	0.54
I_D/I_G	0.85	0.65	0.76

Empirically, the band position can be correlated to the number of atomic layers by Eq. (4.4):

$$wG = 1581.6 + 11/(1 + n^{1.6}) \quad (4.4)$$

where wG is the band position in wave numbers, and n is the number of layers present in the sample. For a single-layer graphene, G appears at around 1587.1 cm^{-1} and as the number of layers increases, the G band shifts downwards [Akbar et al., 2015]. In order to obtain complex numbers, this method could not be used for determining the layer number of GA800, GC600 and GA600 graphene samples.

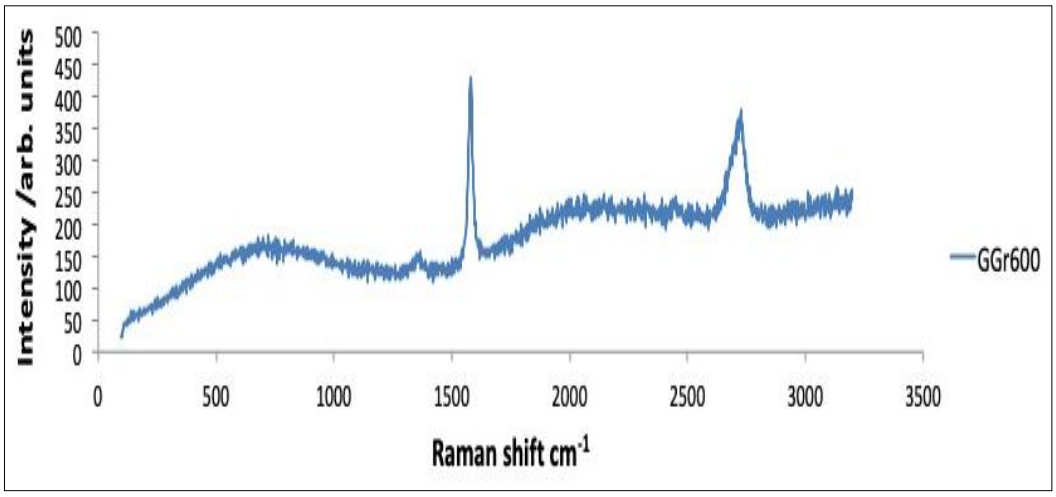

Figure 4.5: Raman spectra of graphene from graphite at 600 °C.

In the Raman spectra (Figure 4.5), temperature change results in a notable increase in the I_G/I_D ratio and the appearance of a broad 2D peak located at around 2600 cm^{-1}, thus implying the increase of the relevance of sp^2 carbon atoms at lower temperatures.

Electrical resistivities of MS-derived graphene products were measured by sourcemeter. Then, electrical conductivities were calculated via $\sigma = l/AR$ by using obtained electrical resistivity data, and these results were presented at Table 4.4.

Table 4.4: Electrical conductivities of MS-derived graphene products.

Graphene products' code	600 °C (S/m)	800 °C (S/m)
GC	0.162	2.92
GS	0.112	12.30
GA	0.224	15.87
GG	0.107	8.54
GX	0.202	5.10
GM	0.198	7.62
GF	0.199	69.38
GGr	1218.9	724.6

As it is seen at Table 4.4, GGr (graphene produced from graphite in a molten salt media) shows highest electrical conductivities among the other MS-derived graphene products that were synthesized. After GGr, GF800 has the second highest value. The electrical conductivities that are obtained at 800 °C are higher than the ones that are obtained at 600 °C. For this reason, it can be concluded that 800 °C is the optimum synthesis temperature when comparing 600 °C.

Table 4.5: Electrical conductivities of commercial graphene, commercial graphite, carbon black, and reduced graphene oxide.

Code	Expansion	Electrical conductivities (S/m)
CG	Commercial graphene	115.71
CGr	Commercial graphite	317.06
CB	Carbon black (Vulcan XC-67)	341.44
RGO	Reduced graphene oxide	195.39

On the other hand, electrical conductivities of commercial graphene (CG), commercial graphite (CGr), carbon black (CB), and reduced graphene oxide which was synthesized by Hummers method (RGO) were measured by 4-point probe

method and compared. According to Table 4.5, CB shows the highest electrical conductivity among the others. Furthermore, by comparing Tables 4.4 and 4.5, it is seen that the electrical conductivity of GGr is very much higher than the electrical conductivity of CG and RGO.

According to the particle size distribution analyses results of MS-derived graphene products; GA800, GGr600, GGr800, and CGr have 911.2, 3108, 943.4, and 915.4 nm particle size respectively.

The surface morphology of the synthesized graphenes were observed by Philips XL 30 SFEG Scanning Electron Microscope (SEM). Figure 4.6 shows the overall morphologies of graphene from fructose synthesized at 800 °C (GF800), graphene from mannose synthesized at 800 °C (GM800), GS600, GX600, GF600, and GM600 that were obtained by SEM.

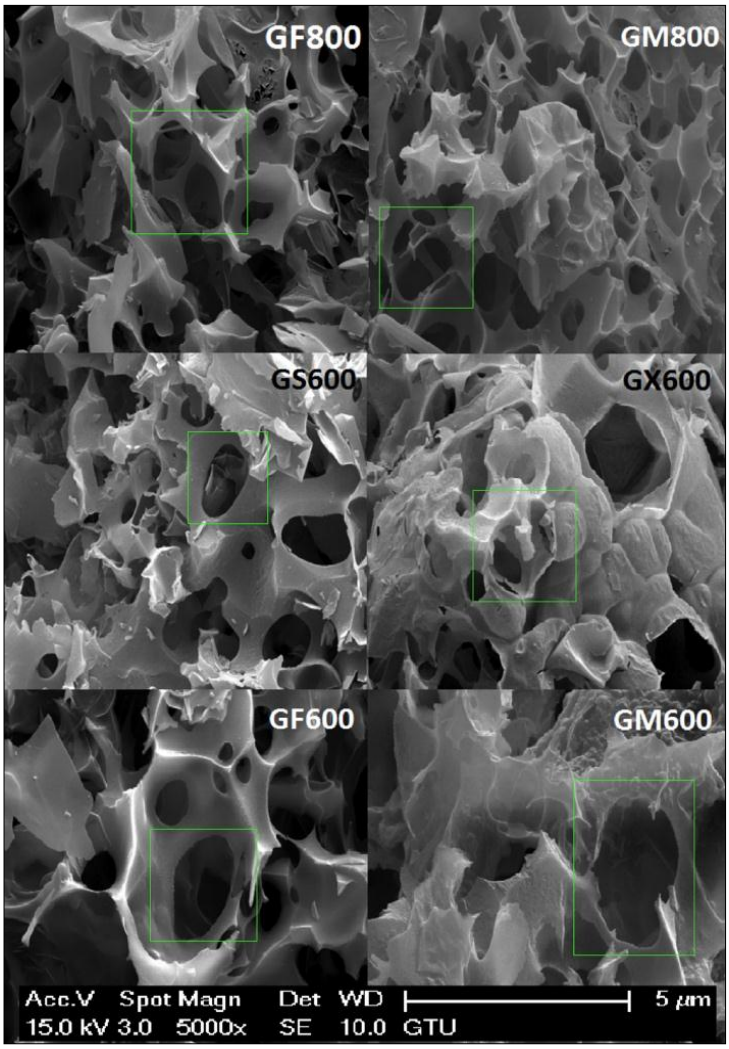

Figure 4.6: SEM images of GF800, GM800, GS600, GX600, GF600, GM600.

The selected images for graphene-like structures observed in small amount in each temperature. These graphene-like structures (highlighted by the green boxes) are produced when saccharide to salt ratio equals to 1/10. As it can be seen in Figure 4.6, these graphene like structures have hexagonal shape and edges.

The presence of different atomic bonds and remaining functional groups can be quantified by means of XPS. The results are presented in Figure 4.7 and Table 4.6 & 4.7.

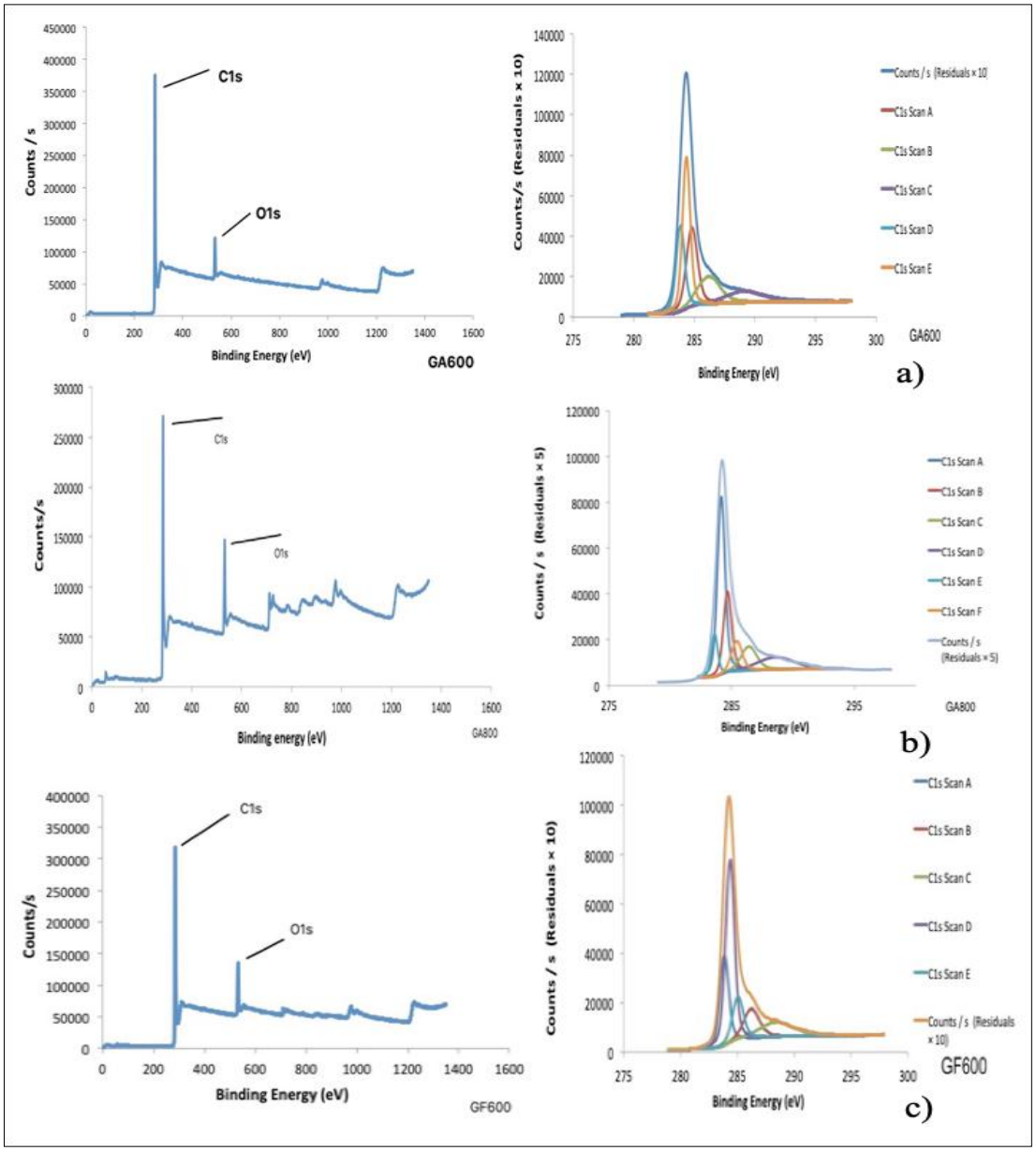

Figure 4.7: Survey-scanned XPS spectra and fine-scanned spectra of a) GA600 b) GA800 and c) GF600.

XPS spectrum of GA600 contains five peaks at 284.79, 286.18, 289.11, 283.85, and 284.33 eV, corresponding to the C-C, C-O-C, O-C=O, C=C and C=C bonds respectively. XPS spectrum of GA800 contains six peaks at 284.16, 284.68, 286.38, 288.58, 283.85, 283.6 and 285.4 eV, corresponding to the C=C, C-C, C-O-C, O-C=O, C=C and C-C bonds. XPS spectrum of GF600 contains five peaks at 283.85, 286.23, 288.45, 284.34 and 285.03 eV, corresponding to the C=C, C-O-C, O-C=O, C=C, and C-C bonds. These results are compatible with the previous studies [Liu et al., 2014], [Gao et al., 2016].

Table 4.6: Contribution from differently bonded carbons extracted through peak de-convolution for C1s region for GA600, GA800 and GF800.

Bond structure	Binding Energy (eV)	Atomic (%)
	GA600	
C-C	284.79	23.05
C-O-C	286.18	16.08
O-C=O	289.11	10.73
C=C	283.85	19.14
C=C	284.33	30.89
C-C	n/a	n/a
	GA800	
C=C	284.16	39.83
C-C	284.68	19.13
C-O-C	286.38	10.93
O-C=O	288.58	12.71
C=C	283.6	8.24
C-C	285.4	9.16
	GF600	
C=C	283.85	20.6
C-O-C	286.23	12.17
O-C=O	288.45	12.95
C=C	284.34	41.62
C-C	285.03	12.65
C-C	n/a	n/a

While sp^3 carbon (C-C) is included in GA600 as 23.05% atomic ratio, it is identified in GA800 as 25.29% and in GF600 as 12.65%. The sp^2 carbon structure (C=C) is included in GA600 as 50.03%, in GA800 as 48.07% and in GF600 as 62.22%. C-O-C structure is determined in GA600 as 16.18%, in GA800 as 10.93%, and in GF600 as 12.17%. O-C=O structure is detected in GA600 as 10.73%, in

GA800 as 12.71% and in GF600 as 12.95%. When the carbon ratio values of the samples are compared, it is understood that GA800 has the highest carbon content with 76.36%. It is followed by GF600 with 74.87% and GA600 with 73.08%.

C1s and O1s regions' atomic ratio values for GA600, GA800 and GF800 are given in Table 4.7. According to these results, it is understood that GA600 has the highest carbon content with 92.22%, and it is followed by GF600 with 88.37%, and GA800 with 83.01%. As a result, it can be concluded that the carbon content of GA slightly decreases by temperature.

Table 4.7: C1s and O1 regions' atomic ratio values for GA600, GA800 and GF800.

	GA600	GA800	GF800
C1s	92.22	83.01	88.37
O1s	7.78	13.65	10.8
Fe2p	n/a	2.19	0.83
N1s	n/a	1.14	n/a

4.1.2. Top-down Approach

As a scope of this method, graphite was used as carbon source and starting material for synthesizing of graphene in molten salt medium. The effect of temperature on product quality was investigated at four temperatures; 500°C, 600 °C, 700 °C and 800 °C. XRD results are summarized in Figure 4.8a; as seen, all of synthesized graphene products gave 2θ°=26.5° peak which is characteristic for graphene [Wazir and Kundi, 2016]. Furthermore, as the temperature increases, the intensity of the 26.5° peak is rising up, in addition this means graphite converts increasingly to the graphene. It can be said that a gradual transition from graphite to graphene was observed due to this decrease in intensity of 2θ° = 26.5°. When previous literature studies are examined, it can be understood that graphite gives a higher intensity peak, while peak intensities of graphene products are lower [Liu et al., 2012], [Liu et al., 2014]. As a result, it can be concluded that gradual formation of graphene was observed in final products.

Structural analyses of graphene products were performed using XRD. Graphene thickness can be calculated by using Scherrer's equation, which is expressed by $D_{002}= K\lambda/B\cos\theta$, where D_{002} is the thickness of crystallite, K is a

constant dependent on the crystallite shape (0.89), λ is the X-ray wavelength, and B is the full width at half maximum (FWHM), and θ is scattering angle. From Scherrer's equation, the number of graphene layers (N_{GP}) can be calculated using the following equation: $N_{GP} = D_{002}/d_{002}$ [Adel et al., 2016].

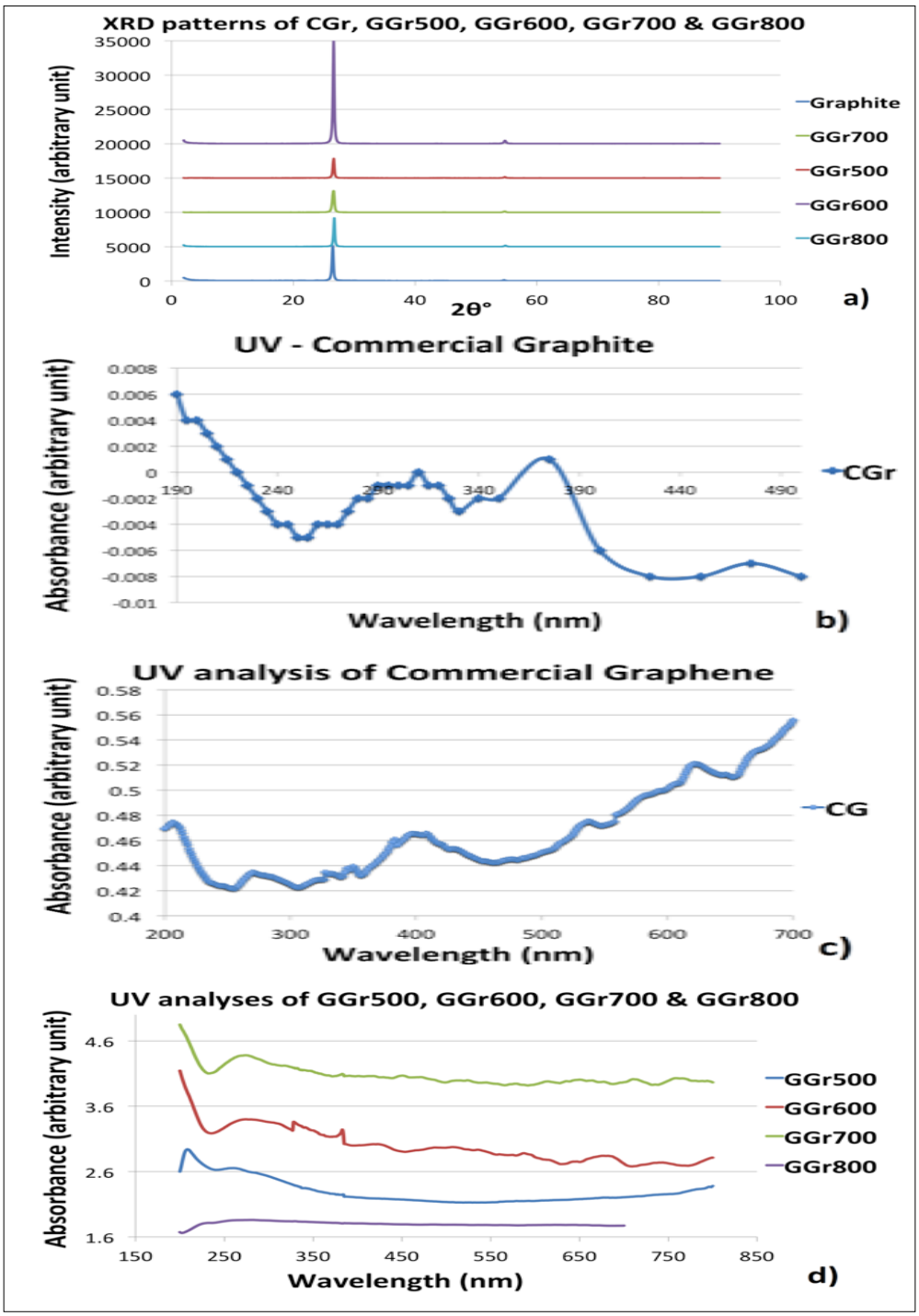

Figure 4.8: a) XRD patterns of CGr, GGr500, GGr600, GGr700 & GGr800 b) UV absorbance peaks of commercial graphite and c) graphene d) UV analyses of obtained graphene products from graphite at different temperatures.

The UV-vis spectrum of the CGr is given Figure 4.8b. According to the obtained spectrum, it gave absorbance peaks around 200 nm and 300 nm. As the previous studies declared that, UV absorbance peaks of graphite are seen at around 200 nm and 280 nm [Uran, 2017], [Wang, 2017]. Thus, these values are compatible with previous literature data. The UV spectrum of the CG is given in Figure 4.8c. According to the obtained spectrum, it gave absorbance peaks around at 200 and 270 nm wavelengths. These values are consistent with the values the study which is presented by previous studies [Wazir, and Kundi, 2016]. The UV spectrum of GGr500, GGr600, GGr700 and GGr800, which is seen in Figure 4.8d, peaked around 275-285 nm. These values are in the same line with the previous references [Wang et al., 2017], [Johra et al., 2014], [Thema et al., 2013].

The particle size analyses results are shown in Figure 4.9. The particle diameters of GGr500, GGr600, GGr700, and GGr800 are 2660, 4205, 3017, and 3459 nm, respectively. When the reaction temperature increases, the particle diameter of the synthesized graphene becomes greater. Botas et al. studied the effect of temperature on the extent of the exfoliation and the reduction of GO. They observed that when they studied at higher temperatures, the crystal size of graphene became closer to that of the graphite crystal [Botas et al., 2013].

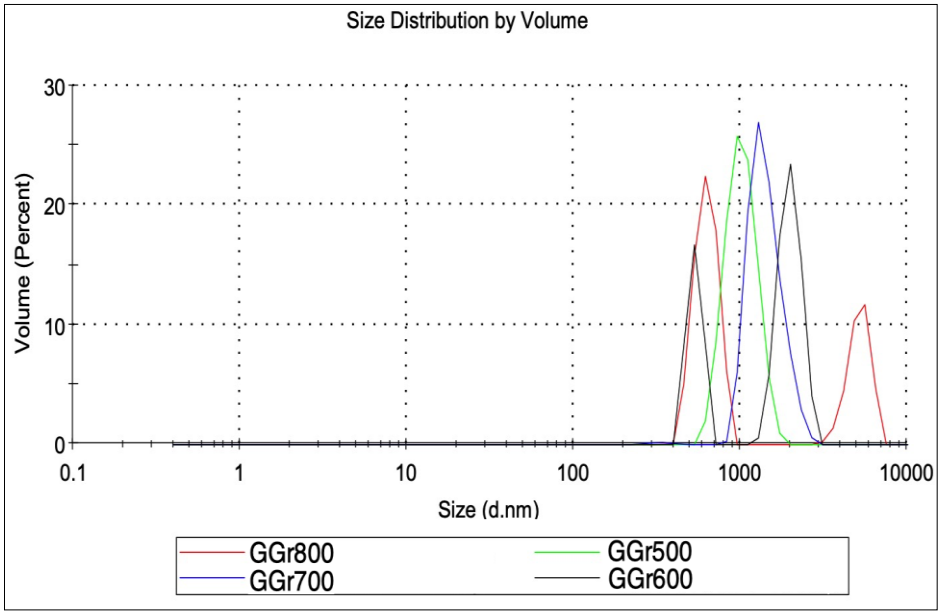

Figure 4.9: Particle size distribution (DLS) analyses of graphene products.

The conductivity values (σ) were estimated according to σ = l/AR. In this equation, R is the electrical resistance of the material, l is the length of the piece of material, and A is the cross-sectional area of the specimen. The results are summarized in Table 4.8.

Table 4.8: Particle size values of synthesized graphene samples and commercial products.

Code	Particle size (nm)	Electrical conductivities (S/m)
CG	2402	115
RGO	738	195
CGr	4180	317
GGr500	2660	1070
GGr600	4205	1219
GGr700	3017	803
GGr800	3459	724

As seen in Table 4.8, electrical conductivity of GGr is higher than electrical conductivities of CG and RGO. Thus, molten salt method created a great impact on conductivity values. The graphene product show a maximum conductivity at 600 °C. When the temperatures increase further to 800 °C, conductivity values decrease from the 1219 to 724 S/m, the particle diameters of the synthesized graphene products increase.

Figure 4.10 shows the typical Raman spectra of the CG, RGO, GGr with different temperatures. The Raman spectrums consist of D, G, and 2D bands located at 1345, 1576, and 2659 cm^{-1}, respectively. For RGO, GGr500, CG, the D band becomes stronger and broader because of the higher level of disorder of the graphene layers, as shown in Figure 4.10.

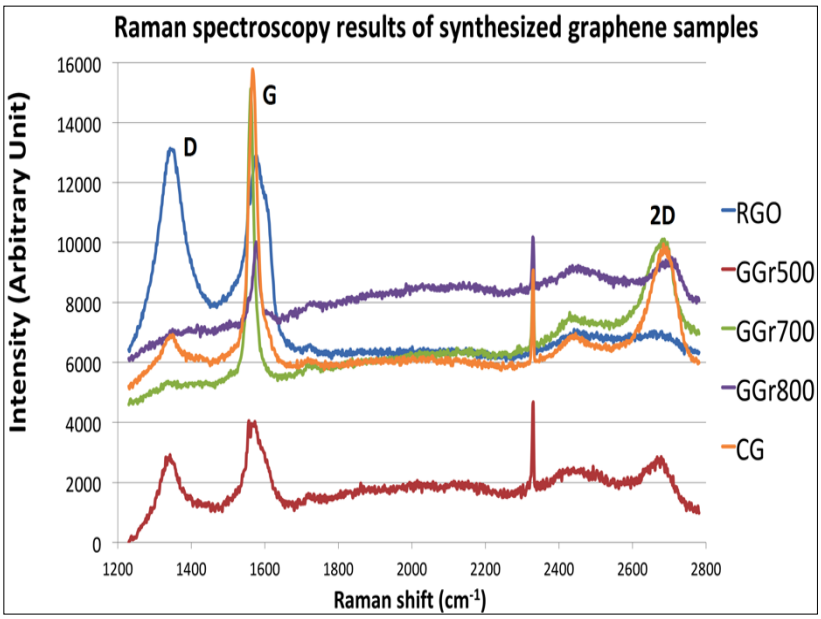

Figure 4.10: Raman spectra of RGO, CG, GGr500, GGr700 and GGr800.

GGr700 and GGr800 show no peaks at the D band, which indicates the formation of well-ordered pristine single-layer graphene without a disordered structure [Dresselhaus et al., 2010], [Ferrari et al., 2006], [Malard et al., 2009]. On the other hand, CG showed a reduced D band compared to the G band ($I_D/I_G > 1/3$), indicating that far fewer defects and functional groups were present in CG. Also, synthesized GGr700, GGr800 samples have smaller D band that indicating good quality and ordered graphene structure. The most prominent features in the Raman spectra of monolayer graphene are the so-called G band appearing at 1582 cm^{-1}. The G band is associated with the doubly degenerate (in-plane transverse acoustic-iTO and longitudinal optic-LO) phonon mode (E2g symmetry) at the Brillouin zone center (Γ point). In fact, the G-band is the only band coming from a normal first order Raman scattering process in graphene [Jorio et al., 2011]. Therefore, it can be understood that GGr700 has the highest G band and includes mostly sp^2 carbon content systems. In addition, there is a peak locating at 2450 cm^{-1}.

As seen in Table 4.9, graphene layer number of graphite is calculated as 10, while layer number of the CG is determined as 2. In the case of products obtained in this study, this number decreases to between 2 - 4 when graphite is converted to the graphene. Therefore, it can be concluded that most of the synthesized graphene samples include 2 layers in average. This value is compatible with CG's layer number.

Table 4.9: Layer numbers of synthesized graphene samples and commercial products.

Code	Expansion	Layer Numbers from Raman results
CG	Commercial graphene	2
CGr	Commercial graphite	10
GGr500	graphene from graphite in a molten salt media at 500° C	2
GGr600	graphene from graphite in a molten salt media at 600° C	4
GGr700	graphene from graphite in a molten salt media at 700° C	2
GGr800	graphene from graphite in a molten salt media at 800° C	3

In the Raman spectra (Figure 4.10), chemical change of graphite to graphene results in a notable decrease in the I_D/I_G ratio (Table 4.10) and the appearance of a broad 2D peak located at around 2600 cm^{-1}, thus implying the increase of the relevance of sp^2 carbon atoms at higher heating temperatures.

Table 4.10: I_D/I_G ratio of synthesized graphene and commercial products.

Sample name	I_D/I_G
GGr500	0.7389
GGr600	0.3179
GGr700	0.1109
GGr800	0.3263
CG	0.1762
RGO	1.0407

According to these results, while the temperature rises from 500°C to 700 °C, I_D/I_G ratio decreases. I_D/I_G ratio of CG is 0.1762 and I_D/I_G ratio of RGO is 1.0407. The intensity ratio (I_D/I_G) is about 0.6 for the few layers and 0.4 for single layer one,

which is much less than most chemical reduction reports [Galindo et al., 2014]. According to I_D/I_G values; GGr600, GGr700 and GGr800 have single layer, GGr500 has few layers, and RGO has multi layers. Therefore, it can be concluded that the reaction temperature between 600°C to 800 °C has positive effect on the quality of graphene product.

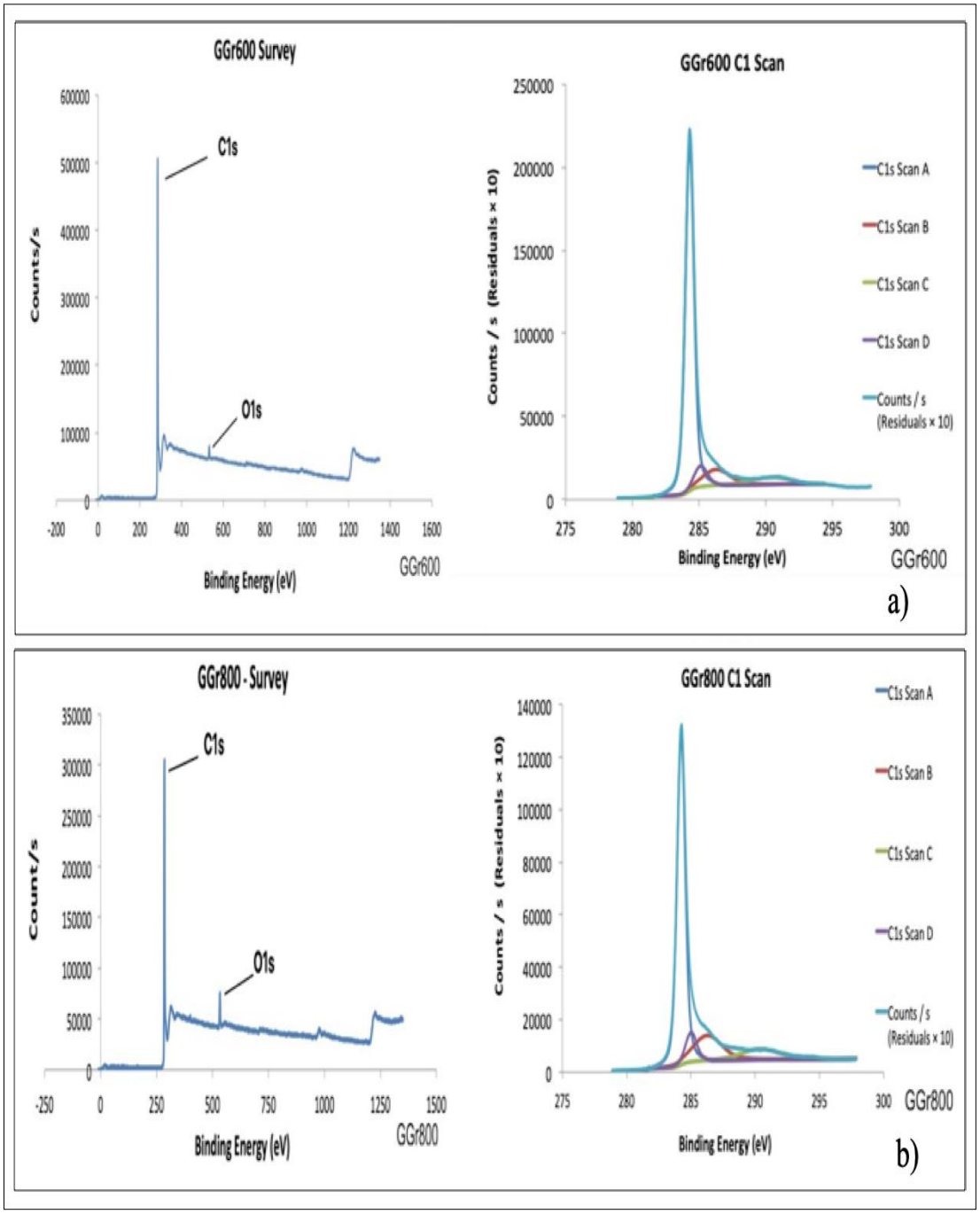

Figure 4.11: Survey-scanned XPS spectra and fine-scanned spectra of a) GGr600 and b) GGr800.

The presence of different bonded carbon atoms and remaining functional groups can be quantified with X-ray photoelectron spectroscopy (XPS; Figure 4.11, Table 4.11, Table 4.12). XPS spectrum of GGr600 contains four peaks at 284.3, 286.26, 290.34, and 285.11 eV, corresponding to the C=C, C-O-C, O-C=O, and C=C bonds. XPS spectrum of GGr800 contains four peaks at 284.24, 286.28, 290.37, and 285.02 eV, corresponding to the C=C, C-O-C, O-C=O, and C-C bonds. These results are compatible with and supported by the previous studies [Liu et al., 2014], [Gurunlu and Bayramoglu, 2019], [Johra et al., 2014], [Gao et al., 2016].

Table 4.11: Contribution from differently bonded carbons extracted through peak de-convolution for C1s region for GGr600, and GGr800.

	GGr600		GGr800	
Bond Structure	Binding energy peaks (eV)	Atomic %	Binding energy peaks (eV)	Atomic %
C=C	284.3	79.86	284.24	64.56
C-O-C	286.26	10.93	286.28	17.53
O-C=O	290.34	7.13	290.37	9.82
C-C	285.11	7. 08	285.02	8.09

The sp^2 carbon structure (C=C) is included in GGr600 as 79.86%, in GGr800 as 64.56%. C-O-C structure is determined in GGr600 as 10.93%, and in GGr800 as 17.53%. O-C=O structure is detected in GGr600 as 7.13%, and in GGr800 as 9.82. While sp^3 carbon (C-C) is included in GGr600 as 7.08% atomic ratio, and it is identified in GGr800 as 8.09%. When the carbon ratio values of the samples are compared, it is understood that GGr600 has the highest carbon content with 86.94%.

On the other hand, the carbon content of GGr600 is 72.65% C1s and O1s regions' atomic ratio values for GGr600, and GGr800 are given in Table 4.11. Although it is expected that the graphitic carbon content is higher at high carbonization temperatures, the oxygen derivative from the post-reaction processes at 800 °C may interact with the carbon in the environment, increasing the percentage of functional groups in the final product and causing the graphitic carbon percentage to

decrease. C1s and O1s regions' atomic ratio values for GGr600, and GGr800 are given in Table 4.12.

Table 4.12: C1s and O1 regions' atomic ratio values and peak for GGr600, and GGr800.

	GGr600		GGr800	
	Peak Binding energy (eV)	Atomic %	Peak Binding energy (eV)	Atomic %
C1s	284.8	97.9	284.8	93.81
O1s	532.02	2.1	532.65	5.45
N1s	n/a	n/a	400.26	0.74

According to these results, it is understood that GGr600 has the highest carbon content with 97.9%, and it is followed by GGr800 with 93.81%. As a result, it can be concluded that the carbon content of GGr slightly decreases by temperature. Oxygen content was most likely formed during the post-synthesis treatments such as washing with water to remove molten salt from the reaction output and stored by physical or chemical adsorption. These processes also lead to some observed functionalities, despite the fact that the samples have been dried in vacuum before measurement.

The SEM images of graphene products are given in Figure 4.12. SEM image of GGr600 showing sheet-like structures; flakes, edges and layers are clearly seen. GGr500, GGr700 and GGr800 include the overlapping layers of graphene flakes with arbitrary shapes and random in-plane orientation. These chevron-fold structures and flakes highlight the graphene-like formations [Liu et al., 2014], [Gao et al., 2016].

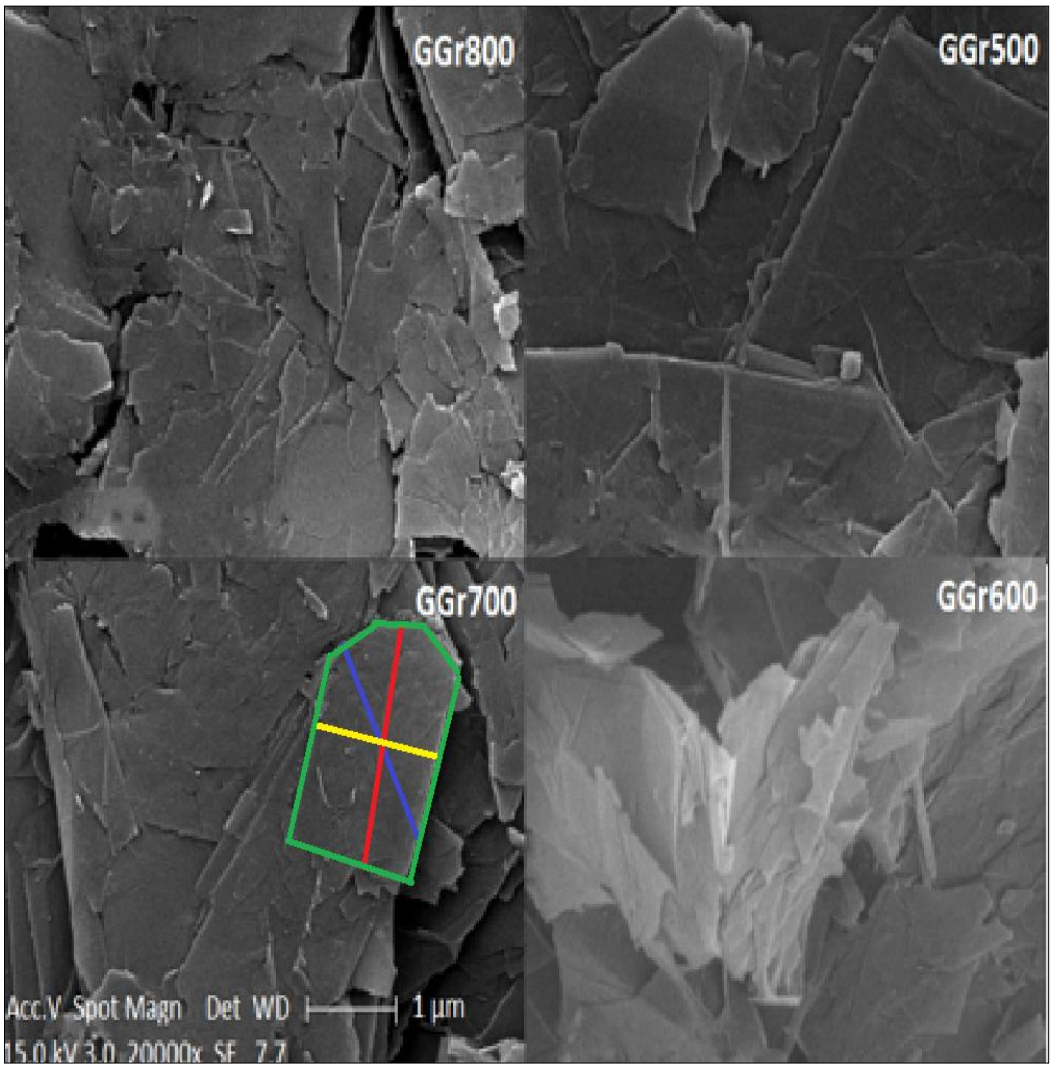

Figure 4.12: SEM images of graphene products.

These flakes have with different size and shape. Edges and intersecting lines of a flake were drawn, and the intersecting lines were used for determining the average flake size. The average size of flakes observed in SEM images was calculated as 2 µm by using Eq. (4.5) which was derived by a previous paper [Malekpour et al., 2014]:

$$L = (L_{Blue} + L_{Red} + L_{Yellow})/3 \quad (4.5)$$

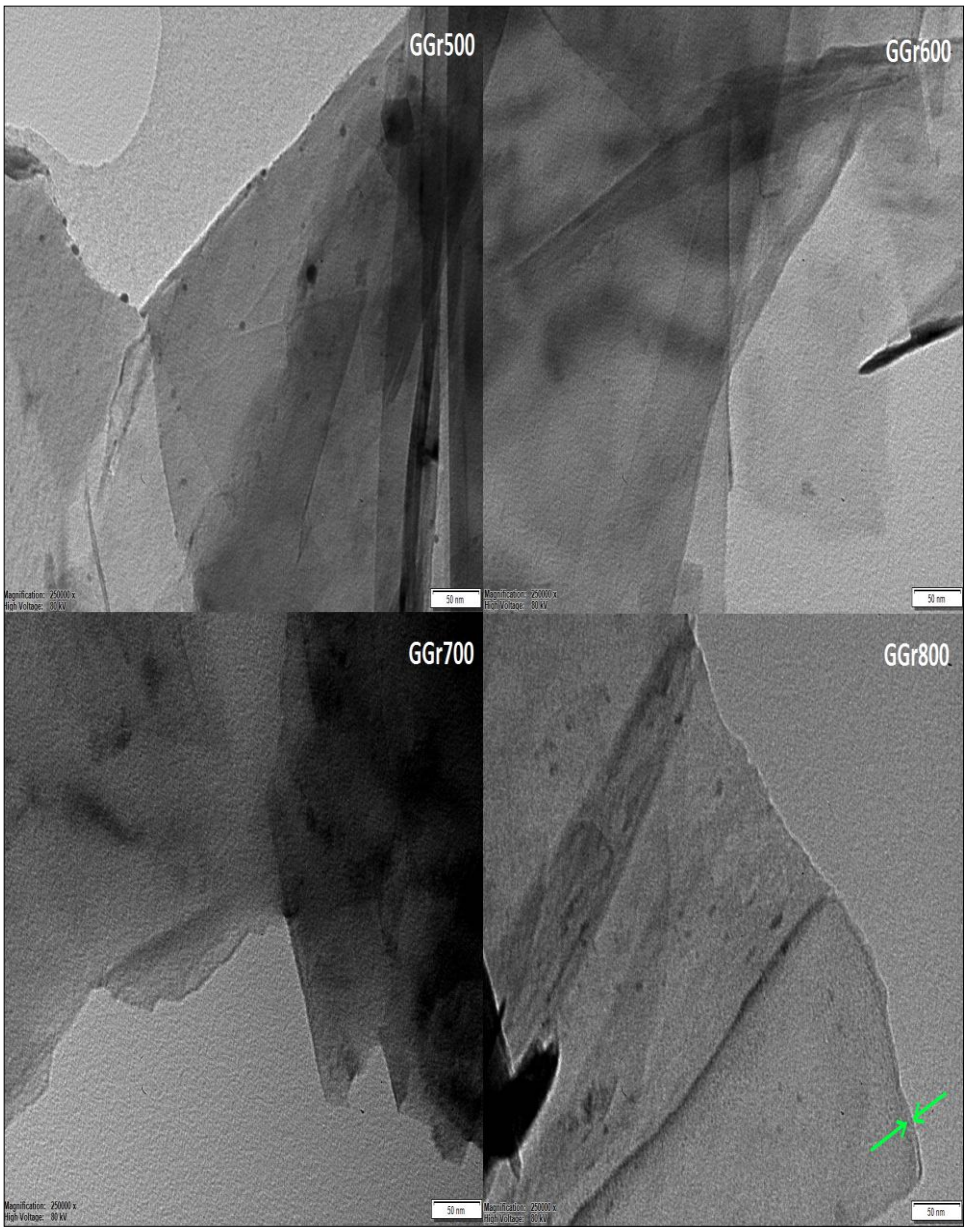

Figure 4.13: TEM images of graphene products.

The sheetlike structure is further confirmed with transmission electron microscopy (TEM) imaging. TEM images show that the graphene-like structure with different thickness, ranging from 5 nm to 9 nm, indicate the presence of a few-layer graphene in Figure 4.13. Thicker layers are observed in significant amounts indicating that most of the graphene samples have few and multi layers. This deviation from the ideal thickness of 0.335 nm (interlayer distance in graphite along the c axis) for chemically derived single-layer graphene can be explained by the presence of structural disorder and remaining attached functional groups [Liu et al., 2014].

The AFM characterization of final graphene products (GGr500, GGr600, GGr700, and GGr800) was performed to measure the surface roughness and thickness to determine the optimal solvent type for graphene growth. The AFM characterization results of samples (GGr500, GGr600, GGr700, and GGr800) are summarized in Figure 4.14.

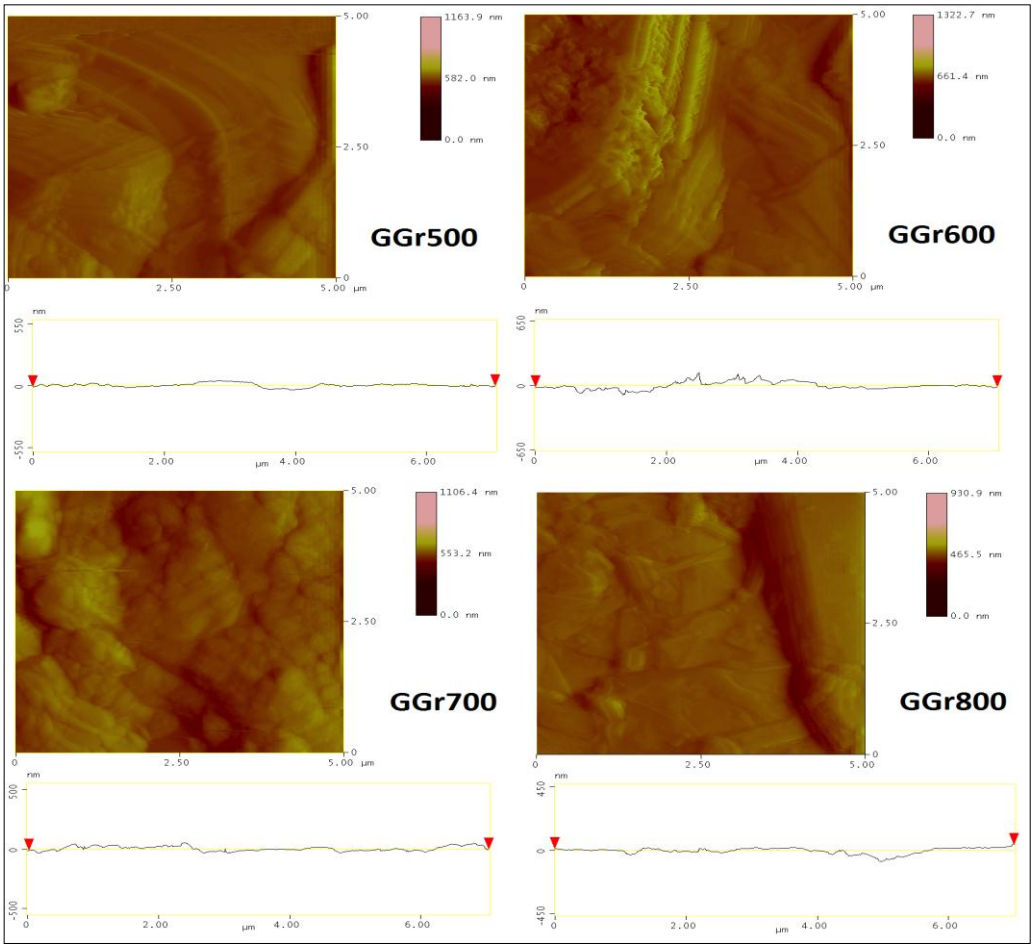

Figure 4.14: AFM images and line profiles of graphene samples.

The Ra values of GGr500, GGr600, GGr700, and GGr800 are 13.052, 30.110, 17.431, and 16.982 nm, respectively. The Rq values of GGr500, GGr600, GGr700, and GGr800 are 21.969, 36.234, 33.244, and 24.348 nm, respectively. The RMS values of GGr500, GGr600, GGr700, and GGr800 are 17.491, 38.027, 20.404, and 22.120 nm, respectively. Vertical distance denotes the thickness of graphene and it is determined for GGr500, GGr600, GGr700, and GGr800 as 7.298, 1.500, 7.406, and 27.695 nm, respectively. The layer numbers were calculated via Eq. 2.1. The layer

numbers of GGr500, GGr600, GGr700, and GGr800 are 21, 3, 21, and 81, respectively. According to AFM results, best results are obtained at 600 °C temperature.

Overall, a green and scalable graphene synthesis in molten salt media through the exfoliation of graphite is examined by X-Ray Diffraction (XRD), Ultraviolet Visible (UV-vis) spectroscopy, particle size analyses, electrical conductivity measurements, X-Ray Photoelectron Spectroscopy (XPS), and Raman spectroscopy, TEM, SEM, AFM.

According to XRD results, all of synthesized graphene products give 2θ°=26.5° peak which is characteristic for graphene, and most of the synthesized graphene samples include 2 layers in average. These results are supported with the layer numbers that are obtained from Raman results; I_D/I_G results show that most of the graphene products are few layered. The UV-vis spectrum of GGr500, GGr600, GGr700 and GGr800 show peak around 275-285 nm. The particle sizes of the graphene samples are increasing with the temperature increase. Electrical conductivities of GGr samples are 7-10 times higher than electrical conductivity of CG. XPS spectrum of GGr600 and GGr800 contain four peaks at ∼284, 286, 290, and 285 eV, corresponding to the C=C, C-O-C, O-C=O, and C-C bonds. As a XPS results, it can be concluded that the carbon content of GGr slightly decreases by increasing temperature. The Raman spectrums consist of D, G, and 2D bands located at 1345, 1576, and 2659 cm^{-1}, respectively. Synthesized GGr700, GGr800 samples have lower D-band that indicating ordered graphene structure including fewer defects and having good quality. According to I_D/I_G values; GGr600, GGr700 and GGr800 have single layer, GGr500 has few layers, and RGO has multi layers. Thus, it can be concluded that the reaction temperature has positive effect on quality of the graphene.

Graphene morphology was confirmed via both SEM and TEM studies. The average size of flakes observed in the SEM images was calculated as 2 μm. The TEM images show graphene-like structures with different thickness, ranging from 5nm to 9 nm, indicating the presence of few-layer graphene. The layer numbers of GGr500, GGr600, GGr700, and GGr800 are calculated via AFM results as 21, 3, 21, and 81, respectively. Thus, it can be concluded that lower temperature gives better results.

4.2. Microwave (MW) Assisted Method Results

All the results of ammonia tests were summarized in Table 4.13. According to the results; sonication did not create a positive effect on electrical conductivity of final product. Lower temperature conditions give better yield and electrical conductivity results.

Table 4.13: Results of experiments that were done by using ammonia.

Exp. No	Carbon source	Solvent	Sonication step	React. Cond.	Yield (%)	Elec. cond. (S/m)	E. Cond. (After annealing) (S/m)
1	Natural graphite (0.5 g)	25% Ammonia	-	120 °C, 1 bar, 50 watt	94	52.44	58.114
2	Natural graphite (0.5 g)	25% Ammonia	-	120 °C, 1 bar, 50 watt	89	12.8	30.647
3	Natural graphite (0.5 g)	25% Ammonia	30’ mode 5 power 50%	200 °C, 1 bar, 50 watt	53.5	9.06	12.047

According to these results which were given in Table 4.13; low temperature showed better electrical condcutivity results. Sonication step created negative effect on electrical conductivity results. Also, after annealing step, electrical conductivity results slightly increased.

Another set of experiment were done in order to compare the effect of different solvents on graphene synthesis via microwave energy. The results of microwave tests that were conducted by using N,N-Dimethyl formamide (DMF), ethylene glycol (EG) and ethylene diamine (ED) were given in Table 4.14.

Table 4.14: Microwave tests that were conducted by using DMF, EG and ED.

Exp. No	Carbon source	Solvent	Sonication step	React. Cond.	Yield (%)	Elec. cond. (S/m)
4	Natural graphite (0.1 g)	DMF (50 ml)	10', 200 W, 20 kHz, mode 5, power 50%	30', 180 °C	60	22.7
5	Natural graphite (0.1 g)	EG (50 ml)	10', 200 W, 20 kHz, mode 5, power 50%	30', 180 °C	88	6
6	Natural graphite (0.1 g)	ED (50 ml)	10', 200 W, 20 kHz, mode 5, power 50%	30', 180 °C	75	7.1

According to the results which were given in Table 4.14; the reaction yields of DMF, EG, and ED are 60, 88, and 75%, respectively. The electrical conductivity values of DMF, EG, and ED are 22.716, 6.0002, 7.0967 S/m, respectively. It can be concluded that; G-DMF shows better conductivity performance.

XRD spectrums of MW assisted expanded graphite products which were obtained in different solvents such as EG, ammonia, and DMF were given in Figure 4.15, 4.16, and 4.17, respectively. Also, XRD spectrum of natural graphite was given in Figure 4.18.

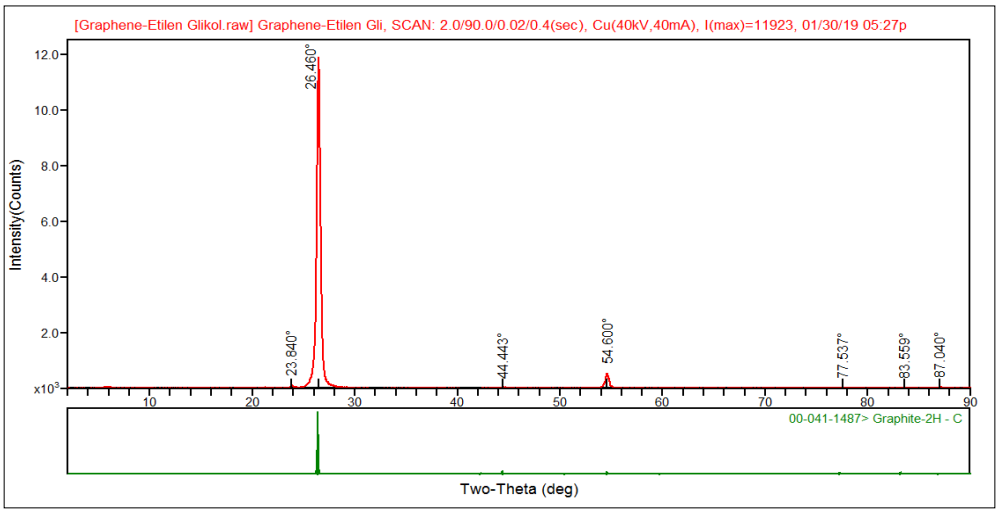

Figure 4.15: XRD spectrum of expanded graphite products, which was obtained in EG by using MW energy.

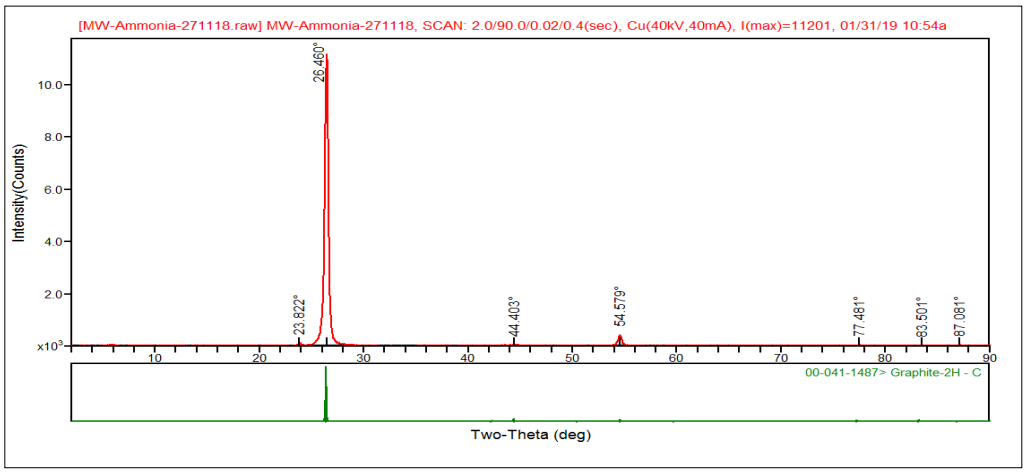

Figure 4.16: XRD spectrum of expanded graphite products, which was obtained in ammonia by using MW energy.

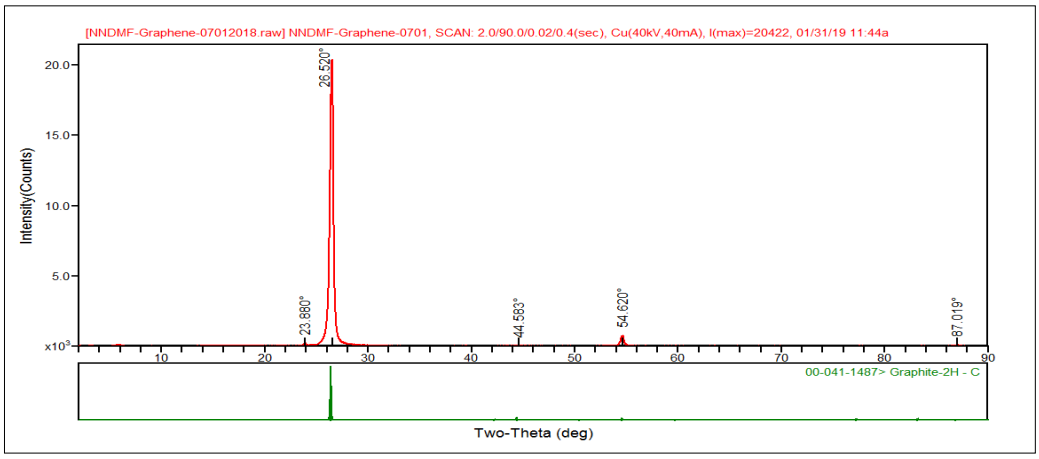

Figure 4.17: XRD spectrum of expanded graphite products, which was obtained in DMF by using MW energy.

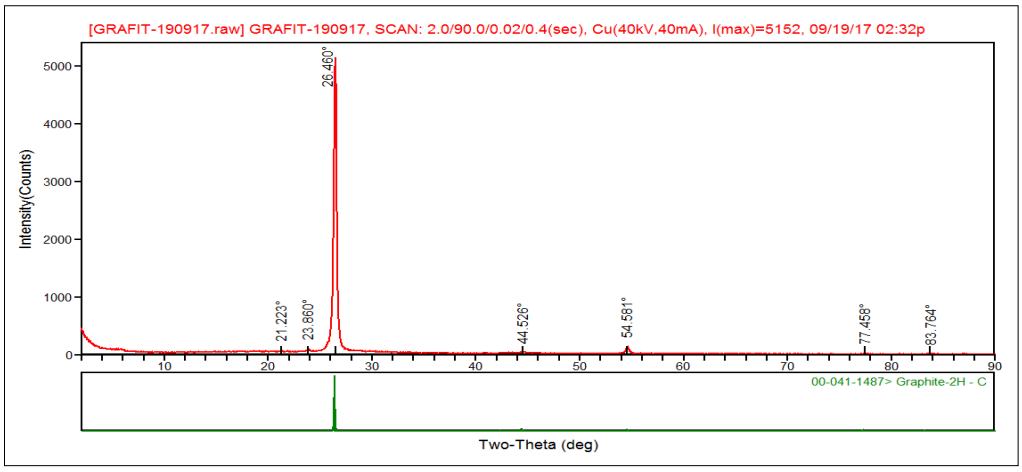

Figure 4.18: XRD spectrum of Natural graphite.

According to XRD results; all the spectrums show the 002 peak of graphite was predominant in all the four types of graphite, at 2 θ° = 26.44° peak, which is characteristic for graphite. Natural graphite shows highest intensity peak at 2θ° = 26.44. The intensity of other two peaks 101, 004 was low at all the spectrums. Layer numbers of final products calculating by using XRD data were presented at Table 4.15. Layer numbers of expanded graphite products, which were obtained in EG, ammonia, and DMF by using MW energy, were calculated as 1.5 for all solvents. Layer number of natural graphite was calculated as 1.75 by the help of XRD result.

Table 4.15: Layer numbers of final products calculating from XRD results.

Code	Layer number
Ethylene glycol (EG)	1.5
Ammonia	1.5
N,N-Dimethyl formamide (DMF)	1.5
Natural graphite	1.75

The results of another experiment plan which covering the usage of wide scale of solvents including n-Hexadecane (n-Hexa), Dimethylsulfoxide (DMSO), Sodium Hydroxide (50% aq.) (NaOH), 1-octanol (OCTA), Perchloric acid (PA), N,N-Dimethyl formamide (DMF), Ethylene glycol (EG), and Ethylene diamine (ED) were presented in Table 4.16. According to the results, G-DMF showed the highest electrical conductivity. Electrical conductivities of MW assisted graphene products were higher when the used chemicals have 2 - 4 Debye (D) dipole moments. These results are compatible with the dielectric constants and surface tensions of the used chemicals. Layer numbers were calculated by Scherrer equation and the half-width of the diffraction line β(2θ) (in rad) was taken as the experimental half-width (βexp) and was corrected for experimental broading (βinstr) as described in Saberi et al.'s study [Saberi et al., 2007]. Layer numbers show distribution between 10 - 16. EG showed the thinnest layer number with the value of 5.5, which is seen at Table 4.16. Solvents that have surface tension bigger than 40 mN/m show better layer number results. Briefly, as the surface tensions increased, layer numbers decreased. These results are supported with Hernandez et al. study [Hernandez et al., 2008]. When the dielectric constants (ε) get larger, electrical conductivity values of synthesized products increased.

Table 4.16: Electrical conductivities, dipole moments, layer numbers and dielectric constants of MW supported graphene products.

Solvent	Dipole moment (Debye)	Dielectric constant (ε)	Layer number	Surface Tension @ 20 °C (mN/m)	Electrical conductivity of obtained product (S/m)
n-Hexadecane	0.06	2	15.81	27.47	8.1739
Dimethylsulfoxide	3.96	46.7	12.36	43.54	7.5809
Sodium Hydroxide (50% aq.)	6.832	57.5	10.33	74.35	10.664
1-octanol	1.76	3.4	14.02	27.6	1.7842
Perchloric acid	2.1456	115	10	69.69	20.619
N,N-Dimethyl formamide	3.86	36.7	15	37.1	22.716
Ethylene glycol	2.746	37	5.5	47.7	6.002
Ethylene diamine	1.83	16	10.61	42	7.0967

All XRD spectrums showed peak at 26.5° which can be seen in Figure 4.19. XRD spectra of G-PA also proved that graphite peak at 26.5° shows minimum intensity.

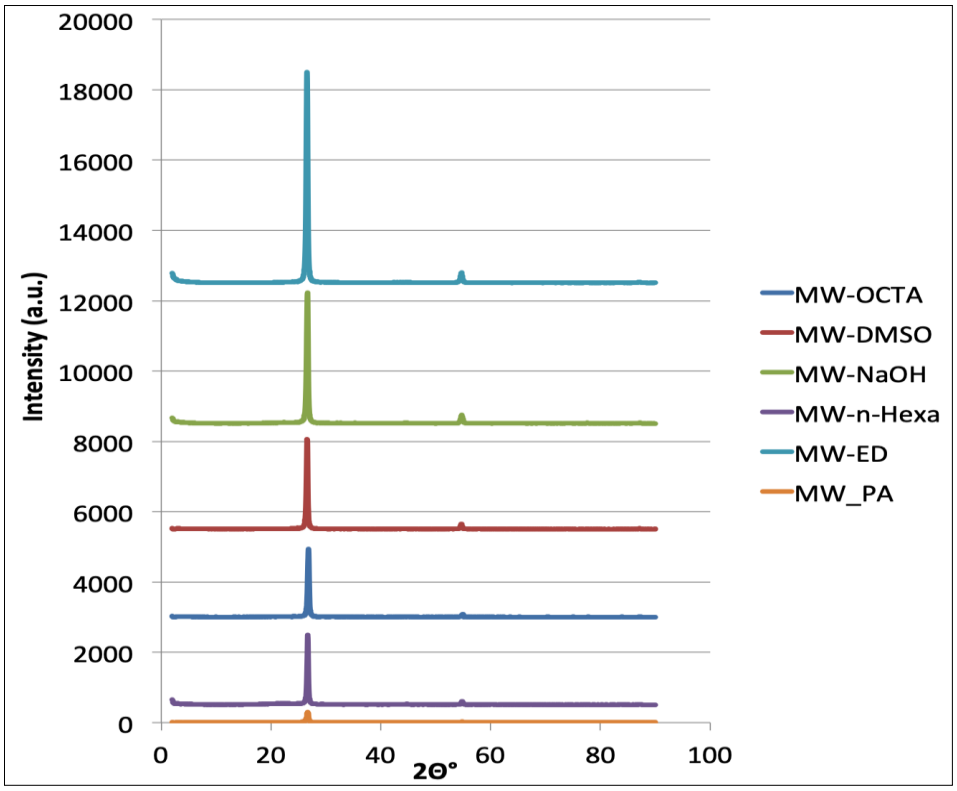

Figure 4.19: XRD spectrums of MW supported synthesized graphene products.

Electrical conductivities of MW assisted graphene products were higher when the used chemicals have 2 - 4 Debye (D) dipole moments as seen as in Figure 4.20.

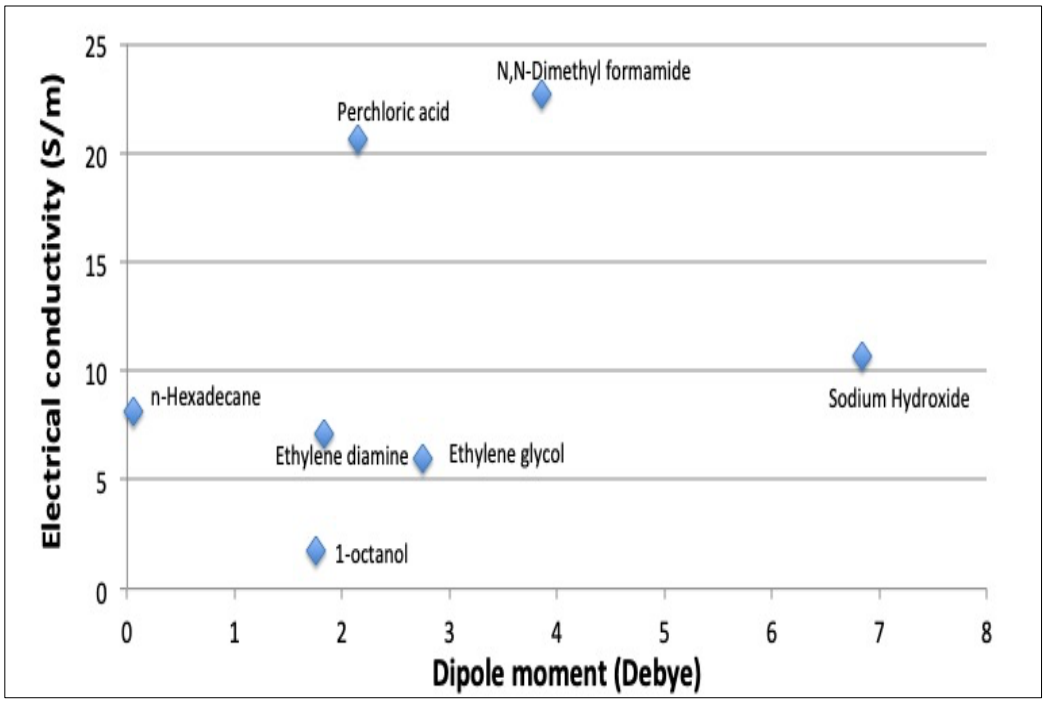

Figure 4.20: Relation between electrical conductivity and dipole moment.

PA showed the optimum electrical conductivity and layer number values for the MW assisted graphene synthesis as seen in Figure 4.21.

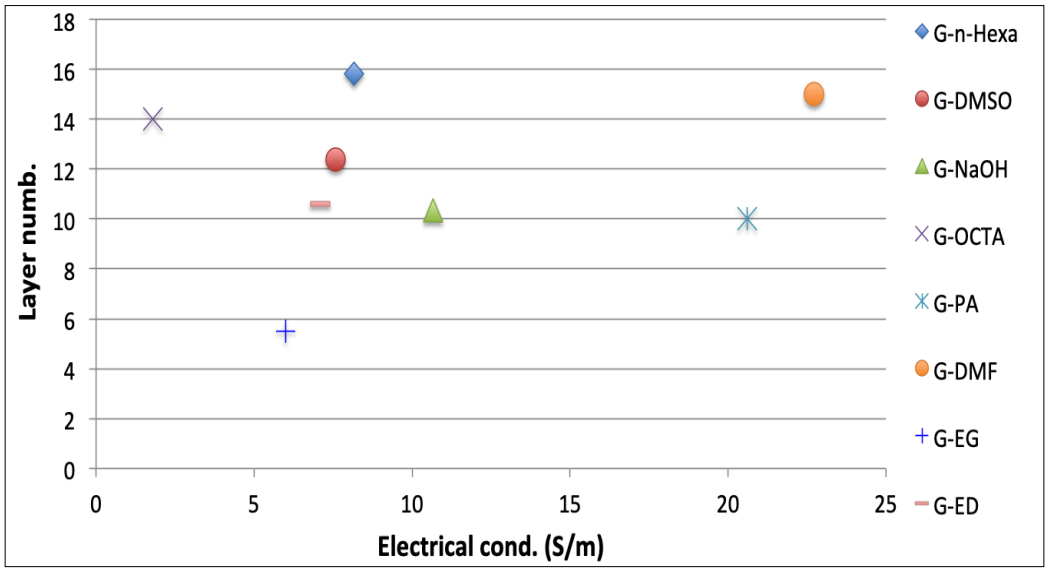

Figure 4.21: Relation between layer numbers and electrical conductivity.

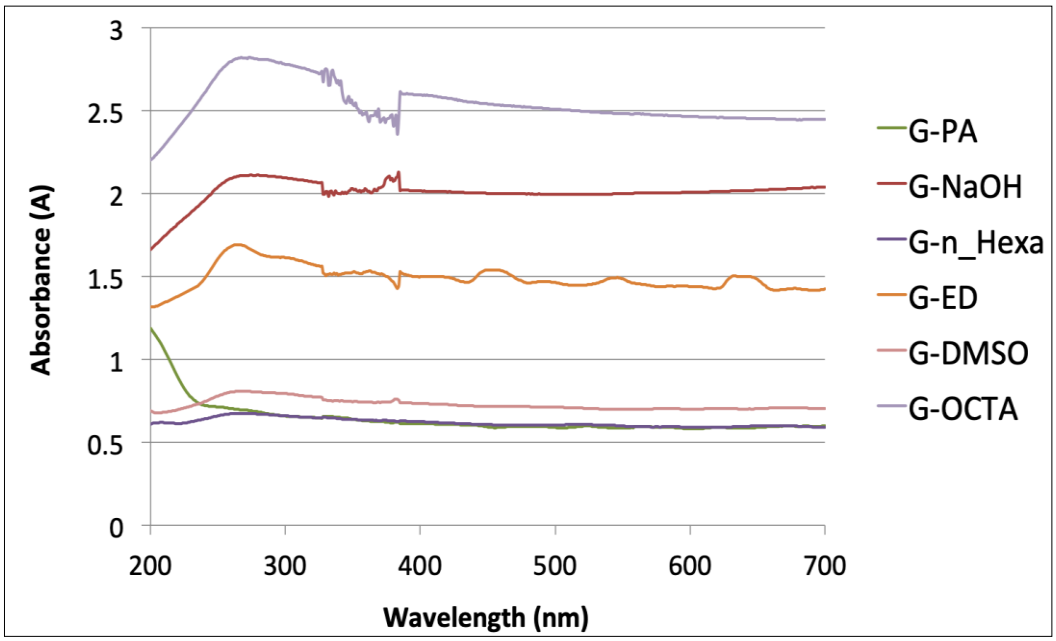

Figure 4.22: UV spectrums of MW based synthesized graphene products.

According to the UV-vis spectrums of MW-assisted graphene samples, which are presented in Figure 4.22, synthesized graphene samples, which were labeled as G-PA, G-NaOH, G-n-Hexa, G-ED, G-DMSO, and G-OCTA showed peak at 265 nm wavelength that referring sp^2 C=C bonds. This result is in line with the previous lierature [Johra et al., 2014].

4.3. Ultrasound (US) Assisted Method Results

The US-assisted synthesized graphene products were characterized by using UV-vis spectroscopy, AFM Spectroscopy, and DLS analysis. UV-vis spectrums of US-assisted graphene products are presented in Figure 4.23. Coleman's team calculated the absorption coefficient of graphene dispersion via UV/vis spectroscopy. Concisely, with the help of the Beer-Lambert law, absorption coefficient ($A = \alpha cl$) of graphene could be found by using dispersion at specific concentrations [Hernandez et al., 2008], [Khan et al., 2010], [Lotya et al., 2010], [Lotya et al., 2009], [Khan et al., 2011]. UV–Vis absorbance spectroscopy was conducted at fixed wavenumbers of 253 nm for graphene. A piercing peak at 210 nm can be noticed and one more peak around 226 nm with a little bit less intensity of absorption peak is also observed due to Π-Π* bondings of the C-C aromatic rings.

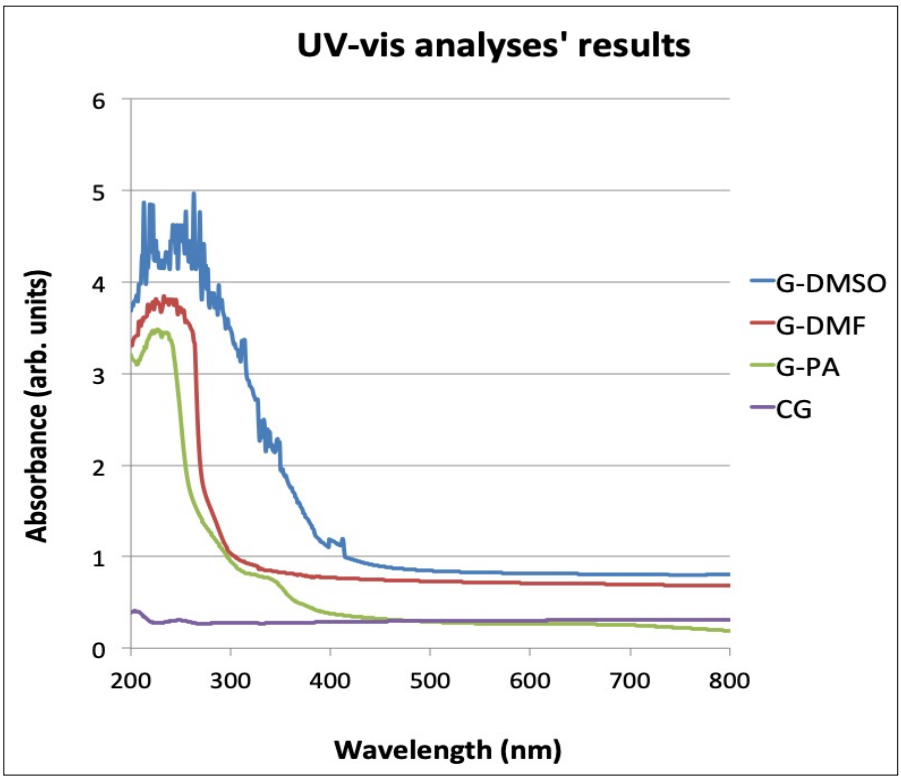

Figure 4.23: UV-Vis spectrums of US-assisted graphene products and CG.

The obtained graphene samples, which are labeled as G-DMSO, G-DMF and G-PA, show peak at 265 nm wavelength that referring sp^2 C=C bonds [Johra et al., 2014].

AFM characterization of final graphene products (G-DMF, G-DMSO, G-PA) were conducted to determine the optimal growth condition by measuring surface roughness and thickness. The Ra values of G-DMSO, G-DMF, and G-PA are 2.937, 6.343, and 10.103 nm, respectively. The Rq values of G-DMSO, G-DMF, and G-PA are 3.471, 8.046, and 11.748 nm, respectively. The RMS values of G-DMSO, G-DMF, and G-PA are 5.675, 8.842, and 11.910 nm, respectively. Vertical distance denotes the thickness of graphene and it is determined for G-DMSO, G-DMF, and G-PA as 1.638, 2.151, and 10.754 nm, respectively. The layer numbers were calculated via Eq. 2.1. The layer numbers of G-DMSO, G-DMF, and G-PA are calculated as 4, 5, and 31, respectively. According to AFM results, best result was obtained with DMSO. All these results confirmed that the G-DMSO materials had fewer layers and defects.

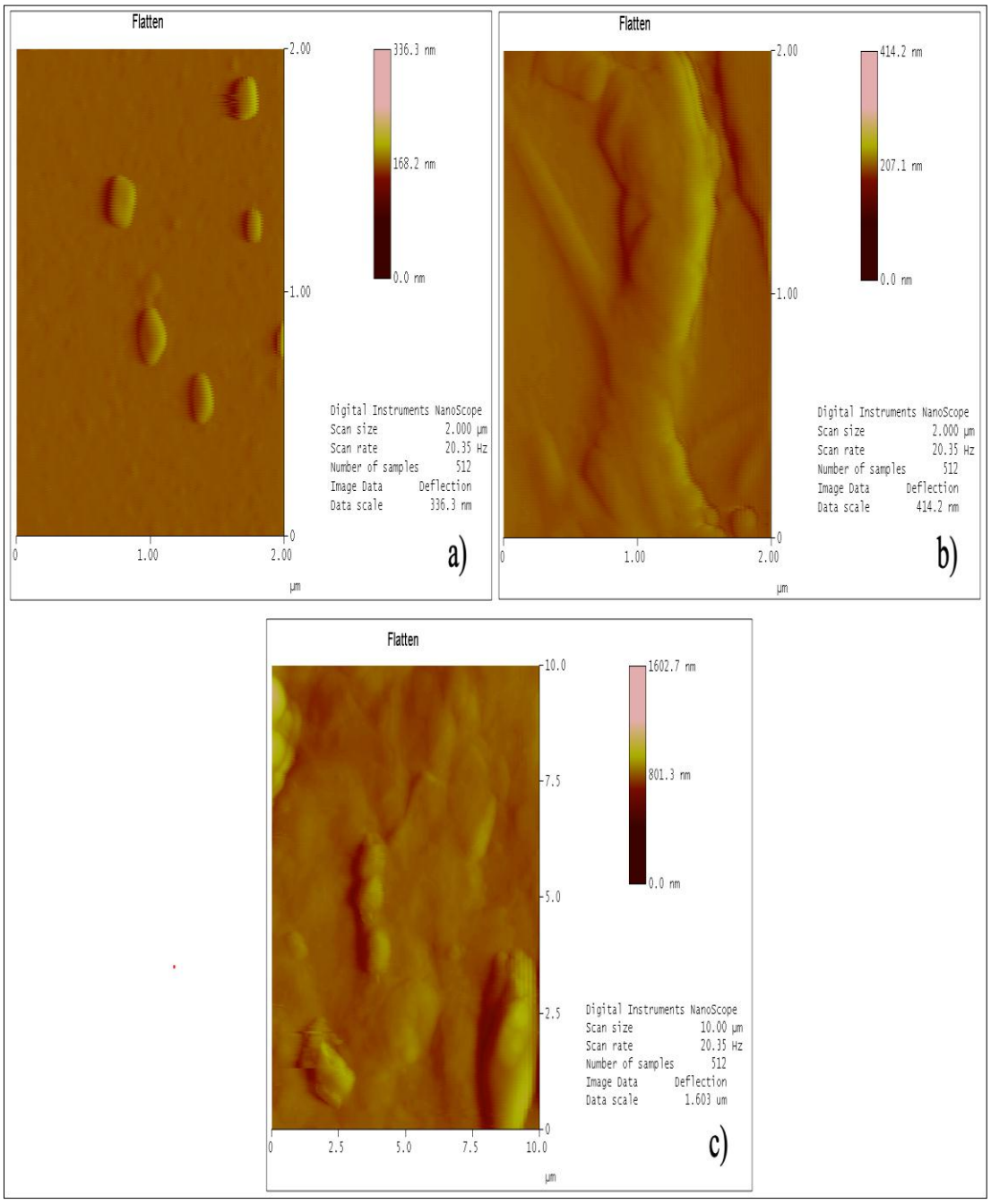

Figure 4.24: AFM results of US-assisted graphenes a) G-DMSO, b) G-DMF, and c) G-PA.

Although these techniques can determine the size of graphene products, dynamic light scattering (DLS) is also helpful to measure the particle size. It is an easy and quick method for evaluating the size of graphene samples [Lotya et al., 2013]. The size distribution of the synthesized graphene samples using DLS are shown in Figure 4.25.

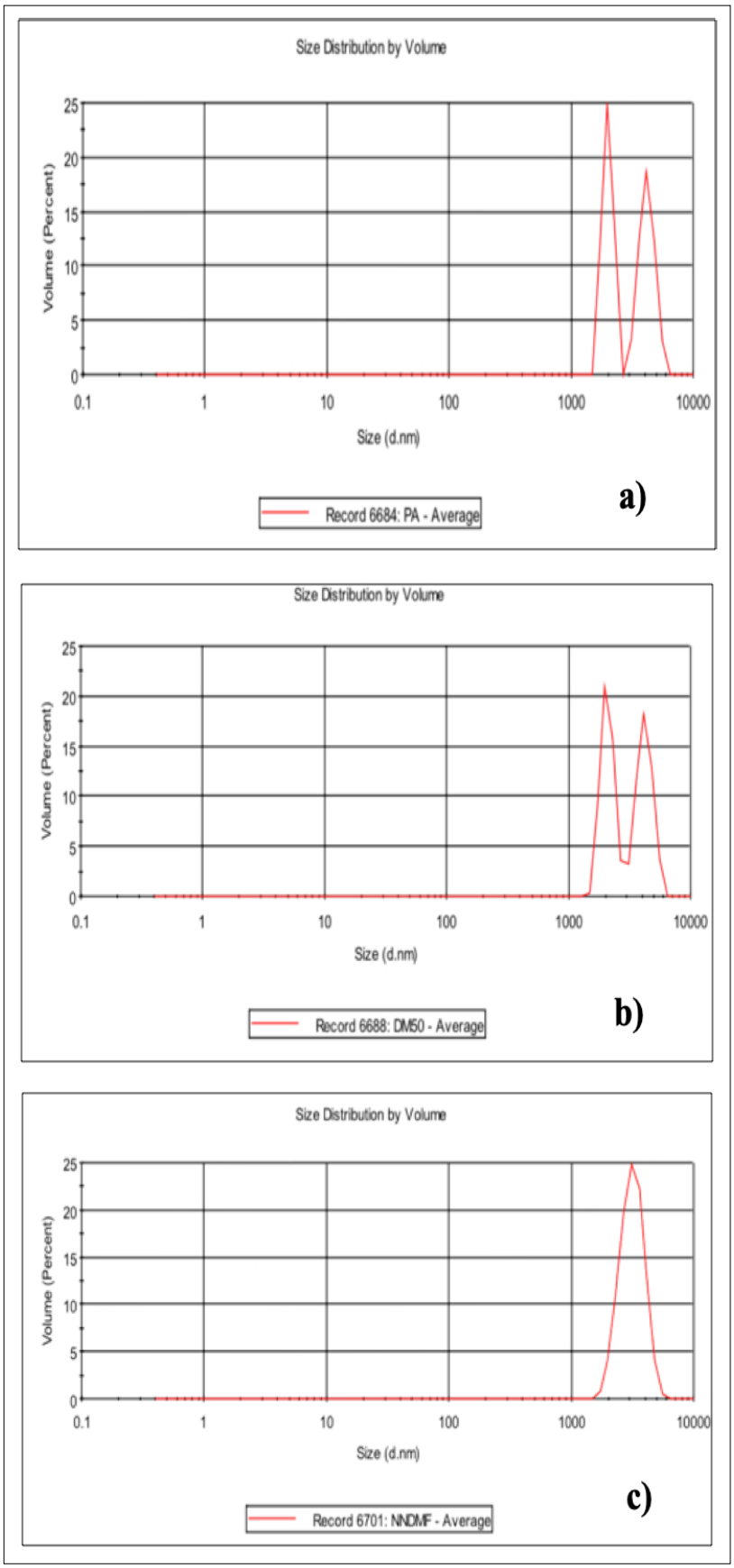

Figure 4.25: DLS analysis results of synthesized samples a) G-PA, b) G-DMSO, c) G-DMF.

It is a versatile method and represents repeatable and non-detrimental analysis results. DLS gives the hydrodynamic radius (R_h), which is described as the radius of an equivalent hard sphere diffusing at the same rate as the particle under observation, and so it is indicative of the apparent size adopted by the graphene samples in the aqueous dispersion.

Table 4.17: Particle size results of US-assited synthesized samples.

Sample Name	Z-Ave (d.nm)
G-DMF	3846
G-DMSO	6938
G-PA	7137

Z-average hydrodynamic radius (R_h) of G-DMF is 3846 nm, R_h of G-DMSO is 6930 nm, and R_h of G-PA is 7137 nm as it is summarized in Table 4.17. According to these results, DMF provides graphene products with smallest particle size.

5. CONCLUSION

As a scope of this study; firstly, a green, low-cost, one-step method was developed for growth of graphene from saccharides in molten salt medium. SEM and Raman spectroscopy characterizations confirmed the morphology and high quality of these graphene products. Yields of graphene products which are obtained at 600 °C temperature are higher than at 800 °C temperature. Most of the saccharides based graphene products gave peak at 2θ = 23° on their XRD patterns. Also, as the reaction temperature was increased from 600 °C to 800 °C, amorphous structure were observed at the XRD spectrums of some final products and layer numbers of the products increased. According to XPS results, graphene products that were synthesized at 600 °C have higher carbon content than the ones that were synthesized at 800 °C. Temperature built an insignificant positive effect only on the electrical conductivities of the graphene samples. Molten salt media enhanced the microstructure and porosity of the graphenes. These graphene substances include few-layers. The saccharide-based graphenes were highly hydrophobic and showed significant capacity and selectivity for absorption of organic molecules. These results can be a novel synthetic route to produce carbon materials from various mono/polysaccharides.

Secondly, a green and scalable graphene synthesis in molten salt media via the exfoliation of graphite was conducted. Then, final products of this second method were examined by X-Ray Diffraction (XRD), Ultraviolet Visible (UV-vis) spectroscopy, particle size analyses (DLS), electrical conductivity measurements, X-Ray Photoelectron Spectroscopy (XPS), and Raman spectroscopy, TEM, SEM, and AFM. According to XRD results, all graphene products gave peak at 2θ°=26.5° which is characteristic for graphene, and most of the synthesized graphene samples include 32 layers in average. These results are supported by the layer numbers that were calculated from Raman results; I_D/I_G results showed that most of the graphene products are multi layered. The UV-vis spectrum of GGr500, GGr600, GGr700 and GGr800 show peak around 275-285 nm. The particle sizes of the graphene samples are increasing with the temperature increase. Electrical conductivities of GGr samples are 7-10 times higher than electrical conductivity of CG. XPS spectrum of GGr600 and GGr800 contain four peaks at ∼284, 286, 290, and 285 eV,

corresponding to the C=C, C-O-C, O-C=O, and C-C bonds. According to XPS results, it can be concluded that the carbon content of GGr slightly decreases by increasing temperature. The Raman spectrums consist of D, G, and 2D bands located at 1345, 1576, and 2659 cm^{-1}, respectively. GGr700, GGr800 samples have lower D-band that indicating ordered graphene structure including fewer defects and having good quality. According to I_D/I_G values; GGr600, GGr700 and GGr800 have single layer, GGr500 has few layers, and RGO has multi layers. Thus, it can be concluded that the reaction temperature has positive effect on quality of the graphene. Graphene morphology was confirmed via both SEM and TEM studies. The average size of flakes observed in the SEM images was calculated as 2 μm. The TEM images show graphene-like structures with different thickness, ranging from 5nm to 9 nm, indicating the presence of few-layer graphene. The layer numbers of GGr500, GGr600, GGr700, and GGr800 are calculated via AFM results as 21, 3, 21, and 81, respectively. Thus, it can be concluded that lower temperature gives better results.

Thirdly, microwave (MW)-assisted method was developed. Although many solvents have been studied, carbon product, which was synthesized in DMF, showed the highest electrical conductivity. Electrical conductivities of MW-assisted graphene products were higher when the used solvents have 2 - 4 Debye (D) dipole moments. These results are compatible with the dielectric constants and surface tensions of the used chemicals. Layer numbers show distribution between 10 - 16. EG has minimum layer number with the value of 5.5. Solvents that have surface tension bigger than 40 mN/m show better layer number results. When the dielectric constants (ε) get larger, electrical conductivity values of synthesized products increased. As the surface tensions increased, layer numbers decreased. PA showed the optimum electrical conductivity and layer number values for the MW-assisted graphene synthesis. According to the UV-vis spectrums of MW assisted graphene samples. The obtained graphene samples, which were labeled as G-PA, G-NaOH, G-n-Hexa, G-ED, G-DMSO, and G-OCTA showed peak at 265 nm wavelength that referring sp^2 C=C bonds.

Fourthly, ultrasound (US)-assisted method was studied. Graphene samples were easily synthesized via solution-based process. According to the UV-vis spectrums, all graphene products gave peak at 265 nm wavelengths, which may be caused by the ultrasonication required for proper suspension using the solution-based process. Also, as a result of AFM analyses, G-DMSO has four layers, G-DMF has

five layers and G-PA has thirty-one layers. It can be understood that DMSO shows better solvent effect on graphite exfoliation by sonication process. Z-average hydrodynamic radius (R_h) of G-DMF is 3846 nm, R_h of G-DMSO is 6930 nm, and R_h of G-PA is 7137 nm. It can be concluded that, DMF provides graphene products with smallest particle size.

REFERENCES

Adel M., El-Maghraby A., El-Shazly O., El-Wahidy E. F., Mohamed M. A. A., (2016), “Synthesis of few-layer graphene-like nanosheets from glucose: New facile approach for graphene-like nanosheets large scale production”, Journal of Materials Research”, 31 (4), 455-467.

Ajayan P. M., Ebbesen T. W., Ichihashi T., Iijima S., Tanigaki K., Hiura H. (1993), “Opening carbon nanotubes with oxygen and implications for filling”, Nature, 362 (6420), 522-525.

Akbar F., Kolahdouz M., Larimian S., Radfar B., Radamson H. H., (2015), “Graphene synthesis, characterization and its applications in nanophotonics, nanoelectronics, and nanosensing”, J Mater Sci: Mater Electron 26: 4347.

Al-Hazmi F. S., Al-Harbi G. H., Beall G. W., Al-Ghamdi A. A., Obaid A. Y., Mahmoud W. E., (2015), “One pot synthesis of graphene based on microwave assisted solvothermal technique”, Synthetic Metals, 200, 54-57.

Allen M. J., Tung V. C., Kaner R. B., (2010), “Honeycomb carbon: a review of graphene”, Chem. Rev., 110 (1), 132-145.

Alsmeyer D. C., McCreery R. L., (1992), “In situ Raman monitoring of electrochemical graphite intercalation and lattice damage in mild aqueous acids”, Anal Chem, 64 (14), 1528-1533.

An X., Simmons T., Shah R., Wolfe C., Lewis K. M., Washington M., Nayak S. K., Talapatra S., Kar S., (2010), “Stable aqueous dispersions of noncovalently functionalized graphene from graphite and their multifunctional high-performance applications”, NanoLett., 10, 4295-4301.

Berger C., Song Z., Li T., Li X., Ogbazghi A. Y., Feng R., Dai Z., Marchenkov A. N., Conrad E. H., First P. N., de Heer W. A., (2004), “Ultrathin epitaxial graphite: 2D electron gas properties and a route toward graphene-based nanoelectronics”, J. Phys. Chem. B, 108, 19912-19916.

Bhuyan M. S. A., Uddin M. N., Islam M. M., Bipasha F. A., Hossain S. S., (2016), “Synthesis of graphene”, Int. Nano Lett, 6 (2), 65-83.

Blake P., Brimicombe P. D., Nair R. R., Booth T. J., Jiang D., Schedin F., Ponomarenko L. A., Morozov S. V., Gleeson H. F., Hill E. W., Geim A. K., Novoselov K. S., (2008), “Graphene-based liquid crystal device”, Nano Lett., 8 (6) 1704-1708.

Bonaccorso F., Lombardo A., Hasan T., Sun Z., Colombo L. Ferrari A. C., (2012), “Production and processing of graphene and 2D crystals”, Materials Today, 15 (12) 564-589.

Botas C., Álvarez P., Blanco C., Santamaría R., Granda M., Gutiérrez M. D., Rodríguez-Reinoso F.; Menéndez R., (2013), “Critical temperatures in the synthesis of graphene-like materials by thermal exfoliation-reduction of graphite oxide”, Carbon, 52, 476-485.

Cameron J. S., Ashley D. S., Andrew J. S., Joseph G. S., Christopher T. G., (2016), “Accurate Thickness Measurement of Graphene”, Nanotechnology, 27 (12), 125704.

Ciesielski A., Samori P., (2014), “Graphene via sonication assisted liquid-phase exfoliation”, Chem. Soc. Rev., 43, 381-398.

Chen Y., Zhao H., Sheng L., Yu L., An K., Xu J., Ando Y., Zhao X., (2012), “Mass-production of highly-crystalline few-layer graphene sheets by arc discharge in various H_2–inert gas mixtures”, Chem. Phys. Lett., 538 (11), 72-76.

Choi W., Lee J.-w., (2011), “Graphene: Synthesis and Applications”, 1st edition, CRC Press, Taylor and Francis Group.

Choucair M., Thordarson P., Stride J. A., (2009), “Gram-scale production of graphene based on solvothermal synthesis and sonication”, Nat. Nanotechnol., 4 (1), 30-33.

Chun W. W., Leng T. P., Osman A. F., Keat Y. C., (2018), “Mechanical Properties and Morphology of Epoxy/Graphene Nanocomposite Using Bath Sonication and Tip Sonication”, Solid State Phenomena, 280, 258-263.

Dhar S., Barman A. R., Ni G. X., Wang X., Xu X. F., Zheng Y., Tripathy S., Ariando, Rusydi A., Loh K. P., Rubhausen M., Castro Neto A. H., Őzyilmaz B., Venkatesan T. (2011), A new route to graphene layers by selective laser ablation, AIP Advances, 1 (2), 022109.

Dresselhaus M. S., Jorio A., Hofmann M., Dresselhaus G., Saito R., (2010), “Perspectives on carbon nanotubes and graphene Raman spectroscopy”, Nano Letters, 10 (3), 751-758.

Du F., Ma Y., Lv X., Huang Y., Li F., Chen Y., (2006), “The synthesis of single-walled carbon nanotubes with controlled length and bundle size using the electric arc method”, Carbon, 44 (7), 1327-1330.

Ferrari A. C., Robertson J., (2000), “Interpretation of Raman spectra of disordered and amorphous carbon”, Physical Review B, 61, 14095-14107.

Ferrari A. C., (2007), “Raman spectroscopy of graphene and graphite: Disorder, electron–phonon coupling, doping and nonadiabatic effects”, Solid State Communications, 143 (1-2), 47-57.

Ferrari A. C., Bonaccorso F., Fal'ko V., Novoselov K. S., Roche S., Bøggild P., Borini S., Koppens F. H. L., Palermo V., Pugno N., Garrido J. A., Sordan R., Bianco A., Ballerini L., Prato M., Lidorikis E., Kivioja J., Marinelli C., Ryhänen T., Morpurgo A., Coleman J. N., Nicolosi V., Colombo L., Fert A., Garcia-Hernandez M., Bachtold A., Schneider G. F., Guinea F., Dekker C., Barbone M., Sun Z., Galiotis C., Grigorenko A. N., Konstantatos G., Kis A., Katsnelson M., Vandersypen L., Loiseau A., Morandi V., Neumaier D., Treossi E., Pellegrini V., Polini M., Tredicucci A., Williams G. M., Hee Hong B., Ahn J.-H., Min Kim J., Zirath H., van Wees B. J., van der Zant H., Occhipinti L., Di Matteo A., Kinloch I. A., Seyller T., Quesnel E., Feng X., Teo K., Rupesinghe N., Hakonen P., Neil S. R. T., Tannock Q., Löfwander T., Kinaret J., (2015), "Science and technology roadmap for graphene, related two-dimensional crystals, and hybrid systems", Nanoscale, 7 (11), 4598-4810.

Galindo B., Gil Alcolea S., Gómez J., Navas A., Ortega Murguialday A., Pérez Fernandez M., Puelles R. C., (2014), "Effect of the number of layers of graphene on the electrical properties of TPU polymers", IOP Conf. Ser.: Mater. Sci. Eng., 64, 012008.

Gao G., Liu D., Tang S., Huang C., He M., Guo Y., Sun X., Gao B., (2016), "Heat-Initiated Chemical Functionalization of Graphene", Scientific Reports, 6, 20034.

Garaj S., Hubbard W., Golovchenko J. A., (2010), "Graphene synthesis by ion implantation", Applied Physics Letters, 97, 183103.

Geim A. K., Novoselov K. S., (2010), "The rise and rise of graphene", Nature Nanotechnology, 5, 755.

Gurunathan S., Han J., Kim J. H., (2013), "Humanin: a novel functional molecule for the green synthesis of graphene", Colloids and Surfaces B: Biointerfaces, 111, 376-383.

Gurunlu B., Bayramoglu M., (2019), "One Step Synthesis of Graphene-Like Structures by Carbonization of some Carbohydrates in Molten Salt Media", Journal of Nano Research, 59, 166-179.

Hernandez Y., Nicolosi V., Lotya M., Blighe F. M., Sun Z., De S., McGovern I. T., Holland B., Byrne M., Gun'ko Y. K., Boland J. J., Niraj P., Duesberg G., Krishnamurthy S., Goodhue R., Hutchison J., Scardaci V., Ferrari A. C., Coleman J. N., (2008), "High-yield production of graphene by liquid-phase exfoliation of graphite", Nat. Nanotechnol., 3, 563-568.

Janowska I., Chizari K., Ersen O., Zafeiratos S., Soubane D., Costa V. D., Speisser V., Boeglin C., Houllé M., Bégin D., Plee D., Ledoux M.-J., Huu P.-C., (2010), "Microwave Synthesis of Large Few-Layer Graphene Sheets in Aqueous Solution of Ammonia", Nano Res., 3 (2), 126-137.

Jiang F., Yu Y., Wang Y., Feng A., Song L., (2017), "A novel synthesis route of graphene via microwave assisted intercalation-exfoliation of graphite", Materials Letters, 200, 39-42.

Johra F. T., Lee J. W., Jung W. G., (2014), “Facile and safe graphene preparation on solution based platform”, Journal of Industrial and Engineering Chemistry, 20 (5), 2883-2887.

Jorio A., Dresselhaus M. S., Saito R., Dresselhaus G., (2011), “Raman Spectroscopy in Graphene Related Systems”, Wiley & Sons Inc.

Kar S., Talapatra S., (2012), “Synthesis of Graphene”. In: B. Bhushan, Editor, “Encyclopedia of Nanotechnology”, Springer, Dordrecht.

Khan U., O’Neill A., Lotya M., De S., Coleman J. N., (2010), “High Concentration Solvent Exfoliation of Graphene”, Small, 6, 864-871.

Khan U., Porwal H., O’Neill A., Nawaz K., May P., Coleman J. N., (2011), “Solvent-Exfoliated Graphene at Extremely High Concentration”, Langmuir, 27, 9077-9082.

Kim K. S., Zhao Y., Jang H., Lee S. Y., Kim J. M., Kim K. S., Ahn J.-H., Kim P., Choi J.-Y., Hong B. H., (2009), “Large-scale pattern growth of graphene films for stretchable transparent electrodes”, Nature, 457, 706-710.

Kötz R., Barbero C., Schnyder B., Haas O., (1993), “Spectroscopic ellipsometry of carbon electrodes during electrochemical activation”, Thin Solid Films, 233 (1-2), 69-73.

Lee S., Lim S., Lim E., Lee K. K., (2010), “Synthesis of aqueous dispersion of graphenes via reduction of graphite oxide in the solution of conductive polymer”, Journal of Physics and Chemistry of Solids, 71 (4), 483-486.

Li N., Wang Z., Zhao K., Shi Z., Gu Z., Xu S., (2010), “Large scale synthesis of N-doped multi-layered graphene sheets by simple arc-discharge method”, Carbon, 48 (1), 255-259.

Li Y., Chen Q., Xu K., Kaneko T., Hatakeyama V. R., (2013), “Synthesis of graphene nanosheets from petroleum asphalt by pulsed arc discharge in water”, Chemical Engineering Journal, 215-216, 45-49.

Liu C., Hu G., Gao H., (2012), “Preparation of few-layer and single-layer graphene by exfoliation of expandable graphite in supercritical N, N-dimethylformamide”, The Journal of Supercritical Fluids, 63, 99-104.

Liu X., Giordano C., Antonietti M. A., (2014), “Facile Molten-Salt Route to Graphene Synthesis”, Small, 10, 193-200.

Lohar D. V., (2017), “Literature Review of Graphene Composites”, International Conference on Recent Trends in Engineering and Science, 6 (1), 475-478.

Lotya M., Hernandez Y., King P. J., Smith R. J., Nicolosi V., Karlsson L. S., Blighe F. M., De S., Wang Z. M., McGovern I. T., Duesberg G. S., Coleman J. N., (2009), "Liquid Phase Production of Graphene by Exfoliation of Graphite in Surfactant/Water Solutions", J. Am. Chem. Soc., 131, 3611-3620.

Lotya M., King P. J., Khan U., De S., Coleman J. N., (2010), "High-Concentration, Surfactant-Stabilized Graphene Dispersions". ACS Nano, 4, 3155-3162.

Lu H., Woi W. S., Tan X., Gibson C. T., Chen X., Raston C. L., Gordon J. M., Chua H. T., (2015), "Synthesis of few-layer graphene by lamp ablation", Carbon, 94, 349-351.

Lu Z., Sun X., Xiang Y., Washington M. A., Wang G.-C., Lu T.-M., (2017), "Revealing the Crystalline Integrity of Wafer-Scale Graphene on SiO_2/Si: An Azimuthal RHEED Approach", ACS Applied Materials \& Interfaces, 9 (27), 23081-23091.

MacGregor W. S., (1967), "The Chemical and Physical Properties of DMSO", Annals of the New York Academy of Sciences; 141 (1), 3-12.

Malekpour H., Chang K.-H., Chen J.-C., Lu C.-Y., Nika D. L., Novoselov K. S., Balandin A. A., (2014), Nano Lett., 14 (9), 5155-5161.

Matsumoto M., Saito Y., Park C., Fukushima T., Aida T., (2015), "Ultrahigh-throughput exfoliation of graphite into pristine 'single-layer' graphene using microwaves and molecularly engineered ionic liquids", Nature Chemistry, 7, 730-736.

Novoselov K. S., Geim A. K., Morozov S. V., Jiang D., Zhang Y., Dubonos S.V., Grigorieva I. V., Firsov A. A., (2004), "Electric field effect in atomically thin carbon films", Science, 306, 666-669.

Qu J., Luo C., Zhang Q., Cong Q., Yuan X., (2013), "Easy synthesis of graphene sheets from alfalfa plants by treatment of nitric acid", Materials Science and Engineering: B, 178 (6), 380-382.

Park W. K., Yoon Y., Kim S., Choi S. Y., Yoo S., Do Y., Jung S., Yoon D. H., Park H., Yang W. S., (2017), "Toward Green Synthesis of Graphene Oxide Using Recycled Sulfuric Acid via Couette–Taylor Flow", ACS Omega, 2 (1), 186-192.

Raccichini R., Varzi A., Passerini S., Scrosati B., (2014), "The role of graphene for electrochemical energy storage", Nature Materials, 14, 271-279.

Randviir E. P., Brownson D. A. C., Banks C. E., (2014), "A decade of graphene research: Production, applications and outlook", Mater. Today, 17, 426-432.

Ravani F., Papagelis K., Dracopoulos V., Parthenios J., Dassios K. G., Siokou A., Galiotis C., (2013), "Graphene production by dissociation of camphor molecules on nickel substrate", Thin Solid Films, 527, 31-37.

Ray A. K., Chatterjee S., Singh J. K., Bapari H., (2015), “Thermal Exfoliation of Natural Cellulosic Material for Graphene Synthesis”, J. of Materi Eng and Perform, 24 (1), 80-84.

Rollings E., Gweon G.-H., Zhou S. Y., Mun B. S., McChesney J. L., Hussain B. S., Fedorov A. N., First P. N., de Heer W. A., Lanzara A., (2006), “Synthesis and characterization of atomically thin graphite films on a silicon carbide substrate”, J. Phys. Chem. Solids, 67, 2172-2177.

Saberi A., Alinejad B., Negahdari Z., Kazemi F., Almasi A., (2007), “A novel method to low temperature synthesis of nanocrystalline forsterite”, Materials Research Bulletin, 42 (4), 666-673.

Schniepp H. C., Li J.-L., McAllister M. J., Sai H., Herrera-Alonso M., Adamson D. H., Prud'homme R. K., Car R., Saville D. A., Aksay I. A., (2006), “Functionalized Single Graphene Sheets Derived from Splitting Graphite Oxide” The Journal of Physical Chemistry B, 110 (17), 8535-8539.

Schnyder B., Alliata D., Kötz R., Siegenthaler H., (2001), “Electrochemical intercalation of perchlorate ions in HOPG: an SFM/LFM and XPS study”, Appl. Surf. Sci., 173 (3-4), 221-232.

Shen B., Ding J., Yan X., Feng W., Li J., Xue Q., (2012), “Influence of different buffer gases on synthesis of few-layered graphene by arc discharge method”, Appl. Surf. Sci., 258 (10) 4523-4531.

Sridhar V., Jeon J.-H., Oh I.-K., (2010), “Synthesis of graphene nano-sheets using eco-friendly chemicals and microwave radiation”, Carbon, 48 (10), 2953-2957.

Subrahmanyam K. S., Panchakarla L. S., Govindaraj A., Rao C. N. R., (2009), “Simple method of preparing graphene flakes by an arc-discharge method”, J. Phys. Chem. C, 113 (11), 4257-4259.

Tassin P., Koschny T., Soukoulis C. M., (2013), “Graphene for Terahertz Applications”, Science, 341 (6146), 620-621.

Thema F. T., Moloto M. J., Dikio E. D., Nyangiwe N. N., Kotsedi L., Maaza M., Khenfouch M., (2013), “Synthesis and Characterization of Graphene Thin Films by Chemical Reduction of Exfoliated and Intercalated Graphite Oxide”, Journal of Chemistry, 2013, 150536, 1-6.

Tsang S. C., Harris P. J. F., Green M. L. H., (1993), “Thinning and opening of carbon nanotubes by oxidation using carbon dioxide”, Nature, 362, 520-522.

Uran S., Alhani A., Silva C., (2017), “Study of ultraviolet-visible light absorbance of exfoliated graphite forms”, AIP Advances, 7 (3), 035323.

Wakeland S., Martinez R., Grey J. K., Luhrs C. C., (2010), “Production of graphene from graphite oxide using urea as expansion–reduction agent”, Carbon, 48 (12), 3463-3470.

Wang G., Xing W., Zhuo S., (2012), “The production of polyaniline/graphene hybrids for use as a counter electrode in dye-sensitized solar cells”, Electrochimica Acta, 66, 151-157.

Wang X. K., Lin X. W., Dravid V. P., Ketterson J. B., Chang R. P. H., (1995), “Carbon nanotubes synthesized in a hydrogen arc discharge”, Appl. Phys. Lett., 66 (18), 2430-2432.

Wang C., Zhan L., Qiao W., Ling L., (2011), “Preparation of graphene nanosheets through detonation”, New Carbon Materials, 26 (1), 21-25.

Wang S., Wang C., Ji. X., (2017), “Towards understanding the salt-intercalation exfoliation of graphite into graphene”, RSC Advances, 7, 52252-52260.

Wazir H., Kundi I. W., (2016), “Synthesis of Graphene Nano Sheets by the Rapid Reduction of Electrochemically Exfoliated Graphene Oxide Induced by Microwaves”, Journal of the Chemical Society of Pakistan, 38 (1), 11-16.

Whitener K. E. Jr., Sheehan P. E., (2014), “Graphene synthesis”, Diamond Relat. Mater., 46, 25-34.

Wu Y., Wang B., Ma Y., Huang Y., Li N., Zhang F., Chen Y., (2010), “Efficient and large-scale synthesis of few-layered graphene using an arc-discharge method and conductivity studies of the resulting films”, Nano Res., 3 (9), 661-669.

Wu Z.-S., Ren W., Gao L., Zhao J., Chen Z., Liu B., Tang D., Yu B., Jiang C., Cheng H. M., (2009), “Synthesis of graphene sheets with high electrical conductivity and good thermal stability by hydrogen arc discharge exfoliation”, ACS Nano, 3 (2), 411-417.

Xu H., Zeiger B. W., Suslick K. S., (2013), “Sonochemical synthesis of nanomaterials”, Chem. Soc. Rev., 42 (7), 2555-2567.

Yi M., Shen Z., (2015), “A review on mechanical exfoliation for the scalable production of graphene”, J. Mater. Chem. A, 3, 11700-11715.

Yu Q., Lian J., Siriponglert S., Li H., Chen Y. P., Pei S-.S., (2008), “Graphene segregated on Ni surfaces and transferred to insulators”, Appl. Phys. Lett., 93 (11), 113103.

Zhang J., Wang E., (1995), “STM investigation of HOPG superperiodic features caused by electrochemical pretreatment”, J Electroanal Chem, 399 (1-2), 83-89.

Zhang L., Ji B., Wang K., Song J., (2014), “Synthesis of nitrogen-doped graphene via solid microwave method”, Materials Science and Engineering B, 185, 129-133.

BIOGRAPHY

Betül Gürünlü was born in 1987, Istanbul. She was graduated from Chemical Engineering Department of Yildiz Technical University in 2009, and then gained her MSc degree from Chemical Engineering Department of Istanbul Technical University in 2012. In 2015, she studied engineering at Sheffield Hallam University in United Kingdom for a year. She is currently doing her PhD on graphene synthesis & characterization, and also working as a research and teaching assistant at Chemical Engineering Department of Gebze Technical University.

APPENDIX

Appendix A: Publications done as a scope of thesis

Gurunlu B., Bayramoglu M., (2019), “Microwave Based Synthesis of Graphene from Graphite by Various Solvents”, Graphene Week 2019, Helsinki, Finland, 23-27 September.

Gurunlu B., Bayramoglu M., (2019), “One Step Synthesis of Graphene-Like Structures by Carbonization of Some Carbohydrates in Molten Salt Media”, Journal of Nano Research, 59, 166-179.

Gurunlu B., Bayramoglu M., (2019), “Graphene Synthesis by Ultrasound Energy Assisted Exfoliation of Graphite in Various Solvents”, Graphene2019: 9th edition of largest European Conference and Exhibition in Graphene and 2D Materials, Rome, Italy, 25-28 June.

Gurunlu B., Bayramoglu M., (2018), “Green Synthesis of Graphene in Molten Salt Media”, 20th International Conference on Materials, Method and Technologies, Elenite, Bulgaria, 26-30 June.